Arabidopsis inositol polyphosphate kinase activities regulate COP9 deneddylation functions in phosphate-homeostasis

Yashika Walia[a1#], Medha Noopur[a#], Bhaskar Chandra Sahoo[a], Ishana Bhattacharya[a], Mritunjay Kasera[a2], Naga Jyothi Pullagurla[b], Shobhita Saxena[c], Guizhen Liu[d], Gabriel Schaaf[e], Henning Jessen[d], Debabrata Laha[b], Souvik Bhattacharjee[c], Saikat Bhattacharjee[a#*]

[a]Laboratory of Signal Transduction and Plant Resistance, UNESCO-Regional Centre for Biotechnology (RCB), NCR Biotech Science Cluster, 3rd Milestone, Faridabad-Gurgaon Expressway, Faridabad- 121001, Haryana, India.

[b]Department of Biochemistry, Indian Institute of Science, Bengaluru-560 012, Karnataka, India.

[c]Special Centre for Molecular Medicine, Jawaharlal Nehru University, New Delhi-110067, Delhi, India.

[d]Faculty of Chemistry and Pharmacy & CIBSS-The Center for Biological Signalling Studies, University of Freiburg, Freiburg 79104, Germany.

[e]Department of Plant Nutrition, Institute of Crop Science and Resource Conservation, Rheinische Friedrich-Wilhelms-Universität Bonn, 53115 Bonn, Germany.

# Equal contribution

*Corresponding author:
Saikat Bhattacharjee
saikat@rcb.res.in
Tel: (+91) 129-2848837

Running title: InsPs regulate CRL-CSN dynamics in *A. thaliana*

---

[1] Present address: Maharishi Markandeshwar (deemed to be) University, Mullana-Ambala, Haryana-133207. India.

[2] Present address: Division of Biological Sciences, University of California, San Diego, La Jolla, CA 92093. USA.

Abstract

Plant Cullin RING Ubiquitin E3 ligases (CRLs) facilitate targeted protein degradation during physiological development and adaptation to stress. The deneddylase activity of COP9 signalosome (CSN) regulates cellular ratios of neddylated cullins available for the continuum of CRL functions. While selective inositol polyphosphates (InsPs) function as co-factors in plant responses involving the ubiquitylation of negative regulators, a relationship to CSN-CRL activities has not yet been established. Here, we show that the two *Arabidopsis thaliana* InsP-kinases IPK1 and ITPK1 physically interact and metabolically connect with the CSN holo-complex to modulate cullin deneddylation efficiency. Specifically, functional deficiency of ITPK1 lowers cullin deneddylation rates and disrupts the dissociation equilibrium of CSN5, the deneddylase catalytic subunit, and CUL1 with the holo-complex. Our results identify a novel auto-regulatory switch of CSN functions, defined by deneddylation activity. We further demonstrate that phosphate starvation response (PSR), which is induced in Pi-starved wild-type plants and constitutive in the above InsP-kinase mutants, is orchestrated in part by reduced deneddylation rates that, in turn, affect the stability of SPX4, a key negative regulator of PSR. Pharmacological inhibition of cullin neddylation stabilizes SPX4 and impairs PSR, thus linking CSN-CRL dynamics to phosphate (Pi)-sensing. Conversely, when exposed to compounds that inhibit CSN5 deneddylase activity, wild-type plants display phenotypes similar to the above InsP-kinase mutants. Overall, our data reveal that the regulation of plant Pi-starvation responses by specific InsP-kinases is caused by a direct role of these kinases in balancing coordination between CRL-CSN activities.

Keywords

Inositol polyphosphates; COP9 signalosome; inositol hexakisphosphate ($InsP_6$) kinase 1; inositol 1,3,4-trisphosphate 5/6-kinase 1; $InsP_7$, deneddylation; phosphate homeostasis; phosphate-starvation response; Cullin RING ubiquitin ligase; ubiquitination; SPX4

The versatile functions of soluble inositol polyphosphates (InsPs) in cellular processes in eukaryotes result from their propensity for being differentially phosphorylated by a relatively largely conserved set of InsP-kinases (Kim et al., 2024; Laha et al., 2021; Monserrate and York, 2010; Shears and Wang, 2019; Wilson et al., 2013). In plants, particular InsPs have been linked to phytohormone perception, inorganic phosphate (Pi)-homeostasis, mRNA export, meristem maintenance, and plant immunity (Alcazar-Roman et al., 2010; Dong et al., 2019; Gillaspy, 2013; Gulabani et al., 2022; Jia et al., 2019; Kuo et al., 2014; Kuo et al., 2018; Laha et al., 2015; Laha et al., 2016; Laha et al., 2019; Laha et al., 2021; Laha et al., 2022; Murphy et al., 2008; Poon et al., 2020; Pullagurla et al., 2024; Ren et al., 2024; Riemer et al., 2021; Stevenson-Paulik et al., 2005; Wild et al., 2016; Williams et al., 2015; Zhu et al., 2009). The synthesis of the fully phosphorylated *myo*-inositol derivative, $InsP_6$ (*myo*-inositol-1,2,3,4,5,6-hexakisphosphate, also known as phytic acid), from $InsP_5$ [2OH] is catalyzed by INOSITOL PENTAKISPHSPHATE 2-KINASE 1 (IPK1) and is sequentially (pyro)-phosphorylated by INOSITOL 1,3,4-TRISPHOSPHATE 5/6-KINASES (ITPK1/2) and then by DIPHOSPHOINOSITOL PENTAKISPHOSPHATE KINASES (VIH1/2) to generate the energy-rich phosphoanhydride bond-containing inositol pyrophosphates, including various $InsP_7$ isomers and $InsP_8$ (Adepoju et al., 2019; Desai et al., 2014; Laha et al., 2015; Laha et al., 2019; Laha et al., 2022; Pullagurla et al., 2024; Riemer et al., 2021; Stevenson-Paulik et al., 2005; Whitfield et al., 2020; Zhu et al., 2019). Recent studies have indicated (or have proposed) that $InsP_6$, and more recently 5-$InsP_7$, promote auxin-receptor complex formation that may eventually drive the degradation of AUX/IAA repressors, whereas $InsP_8$ may similarly facilitate targeting of JASMONATE ZIM-DOMAIN (JAZ) repressors (Laha et al., 2015; Laha et al., 2022; Pullagurla et al., 2023; Sheard et al., 2010; Tan et al., 2007). Interestingly, the cognate substrate receptors TRANSPORT INHIBITOR RESPONSE 1 (TIR1) and CORONATINE INSENSITIVE 1 (COI1) belong to the F-box family proteins and are components of typical SCF (ASK1/SKP1-Cullin-F-Box; SCF^{TIR1} and SCF^{COI1})-type E3 ubiquitin ligases (Gray et al., 1999; Gray et al., 2001; Sheard et al., 2010; Tan et al., 2007; Williams et al., 2019; Xu et al., 2002).

InsPs have also been recently implicated as sensors of phosphate (Pi)-status in plants (Cridland and Gillaspy, 2020; Dong et al., 2019; Guan et al., 2022; Kuo et al., 2018; Pullagurla et al., 2024; Ried et al., 2021; Riemer et al., 2021; Stevenson-Paulik et al., 2005; Wild et al., 2016; Zhu et al., 2019). Under low Pi-availability from the soil, a highly organized adaptive cascade of events collectively termed phosphate starvation response (PSR) is activated. Such events

include the upregulated expression of phosphate-starvation inducible (*PSI*)-genes such as for Pi-transporters (*PHT*s), phosphatases (*PAP*s), and several micro- (*MIR399*) or non-coding RNAs (*IPS1*), that results in increased Pi mobilization in the rhizosphere/soil, as well as in increased Pi uptake and remobilization from source tissues and intracellular Pi-storage reserves (Ham et al., 2018; Kuo et al., 2014; Puga et al., 2014). In Arabidopsis, PSR-associated transcriptional changes are majorly orchestrated by the MYB-transcription factors PHOSPHATE STARVATION RESPONSE 1 (PHR1) and its closest homolog PHR1-LIKE (PHL1) (Bustos et al., 2010; Sun et al., 2016). These transcription factors bind to partially conserved sequences (*P1BS* elements) present in *PSI*-gene promoters to activate the expression of these genes (Franco-Zorrilla et al., 2004; Rubio et al., 2001; Zhou et al., 2008). In consequence, a *phr1 phl1* double mutant is deficient in *PSI*-gene expression both basally and upon exposure to Pi deficiency (Kuo et al., 2014).

The stand-alone SPX (SYG1/Pho81/XPR1)-domain-containing proteins SPX1/2 act as negative regulators of PHR1/PHL1 functions in maintaining phosphate homeostasis. Following the first report that SPX domains can bind specific InsPs, it was subsequently demonstrated that under Pi-replete conditions, SPX-type proteins require $InsP_8$ as a co-factor to bind PHR1 and suppress its transcriptional activity (Dong et al., 2019; Wild et al., 2016; Zhu et al., 2019). Upon Pi starvation, intracellular $InsP_8$ levels are reduced, relieving SPX1-tethered inhibitions on PHR1, thus allowing successful transduction of PSR (Dong et al., 2019; Riemer et al., 2021) In $InsP_8$-deficient *ipk1-1*, *itpk1-2*, *vih1 vih2*, or *spx* mutants, released PHR1 causes constitutive activation of *PSI*-gene expressions, even under Pi-sufficient conditions, accumulating high endogenous Pi levels (Dong et al., 2019; Kuo et al., 2018; Puga et al., 2014; Riemer et al., 2021; Zhu et al., 2019). Besides the well-established role of InsPs in modulating PSR by allosteric regulation of SPX proteins (Dong et al., 2019; Ried et al., 2021; Riemer et al., 2021; Wild et al., 2016; Zhu et al., 2019), there is recent evidence that the cellular Pi status has a direct role in regulating SPX protein stability. Pi-starvation was shown to promote ubiquitylation of at least two SPX proteins (Lv et al., 2014; Osorio et al., 2019; Zhong et al., 2018). Furthermore, the identification of E3 ubiquitin ligases that target rice SPX4 upon Pi-starvation (Ruan et al., 2019) when consolidated with specific InsP-requirement as co-factors affecting the fate/function of hormonal repressors (Laha et al., 2015; Laha et al., 2022) implies that $InsP_7$/$InsP_8$ are biochemical regulators of stimulus-dependent substrate stabilities.

In a typical eukaryotic cell, ~20% of targeted protein degradations are mediated by Cullin RING ubiquitin ligases (CRLs), the largest subfamily among the E3 ubiquitin ligase family

114 (Soucy et al., 2009; Sun et al., 2002). A modular CRL contains a Cullin (CUL) scaffold (CUL1-
115 4 in Arabidopsis), an E2-interacting RING-type Rbx/Roc protein, CUL member-guided
116 substrate adaptor and a ubiquitination target-specified substrate receptor (Hotton and Callis,
117 2008; Hua and Vierstra, 2011; Zheng et al., 2002). CRLs require covalent modification of a
118 Nedd8 moiety on CULs (a process termed as neddylation) (Sun et al., 2002) for activation and
119 complex formation with specific co-receptors, adapters and with the ubiquitin E2 enzyme for
120 subsequent degradation of targeted substrates (Schwechheimer, 2018). In the absence of
121 cognate substrates, CRLs become vulnerable to self-ubiquitylation and are protected by the
122 Constitutive photomorphogenesis 9 signalosome (CSN), an evolutionarily conserved eight-
123 subunit (CSN1-8) macromolecular complex (Chamovitz and Segal, 2001; Dubiel et al., 2015;
124 Stuttmann et al., 2009; Wu et al., 2006). The CSN5 subunit in this holo-complex contains an
125 MPN^{+}/JAMM metalloprotease motif that catalytically removes Nedd8 (deneddylation) from
126 CULs, preventing their self-degradation (Cope et al., 2002). Interaction changes between CRL
127 and CSN affect the cellular ratio of neddylated CUL:unneddylated CUL (CUL^{Nedd8}:CUL)
128 (Scherer et al., 2016). CUL deneddylation promotes CRL disassembly from the holo-complex
129 and is essential for its functional recycling and establishing associations with newer substrate
130 co-receptors and adapters. Biochemical modes of a CSN operation, including its dynamic
131 rearrangements upon CRL binding, have been gradually unraveled at the structural and
132 functional levels (Dubiel et al., 2015; Enchev et al., 2012; Lingaraju et al., 2014). From these
133 studies, it is evident that optimal CRL activity necessitates regulated cullin
134 neddylation/deneddylation cycles. Recent breakthroughs have revealed highly localized,
135 coordinated activities of mammalian IP5K with IP6K1 in providing $InsP_6$ and $InsP_7$ to
136 strengthen and loosen CRL-CSN associations, respectively (Lin et al., 2020; Rao et al., 2014;
137 Scherer et al., 2016). However, despite the reported interactions between the Arabidopsis
138 ITPK1 or of SCF^{TIR1}/SCF^{COI1} components with the CSN subunits (Feng et al., 2003; Qin et al.,
139 2005; Schwechheimer, 2001) and the implicated role of InsPs as co-factors in response
140 adaptations that require degradation of specific repressors (Laha et al., 2015; Laha et al., 2022;
141 Osorio et al., 2019), the ternary relationship that directly demonstrates the functional
142 coordination between (any) InsP-kinase with CRL and CSN activities, has not been shown so
143 far.

144 Here, we show that, in Arabidopsis, the metabolically linked pair IPK1 and ITPK1 form a
145 previously unrecognized association within the CSN holo-complex and moderate CUL1
146 deneddylation efficiency, likely via $InsP_7$ synthesis. The corresponding InsP-kinase mutants

147 display enhanced CUL1^{Nedd8} levels due to deficient deneddylation rates *in vivo* and *in vitro*.
148 Impaired deneddylation in these mutants perturb the equilibrium of selective holo-complex-
149 associated and -free monomeric CSN subunits and CUL1, highlighting an intricate auto-
150 regulatory mechanism in the holo-complex activities. Furthermore, using various
151 pharmacological inhibitors that perturb CUL^{Nedd8}:CUL ratios, we demonstrate a molecular link
152 between CSN holo-complex deneddylase activities and activation of PSR. In particular, we
153 show that SPX4, a key negative regulator of PSR, is degraded via the CRL pathway upon Pi-
154 starvation. Our data reveal that the maintenance of CSN deneddylase activity and CRL
155 functions are essential to execute a successful PSR in plants. These results unravel novel
156 activities of the plant IPK1-ITPK1 InsP-kinase pair in regulating CSN-CRLs functions during
157 Pi-homeostasis and in responses to Pi-starvation.

158 **Results**

159 **Arabidopsis IPK1 and ITPK1 interact with CSN subunits**

160 Basal neddylation ratios of cullins are skewed in mutants of mammalian IP5K and IP6K (Rao
161 et al., 2014; Scherer et al., 2016). Similar occurrences are not known in any plant InsP kinase
162 mutant. Anti-CUL1 blots on total protein extracts from Arabidopsis *ipk1-1* or *itpk1-2* plants
163 detected considerably higher levels of neddylated-CUL1 (CUL1^{Nedd8}) than in Col-0 (Figure
164 1A). In other InsP-kinases mutants, namely *ipk2β-1* and *itpk4-1*, that share a common global
165 $InsP_6$ deficiency with *ipk1-1* (Kuo et al., 2018; Laha et al., 2015; Laha et al., 2022; Stevenson-
166 Paulik et al., 2005) CUL1^{Nedd8}:CUL1 ratios were similar to Col-0 (Supplemental Figure 1A).
167 Enhanced CUL1^{Nedd8} levels observed in *ipk1-1* or *itpk1-2* were restored to Col-0 levels in the
168 corresponding complemented lines *Myc-IPK1/ipk1-1* or *ITPK1-GFP/itpk1-2*, respectively
169 (Gulabani et al., 2022; Laha et al., 2022) (Supplemental Figure 1B). These results suggest that
170 deficiencies limited and specific to *ipk1-1* or *itpk1-2* plants caused perturbed levels of
171 neddylated CUL1.

172 The COP9 signalosome regulates cullin-deneddylation rates (Lyapina et al., 2001). Previously,
173 mammalian or plant ITPK1 was shown to interact with CSN1 (Qin et al., 2005; Sun et al.,
174 2002). However, their functional implications were not explored. Similarly, human IP5K or
175 IP6K1 enrichments were also shown to co-elute with CSN subunits and cullins (Rao et al.,
176 2014; Scherer et al., 2016). We performed yeast two-hybrid assays to determine physical
177 associations between IPK1 and ITPK1 with various CSN subunits. Both InsP-kinases
178 interacted in yeast with each other and with CSN1 and CSN2 subunits (Supplemental Figure

179 2A-C). However, only IPK1, but not ITPK1, showed interaction with the CSN5 subunit.
180 Similarly, immuno-enriched Myc-IPK1 or ITPK1-GFP from the above-mentioned
181 complemented plant lines also detected CSN1, CSN2, CSN4 subunits and CUL1 in the co-
182 elutes (Figure 1B). Mirroring the Y2H data, CSN5 was only detected in co-elutes from Myc-
183 IPK1 but not ITPK1-GFP enrichments (Figure 1B). Control pulldowns, either from transgenic
184 plants expressing CaMV 35S promoter-driven GFP *(35S:GFP*) using anti-GFP agarose, or
185 from the InsP-kinase complemented lines using IgG-conjugated beads, did not detect any CSN
186 subunits, validating the specificity of the above interactions (Figure 1B; Supplemental Figure
187 1C). In bi-molecular fluorescence complementation (BiFC) assays, IPK1 and ITPK1
188 association with each other or with CSN1, CSN2, or CSN5 were detected as nucleocytoplasmic
189 complexes similar to the localization of the individual proteins (Adepoju *et al.*, 2019)
190 (Supplemental Figure 3A). The negative control protein β-Glucuronidase (GUS), did not
191 interact with either IPK1, ITPK1, CSN1, CSN2, or CSN5, again indicating the specificity of
192 the observed interactions (Supplemental Figure 3B). Mutual interaction between IPK1 and
193 ITPK1 was further validated by co-immunoprecipitation assay (Co-IP) wherein immuno-
194 enrichment of transiently expressed GFP-ITPK1, but not of GFP alone, detected the co-
195 expressed Myc-IPK1 (Supplemental Figure 3C). Consolidated, the results demonstrate *planta*
196 associations between IPK1 and ITPK1 with each other and selective CSN subunits.

197 **Kinase activities of IPK1 or ITPK1 affect their association with the CSN holo-complex**

198 To determine the cellular proportion of IPK1 or ITPK1 pools that associate with the CSN holo-
199 complex, we subjected total protein extracts from Col-0, *Myc-IPK1/ipk1-1* and *ITPK1-*
200 *GFP/itpk1-2* leaves to size-exclusion chromatography, followed by immunoblotting for the
201 CSN1 subunit, Myc-IPK1, or ITPK1-GFP proteins in the collected fractions. The elution
202 profile of the CSN holo-complex and free CSN subunits from plant extracts have been reported
203 earlier (Dohmann et al., 2005; Gusmaroli et al., 2004). CSN1 was used as the representative
204 marker for CSN holo-complex pools since it exclusively partitions into higher molecular
205 weight fractions (~400-600 kDa; termed high molecular weight, HMW). Intriguingly, neither
206 Myc-IPK1 nor ITPK1-GFP proteins were detected in fractions containing CSN1, suggesting
207 that under steady-state, only a minor cellular pool of these InsP-kinases is present with the CSN
208 holo-complex (Supplemental Figure 4A). We then investigated whether the activities of these
209 InsP-kinases influenced their association with the CSN subunits. To this end, GFP alone or
210 GFP-tagged wild-type or kinase-dead versions of IPK1 or ITPK1 cDNAs (accordingly named
211 GFP-IPK1, GFP-ITPK1, GFP-IPK1^{K168A}, or GFP-ITPK1^{D288A}, respectively) were transiently

212 co-expressed with HA-CSN2 in *N. benthamiana* leaves. IPK1^{K168A} harbors a substitution in the
213 conserved kinase motif, whereas the ITPK1^{D288A} contains a similar mutation in the conserved
214 ATP-grasp motif. Thus, these mutant variants are catalytically inactive (Laha et al., 2019;
215 Riemer et al., 2021; Stevenson-Paulik et al., 2005). Anti-GFP immuno-enrichments of the InsP-
216 kinases showed that the kinase-dead IPK1^{K168A} interacted less, whereas more association of
217 ITPK1^{D288A} was observed with CSN2, in comparison to their cognate wild-type proteins
218 (Supplemental Figure 4B). Enrichments of GFP alone did not co-elute HA-CSN2. Interactions
219 between IPK1 and ITPK1 were unaffected by the kinase-site mutations (Supplemental Figure
220 2C).

221 Transgenic Arabidopsis *ipk1-1* plants expressing Cauliflower Mosaic virus (CaMV) 35S
222 promoter-driven *GFP-IPK1*, but not *GFP-IPK1^{K168A}*, transgene restored growth deficiencies
223 and Pi over-accumulation phenotypes of the *ipk1-1* plants, implying functional
224 complementation by the wild-type, but not by the kinase-dead fusion proteins (Figure 1C;
225 Supplemental Figures 5A, B). These results matched earlier reports (Kuo et al., 2014; Kuo et
226 al., 2018). The lines *GFP-IPK1/ipk1-1#12* and *GFP-IPK1^{K168A}/ipk1-1#*3, expressing
227 comparable levels of the respective recombinant proteins, were selected for further assays
228 (Supplemental Figure 5C). Enhanced CUL1^{Nedd8} pools apparent in *ipk1-1*, were restored to
229 wild-type levels in *GFP-IPK1/ipk1-1#12,* but not in *GFP-IPK1^{K168A}/ipk1-1#3* extracts,
230 indicating that the maintenance of CUL1^{Nedd8}:CUL1 homeostasis requires catalytically active
231 IPK1 (Supplemental Figure 5D). Immuno-enrichments detected lower amounts of co-eluted
232 endogenous CSN2 or CSN4 with GFP-IPK1^{K168A}, than GFP-IPK1 (Figure 1E). In Y2H assays,
233 IPK1^{K168A} did not or only weakly interacted with CSN1, CSN2, and CSN5 compared to wild-
234 type IPK1 (Supplemental Figure 2A). When tested similarly for *itpk1-2*, its growth defects
235 were abolished, and high endogenous Pi recovered to wild-type levels, albeit partially, only in
236 the transgenic lines expressing CaMV 35S promoter-driven *GFP-ITPK1*, but not *GFP-*
237 *ITPK1^{D288A}* (Figure 1D; Supplemental Figures 6A, B). Corresponding GFP-ITPK1 fusion
238 proteins were detected in all the above transgenic lines (Supplemental Fig. 6C). We selected
239 *GFP-ITPK1/itpk1-2#7* and *GFP-ITPK1^{D288A}/itpk1-2#3* that expressed nearly similar levels of
240 the GFP-fusion protein for further assays. Enhanced CUL1^{Nedd8} level apparent in *itpk1-2* was
241 recovered only in the *GFP-ITPK1/itpk1-2#7*, but not in the *GFP-ITPK1^{D288A}/itpk1-2#3* extracts
242 (Supplemental Figure 6D). Further, extracts from these lines immuno-enriched with anti-GFP
243 antibody-conjugated agarose beads detected more endogenous CSN2 and CSN4 in GFP-
244 ITPK1^{D288A} co-elutes than GFP-ITPK1 (Figure 1F). In Y2H assays, ITPK1^{D288A} showed

245 stronger interaction with CSN1 or CSN2 and displayed gain-of-interaction with CSN5, which
246 was not detected for ITPK1 (Supplemental Figure 2B). These results, in accordance with the
247 earlier *N. benthamiana* data (Supplementary Figure 4B), implied that the ITPK1 kinase
248 function may diminish its CSN association. Mutual interaction between IPK1 and ITPK1 was
249 mostly unaffected by the kinase-dead mutations (Supplemental Figure 2C). Taken together,
250 our results suggest that IPK1 and ITPK1 catalytic activities have a reverse effect in their
251 association with CSN. While the kinase function of IPK1 promotes its interaction with the CSN
252 subunits, the ITPK1 kinase activity hinders such equivalent associations. Similar results
253 wherein the mammalian kinase-deficient $IP5K^{K138A}$ protein binds poorly, whereas a kinase-
254 dead version of IP6K1 ($IP6K1^{K225/335A}$) binds more robustly to CSN2 or CSN5 have been
255 reported (Rao et al., 2014; Scherer et al., 2016).

256 **Equilibrium of association dynamics of the CSN holo-complex is disrupted in *ipk1-1* and**
257 ***itpk1-2* plants**

258 Locally produced InsPs modulate the tethering efficiencies of cullins to the mammalian CSN
259 (Lin et al., 2020; Scherer et al., 2016). Increased CUL^{Nedd8} levels in the above InsP-kinase
260 mutants may be due to deficient tethering of CUL1 and, hence, decreased deneddylation by the
261 endogenous CSN. To test this, we supplemented Col-0, *ipk1-1,* or *itpk1-2* with purified
262 recombinant CSN2 (His-rCSN2), followed by immuno-enrichments using Ni^{2+}-NTA
263 conjugated agarose beads, and then probing for the presence of relative amounts of CUL1 in
264 the elutes. Detection of similar amounts of CSN1 in the His-rCSN2 enrichments from all three
265 extract types suggested the successful and equal incorporation of the recombinant protein into
266 the respective endogenous holo-complex (Figure 2A). Interestingly, higher levels of CUL1 co-
267 eluted with His-rCSN2 in extracts derived from *ipk1-1* or *itpk1-2* plants than in Col-0 samples
268 (Figure 2A). These included pools of both neddylated- and unneddylated-CUL1. Thus,
269 increased $CUL1^{Nedd8}$ levels in the above InsP kinase mutants were not caused by reduced access
270 of CUL1 to the CSN. Control recombinant GFP (His-rGFP) enrichments from the above plant
271 extracts did not lead to the detection of any of the investigated proteins, validating the
272 specificity of the observed interactions (Supplemental Figure 7A).

273 Selective subunits such as CSN4 and CSN5 are known to undergo dynamic
274 association/dissociation cycles to/from the CSN holo-complex to regulate its deneddylase
275 activity (Dohmann et al., 2005; Enchev et al., 2012; Gusmaroli et al., 2007; Lingaraju et al.,
276 2014; Mosadeghi et al., 2016). Eluates from the above His-rCSN2 enrichments detected more

277 endogenous CSN4 and CSN5 from *ipk1-1* or *itpk1-2* extracts than Col-0 (Figure 2A). Total
278 CSN1, CSN4, or CSN5 levels remained unchanged between the extracts from the different
279 genotypes. We further validated this observation by analyzing the fractionation profile of CSN
280 subunits in Col-0 versus *ipk1-1* and *itpk1-2* extracts via gel-filtration chromatography. Fraction
281 numbers that detected CSN1 were similar between extracts (Supplemental Figure 7B).
282 However, CSN5 and CSN4 profiles from *ipk1-1* and *itpk1-2* revealed comparatively reduced
283 or almost negligible presence, respectively, of these subunits in the lower molecular weight
284 fractions (~100-50 kDa, termed LMW), as compared to Col-0 (Figure 2B). Fractionated
285 extracts from the complemented lines of these two InsP-kinase mutants did not display these
286 differences, indicating that the alterations were due to consequences of *ipk1-1* and *itpk1-2*
287 mutations (Supplemental Figure 7C). Slight fractionation shifts of CUL1, also towards larger
288 HMW pools, were detected in extracts from *ipk1-1* and *itpk1-2* plants, as compared to Col-0
289 (Supplemental Figure 7D). These likely represented the CUL1 pools that were associated more
290 with the CSN (Figure 2A). *In toto*, these results implied that a steady-state association
291 dynamics of specific CSN subunits and CUL1 association with the holo-complex is likely
292 perturbed in *ipk1-1* or *itpk1-2* plants.

293 **Impaired deneddylation activity disrupts CSN equilibrium in the InsP-kinase mutants**

294 Deneddylase activity of CSN5 is active only when it engages with the CSN holo-complex
295 (Gusmaroli et al., 2007). Thus, more CSN5 detected as a part of the holo-complex in *ipk1-1* or
296 *itpk1-2* plants would ideally imply higher deneddylation efficiencies. However, increased
297 $CUL1^{Nedd8}$ levels detected in these mutants contradict this speculation. Indeed, *in-lysate* assays
298 (Lin et al., 2020) demonstrated decreased efficiencies of CUL1-deneddylation in extracts from
299 *ipk1-1* and *itpk1-2* plants, coinciding with an increased CUL1 degradation in these mutant lines
300 (Supplemental Figures 8A, B). Thus, impaired CSN deneddylase activities in *ipk1-1* or *itpk1-*
301 *2* likely cause augmented $CUL1^{Nedd8}$ levels.

302 A deneddylation-deficient CSN5 is known to affect the integration of other CSN subunits, such
303 as CSN4, into the holo-complex (Dohmann et al., 2005; Enchev et al., 2012; Gusmaroli et al.,
304 2007). Using CSN5i-3, a recently reported CSN5-deneddylase inhibitor (Schlierf et al., 2016),
305 we then sought to determine the cause-effect relationship between deneddylation deficiencies
306 and altered CSN subunit partitioning. In Col-0 plants, a dose-dependent increment in
307 $CUL1^{Nedd8}$ levels, coinciding with reduced unneddylated-CUL1, was detected at 24-hpt (hours
308 post-treatment) with CSN5i-3 (Figure 2C). MLN4924, a known small molecule

309 pharmacological inhibitor of CUL-neddylation, was used as a negative control in these tests
310 (Hakenjos et al., 2011; Soucy et al., 2009). Interestingly, fractionation of CSN5i-3-treated Col-
311 0 extracts showed markedly reduced CSN5 levels in LMW pools, a pattern overall resembling
312 profiles observed in *ipk1-1* or *itpk1-2* (Figure 2D). The fractionation profile of CSN1 was
313 unaffected by CSN5i-3 (Supplementary Fig. 8C). The enrichment of supplemented His-rCSN2
314 from CSN5i-3-treated Col-0 extracts detected more CSN4, CSN5, and CUL1 than the control
315 (Figure 2E). These results were also reminiscent of the *ipk1-1* and *itpk1-2* data (Figure 2A),
316 overall suggesting that the deneddylation deficiencies were the primary cause of these
317 retentions in the mutants. Our findings supported earlier reports that a deneddylation deficient
318 recombinant $CSN^{CSN5\text{-}H138A}$ binds neddylated CRLs with higher affinity *in vitro* (Enchev et al.,
319 2012; Füzesi-Levi et al., 2020; Mosadeghi et al., 2016).

320 These results also prompted us to test whether the dissociation dynamics of IPK1 or ITPK1
321 with the CSN holo-complex are also similarly affected by the deneddylase activity. Indeed,
322 His_6-tagged recombinant IPK1 or ITPK1 proteins (hereafter termed as His-rIPK1 or His-
323 rITPK1, respectively), when supplemented to CSN5i-3-treated extracts, bound more CSN4,
324 CSN5, or CUL1 than the mock-treated samples (Figure 2F). Thus, the inhibition of CSN5
325 deneddylation activity also augmented CSN holo-complex associations with IPK1 and ITPK1.
326 This indicates that the deneddylation efficiency of the holo-complex affects the dissociation
327 rates of its mobile subunits CSN4, CSN4 and two InsP-kinases. Interestingly, CSN5i-3
328 treatments did not affect total $InsP_6$ or $InsP_7$ levels, implying that deneddylation inhibition does
329 not interfere *per se* with the two InsP-kinase activities (Supplemental Figure 9).

330 **$InsP_6$ potentiation on CSN deneddylase activity requires a kinase-active ITPK1**

331 The kinase activity of IPK1 promotes its CSN association, whereas a kinetically inactive
332 ITPK1 interacts strongly with CSN (Figures 1C, D; Supplementary Figure 2B). The known
333 metabolic relationship between these two InsP-kinases led us to test whether their cognate
334 catalytic products directly affect the deneddylation activity of the CSN holo-complex. In our
335 assays, purified recombinant mammalian Ubiquitin C-terminal hydrolase-L3 (rUCHL3), a
336 well-known deneddylase, was used as the positive control (Hemelaar et al., 2004; Wada et al.,
337 1998). We noted that endogenous CSN holo-complex (HMW Fraction #9-13), enriched from
338 Col-0, was enzymatically active and successfully deneddylated Nedd8-aminoluciferin (Nedd8-
339 AML) substrate *in vitro* in a dose-dependent manner (Figure 3A). At 10 μM concentration,
340 CSN5i-3 completely inhibited the deneddylation activity, thereby ruling out the contaminating

341 activity of other deneddylases, such as a DENEDDYLASE 1 (DEN1) that may be present in
342 the CSN holo-complex pool (Christmann et al., 2013; Mergner et al., 2015). Of greater purity
343 than the enriched Col-0 CSN holo-complex, rUCHL3 was also a more potent deneddylase.

344 Because $InsP_6$ is commercially available, we first tested whether this metabolite directly affects
345 the deneddylation activity of a plant CSN holo-complex. Remarkably, $InsP_6$ addition enhanced,
346 in a dose-dependent manner, the deneddylation activity of Col-0 CSN holo-complex (Figure
347 3B). Compared to untreated extracts, deneddylation activity was ~90- or ~350-fold higher with
348 50 nM or 100 nM $InsP_6$, respectively. At 300 nM concentration, $InsP_6$ inhibited Nedd8-AML
349 deneddylation, likely due to its known protein-precipitation effects (Ried et al., 2021; Veiga et
350 al., 2006). The lack of commercially available 5-$InsP_7$, the product of ITPK1 kinase activity,
351 prevented us from directly testing the effect of this metabolite in the deneddylation assays.

352 To reaffirm the deneddylation deficiencies in *ipk1-1* or *itpk1*-2 extracts noted earlier
353 (Supplementary Figures 8A, B), CSN holo-complex pools were collected from these mutants,
354 as done for Col-0. At similar total protein concentrations normalized with CSN1, *ipk1-1* or
355 *itpk1-2* CSN holo-complex displayed significantly lower basal and reduced deneddylation
356 kinetics on Nedd8-AML, in comparison to Col-0 (Figure 3C). These results validated our
357 earlier findings of deneddylation deficiencies in *ipk1-1* or *itpk1-2* mutants. Most interestingly,
358 we noted that exogenous supplementation of 50 nM $InsP_6$ in the deneddylation reaction of *ipk1-*
359 *1*, but not in *itpk1-2* or *GFP-ITPK1*^{D288A}*/itpk1-2#3*, improved deneddylation rate of the
360 enriched CSN holo-complex significantly (Figure 3D). These results, consolidated with the
361 earlier data (Figure 3B), implied that the supplemented $InsP_6$ required an enzymatically active
362 ITPK1, and likely $InsP_7$ synthesis, to stimulate deneddylation. Again, the unavailability of
363 commercial 5-$InsP_7$ prevented a direct test of this metabolite in rescuing the deneddylation
364 defects of the InsP-kinase mutants.

365 Similar to the mammalian counterpart, Arabidopsis CSN2 likely binds to $InsP_6$ (Lin et al.,
366 2020). Thus, CSN2, either as a direct competitor and/or allosterically, may limit substrate
367 availability for the enzymatic activity of ITPK1 at the CSN platform. The kinase activity-
368 dependent interaction of IPK1 with the holo-complex (Figure 1D; Supplemental Figures 2A,
369 4B), may ameliorate this suppression either by allosteric interactions with CSN2 or by
370 catalytically providing an increased local concentration of $InsP_6$ substrate to ITPK1. We tested
371 this hypothesis by evaluating the efficiency of $InsP_7$ synthesis by ITPK1, detected via PAGE
372 (Riemer et al., 2021). As anticipated, wild-type ITPK1, but not ITPK1^{D288A}, was enzymatically

373 competent to generate $InsP_7$ from $InsP_6$ (Supplemental Figure 10A). Remarkably, His-rCSN2,
374 added to the reaction, suppressed $InsP_7$ synthesis, whereas the $InsP_6$-binding deficient CSN2
375 (His-rCSN2^{K3A}, harboring alanine substitutions of conserved K64, K67, Q68 residues; Lin et
376 al., 2020) did not (Supplementary Figures 10B, C). Most interestingly, His-rIPK1 added to the
377 reaction, mitigated CSN2-mediated inhibition, increasing $InsP_7$ synthesis by ITPK1 (Figure
378 3E). Cumulatively, these results implied that metabolic coupling between the two InsP-kinases
379 that lead to enzymatic activation of ITPK1 may define the rate-limiting step of deneddylation
380 activity of the holo-complex. This activity, in turn, regulates the association-dissociation
381 dynamics of not only the InsP-kinases but also of CSN5 and CSN4 through feedback
382 mechanisms.

383 **Pi-starvation alters the dynamics of CSN5 and its deneddylase functions**

384 Known consequences in *ipk1-1* and *itpk1-2* mutants are reduced auxin-sensitivity and
385 constitutive PSR (Kuo et al., 2014; Kuo et al., 2018; Laha et al., 2022; Riemer et al., 2021).
386 MLN4924 is known to inhibit the degradation of CRL substrates in Arabidopsis and confer
387 auxin-insensitivity (Hakenjos et al., 2011). To test whether the increased *PSI*-gene expression
388 in the InsP-kinase mutants is linked with deneddylation deficiencies and enhanced CUL^{Nedd8}
389 levels, we treated these mutants with MLN4924. Additionally, upregulated expression of
390 several *PSI*-genes (*PHT1;3, PHT1;2, SPX1*, and *IPS1*), as well as high endogenous Pi-level in
391 these InsP-kinase mutants, were suppressed by MLN4924 (Figure 4A; Supplementary Figure
392 11A). Similarly, MLN4924 also suppressed the induction of *PSI*-genes in Pi-starved Col-0,
393 implying that changes in neddylation-related processes regulate PSR (Figure 4B). Curiously, a
394 prominent increase in CUL1^{Nedd8} levels that was also reversed by MLN4924 was noted in the
395 Pi-starved Col-0 extracts (Figure 4C). Similarly, the resupply of phosphates to the Pi-deprived
396 media also restored CUL1^{Nedd8} amounts to Pi-replete levels, validating that these responses are
397 consequences of Pi-depravation (Figure 4D). Most intriguingly, the CSN5 partitioning profile
398 under the Pi-deplete condition was peculiarly similar to the *ipk1-1* or *itpk1-2* pattern, with
399 higher levels in HMW than LMW fractions (Figure 4E). Resupplied phosphate restored CSN5
400 partitioning changes to the Pi-replete pattern. The elution profile of CSN1 was unaltered in the
401 extracts from the Pi-starved plants (Supplementary Figure 11B).

402 *In lysate* deneddylation assay, performed as earlier, demonstrated that CUL1^{Nedd8} levels were
403 more stable across progressive time points of reaction in Pi-deplete samples than in Pi-replete
404 extracts, indicative of deneddylation deficiencies upon Pi-starvation (Figure 4F, G). However,

405 unlike the data from the InsP-kinase mutants (Supplementary Figure 8A), gradual CUL1
406 instability across progressive time points was not apparent in the Pi-deplete samples. Moreover,
407 deneddylation efficiencies on Nedd8-AML substrate by the enriched CSN holo-complex were
408 lower in the Pi-deplete than in Pi-replete samples (Supplementary Figure 11C). Thus, the
409 enhanced $CUL1^{Nedd8}$ levels associated with PSR are caused by dampened deneddylation
410 activities of the endogenous CSN holo-complex and are similar to the occurrence in the two
411 InsP-kinase mutants. Consolidated, these results implied that Pi-starvation dampens CSN
412 deneddylase activity and the elevated $CULI^{Nedd8}$ is essential for the transduction of PSR.

413 ***csn* mutants or the functional inhibition of CSN5 phenocopy *ipk1-1* or *itpk1-2* properties**

414 Our above results suggested that CSN functions regulate PSR. To determine whether *PSI*-gene
415 expressions are globally affected by functional deficiencies of CSN, we mined the available
416 microarray data of differentially expressed transcripts in the various *csn* null mutants (*csn3*,
417 *csn4* and *csn5ab*) (Dohmann et al., 2008). Strong upregulation in the expression of several *PSI*-
418 genes that were categorized to Pi-remobilization and Pi-transport processes were evident in the
419 transcriptomic data from the *csn* mutants (Supplemental Figure 12). Expression levels of *PHR1*
420 or *PHL1* transcripts remain unaltered in these mutants, similar to *ipk1-1* and *itpk1-2* data (Kuo
421 et al., 2014; Kuo et al., 2018). *IPK1* or *ITPK1* transcript levels are also unaffected in the *csn*
422 mutants. Thus, CSN dysfunctions affect *PSI*-gene expressions.
423 To explore this further, we utilized the *csn5a-2* plants. Reduced cullin deneddylation in this
424 mutant, evident by the enhanced basal $CUL1^{Nedd8}$ levels, has been previously reported
425 (Gusmaroli et al., 2007), and also validated here (Supplementary Figure 1A). Further, we show
426 that CSN holo-complex isolated from *csn5a-2* plants has reduced deneddylase activity on
427 Nedd8-AML (Supplementary Figure 13A). Similar to *ipk1-1* or *itpk1-2*, the *csn5a-2* is also
428 auxin-insensitive (Dohmann et al., 2005; Dohmann et al., 2008; Gusmaroli et al., 2004; Laha
429 et al., 2022). The primary root length of *csn5a-2* plants grown on Pi-replete growth media is
430 slightly shorter than Col-0, a feature also displayed by the *ipk1-1* or *itpk1-2* plants
431 (Supplementary Figures 13B, C) (Riemer et al., 2021). However, endogenous Pi level in this
432 mutant is comparable to Col-0 with slight up-regulation noticed for *PHT1;8,* or *SPX1*
433 expression under Pi-replete conditions (Supplementary Figures 13D, E). $InsP_6$ and $InsP_7$ levels
434 were also comparable to Col-0, indicating that *csn5a-2* mutation does not affect global InsP
435 levels (Supplementary Figures 9A-C). Most interestingly, when Pi-starved, the strong
436 inhibition of primary root length observed for Col-0 was markedly lower in *csn5a-2* or *ipk1-1*
437 plants (Supplementary Figures 13B, C) and similar to *itpk1-2* plants as reported earlier (Riemer

438 et al., 2021). Also, similar to the InsP-kinase mutants, the *csn5a-2* plants were also completely
439 impaired in inducing several *PSI*-genes upon Pi-starvation (Supplementary Figures 13E, F).
440 These results indicated that optimal CSN5 functions are essential for transducing PSR.
441 We also examined the direct effect of CSN5i-3 on Pi-homeostasis and PSR. On Pi-replete Col-
442 0 plants, CSN5i-3 treatment did not dramatically affect *PSI*-gene expressions, implying that
443 inhibited CSN5 or aggravated $CUL1^{Nedd8}$ levels alone cannot trigger PSR (Supplementary
444 Figure 13G). Curiously, upon Pi-starvation, CSN5i-3 suppressed the induction of *PSI*-genes in
445 Col-0 and mirrored MLN4924 effects (Figure 4B), or responses of the *csn5a-2*, *ipk1-1* or *itpk1-*
446 *2* plants, under similar conditions (Supplementary Figure 13E-G). Overall, these results
447 highlight that unregulated dampening of CSN deneddylase activity negatively impacts the
448 induction of *PSI*-genes during PSR.

449 **SPX4 is a target of CRLs**

450 Neddylation of cullins activates CRLs, thereby promoting its assembly with the E2 ubiquitin-
451 conjugating enzyme (UBC) and initiating the ubiquitylation of substrate proteins (Cope et al.,
452 2002; Duda et al., 2008). The rice and Arabidopsis SPX4 proteins are known negative
453 regulators of PSR and undergo rapid turnover when the plants are Pi-deprived (Collins et al.,
454 2024; Lv et al., 2014; Osorio et al., 2019; Ruan et al., 2019). Whether SPX4 proteins are *bona*
455 *fide* targets of CRLs has not yet been directly demonstrated. Increased CUL^{Nedd8} levels
456 prompted us to first evaluate the abundance of global ubiquitin-conjugates in the InsP-kinase
457 mutants. Immunoblot with anti-ubiquitin antibodies detected higher than Col-0 levels of
458 polyubiquitin conjugates in *ipk1-1* and *itpk1-2* extracts but not in their respective
459 complemented lines (Figure 5A). These results suggested that the InsP-kinase mutants display
460 enhanced CRLs-dependent ubiquitylation activities. Interestingly, similar enhancements in the
461 global polyubiquitin conjugates are not apparent in the Pi-starved samples, although a modest
462 increase is detected in the Pi-resupplied extracts (Supplementary Figure 14A). Together, these
463 observations implied that, unlike misregulations that occur in the InsP-kinase mutants,
464 activation of PSR is associated with regulated CRL activities and downstream ubiquitylation
465 of substrates.

466 To elucidate whether the activated CRLs target SPX4 upon Pi-starvation, its levels were
467 evaluated in transgenic plants expressing *SPX4p:SPX4-LUC* (Osorio et al., 2019) grown under
468 Pi-replete and Pi-deplete conditions. SPX-LUC protein levels and LUC activity were lower in
469 Pi-deplete versus Pi-replete plants, in agreement with the degradation of SPX4 under Pi-starved

470 conditions, shown earlier (Figure 5B; Supplementary Figure 14B) (Osorio et al., 2019). Global
471 levels of poly-ubiquitylated SPX4 enriched from Pi-deplete plants were considerably higher in
472 Pi-replete than in Pi-deplete plants (Figure 5D). Further, Pi re-supplementation in the Pi-
473 deplete samples caused a noticeable reduction in the levels of poly-ubiquitylated SPX4.
474 Interestingly, treatment of MLN4924, or MG132, a 26S proteasome inhibitor, under Pi-deplete
475 conditions resulted in increased LUC activity and SPX4-LUC protein levels, similar to the Pi-
476 replete plants, indicating that CRL-dependent ubiquitylation indeed regulates SPX4 turnover
477 upon Pi-starvation (Figures 5B, C; Supplementary Figure 14B) (Osorio *et al.*, 2019). Most
478 remarkably, the presence of CSN5i-3 in the Pi-deplete medium also suppressed SPX4 turnover
479 and completely restored LUC activity or SPX4-LUC protein amounts to Pi-replete levels
480 (Figures 5B, C; Supplementary Figure 14B). *SPX4* transcript levels were mostly unaffected by
481 Pi-starvation in the presence of these inhibitors (Supplementary Figure 14C). Thus, as earlier,
482 irreversible inhibition of the deneddylation function by the endogenous CSN holo-complex
483 impairs the execution of downstream responses to Pi-starvation.
484 To test the fate of SPX4 in *ipk1-1*, we generated *SPX4p:SPX4-LUC/ipk1-1* plants by genetic
485 crossing. Likewise, *SPX4p:SPX4-LUC/ipk2β-1* plants were also generated. Imaging showed
486 that LUC activity was significantly reduced in *ipk1-1*, but not affected in *ipk2β-1* (Figure 5E).
487 Similarly, SPX4-LUC protein levels were lower in *ipk1-1*, but unaffected in the *ipk2β-1*
488 background, implying that IPK1, but not IPK2β, regulates the SPX4 turnover (Figure 5F).
489 Further, levels of poly-ubiquitylated SPX4 were higher in *ipk1-1* than in the control or *ipk2β-*
490 *1* plants (Supplementary Figure 14D). SPX4-LUC protein levels in the *csn5a-2* plants were
491 comparable to the wild-type plants (Supplementary Figure 13H). Transcript levels of *SPX4*
492 were unaffected in either of these mutant backgrounds (Supplementary Figure 14E).
493 Remarkably, SPX4-LUC protein levels and LUC activity in the *SPX4p:SPX4-LUC/ipk1-1*
494 plants were restored to near wild-type levels with either MLN4924 or MG132 treatments,
495 suggesting that enhanced $CUL1^{Nedd8}$ levels caused their heightened turnover in *ipk1-1* (Figure
496 5E, F). Taken together, our results revealed novel dynamics of CSN-CRL functions modulated
497 by IPK1 and ITPK1 activities in the regulation of plant Pi-homeostasis, steady-state levels of
498 SPX4, and its CRL-mediated turnover during adaptation to Pi-starvation.

499 **Discussion**

500 **Kinase activities of IPK1 and ITPK1 regulate their self and CUL1 associations with the**
501 **CSN holo-complex subunits**

502 In this study, we demonstrated that a strategic metabolic coupling of the two Arabidopsis InsP-
503 kinases IPK1 with ITPK1, and more specifically the enzymatic activity of the latter, modulates
504 the deneddylation efficiency of cullins by the CSN holo-complex (Figure 6). Engagements of
505 these two InsP-kinases with the CSN holo-complex are antagonistically affected by their kinase
506 activities. A kinase-deficient IPK1 ($IPK1^{K168A}$) binds weakly, whereas the kinase-deficient
507 ITPK1 ($ITPK1^{D288A}$) associates strongly with the CSN (Figures 1E, F; Supplementary Figures
508 2A, B, 4B). At the CSN platform, where the two InsP-kinase activities are functionally coupled,
509 IPK1 tethering to the holo-complex is promoted by its catalytic activity in generating $InsP_6$.
510 The increased $InsP_6$ levels at this platform relieve the enzymatic suppression of ITPK1, caused
511 either by allosteric interaction with the CSN2 subunit and/or the competitive propensity to bind
512 $InsP_6$ (Figure 3E). Synthesis of $InsP_7$ by ITPK1 (Adepoju et al., 2019; Laha et al., 2019; Riemer
513 et al., 2021; Whitfield et al., 2020) activates the deneddylation activity of the holo-complex,
514 leading to dissociation of this kinase, and likely IPK1, from the CSN platform (Figure 2F).
515 These mechanisms likely define the lack of significant cellular pools of either of the two InsP-
516 kinase enzymes in the CSN holo-complex fractions (Supplementary Figure 3A). The
517 mammalian IP5K and IP6K1 also behave similarly in terms of their kinase-defined associations
518 and dissociation, respectively, with the CSN holo-complex (Rao et al., 2014; Scherer et al.,
519 2016).

520 CUL1 association *per se* with the holo-complex, however, does not seem to require $InsP_6$ since
521 more CUL1 was retained with CSN in the *ipk1-1* plants (Figure 2A). This is contrastingly
522 different from the mammalian CUL4-CSN interactions, which are augmented by the $InsP_6$
523 metabolite (Scherer et al., 2016). It is noteworthy that null mutants of Arabidopsis IPK1 are
524 not viable and that the *ipk1-1* used here is an incomplete loss-of-function allele retaining
525 detectable amounts of $InsP_6$, although significantly lower than the wild-type levels (Gulabani
526 et al., 2022; Kuo et al., 2018; Laha et al., 2015; Laha et al., 2022; Land et al., 2021; Stevenson-
527 Paulik et al., 2005). Thus, either the residual concentrations of $InsP_6$ in *ipk1-1* suffice as a co-
528 factor for the CSN-CRL association, or these interactions in plants have evolved to be
529 independent of this metabolite. Alternatively, changes in other InsPs, such as $InsP_5$ 2-OH,
530 which is highly accumulated in *ipk1-1* plants (Gulabani et al., 2022; Stevenson-Paulik et al.,
531 2005), may also be a contributing factor. Further studies need to clarify whether additional
532 InsPs play a role in this process. Mammalian CUL4-CSN interactions *in vitro* are also

533 strengthened by $InsP_7$, although at a lower efficiency than $InsP_6$ (Scherer et al., 2016).
534 However, again considering that more CUL1 is also retained with CSN2 in *itpk1-2* (Figure
535 2A), which harbors physiological levels of $InsP_6$ but lower level of 5-$InsP_7$ (Laha et al., 2022;
536 Riemer et al., 2021), a role of this metabolite in promoting this tether is again unlikely. These
537 observations instead can be interpreted as deficiencies in CUL1 dissociation from the CSN
538 holo-complex due to lower $InsP_7$ or inactive ITPK1. The same metabolite is also low in *ipk1-*
539 *1* due to the low availability of $InsP_6$ substrate for ITPK1 (Kuo et al., 2018; Laha et al., 2022;
540 Riemer et al., 2021), thus favoring this interpretation. Indeed, 5-$InsP_7$ has been suggested to
541 introduce steric clashes in the interface pocket of the CRL-CSN complex, thereby affecting the
542 stability of this association (Lin et al., 2020). Consolidated, coordinated metabolic activities of
543 the two InsP-kinases affect CUL1 association dynamics with the CSN.

544 While displaying relatedness to the mammalian IP5K and IP6K1 activities (Rao et al., 2014;
545 Scherer et al., 2016), our results raise the question of how ITPK1, a major $InsP_6$-kinase in
546 plants, is evolutionarily endowed with a similar function in coordinating CRL and CSN
547 activities as the mammalian IP6K1, even though these proteins do not share any sequence or
548 structural homology. Perhaps equally surprising is that a mammalian ITPK1 homolog has been
549 reported to engage with the CSN holo-complex (Sun et al., 2002). While it has been shown that
550 mammalian ITPK1 also executes $InsP_6$-kinase activity *in vitro* (Laha et al., 2019), it remains
551 to be determined, whether this homolog has a physiological role *in vivo* as an IP_6-kinase (IP6K)
552 and/or in CRL-CSN activities.

553 **CSN5 deneddylase activity auto-regulates the functional equilibrium of the holo-complex**

554 Previous studies have shown that the CSN holo-complex is structurally intact but functionally
555 inert without CSN5 presence (Lingaraju et al., 2014). The dynamics of holo-complex-
556 associated and free monomeric forms of CSN5 hence play a vital rate-limiting role in
557 maintaining deneddylation homeostasis and basal levels of active CRLs (Wu et al., 2006). Our
558 data here is the first to identify a correlation between the deneddylation activity of holo-
559 complex with the dissociation equilibrium of the catalyzing enzyme CSN5, and of CUL1, and
560 the two InsP-kinase, with/from the CSN platform. Deneddylation defects in the InsP-kinase
561 mutants, or due to CSN5i-3 treatments, ameliorate their dissociation, retaining increased
562 amounts of these proteins with the holo-complex (Figures 2A, B, D, E). An *in vitro*
563 reconstituted holo-complex containing a deneddylation-deficient $CSN5^{H138A}$ protein was
564 shown to bind neddylated CRLs with higher affinity (Lingaraju et al., 2014). Our findings here

565 reveal a key auto-regulatory mechanism that maintains an equilibrium of deneddylation activity
566 of the plant CSN holo-complex. Holo-complex-free lower sub-complexes of CSN4/5 are
567 known to occur in diverse organisms, including in plants, although their individual roles remain
568 mostly unexplored (Dohmann et al., 2005; Fukumoto et al., 2005; Oron et al., 2002). In
569 mammalian cell lines, CSN5 sub-complexes function as a cargo carrier modulating the
570 nucleocytoplasmic export and subsequent CSN-CRL mediated turnover of the tumor
571 suppressor p53, or the cyclin-dependent kinase inhibitor p27 in the cytoplasm (Oh et al., 2006;
572 Tomoda et al., 2002). Whether, in plants, such CSN5 sub-complexes facilitate similar export
573 of substrates to their subsequent fates upon a stimulus awaits further studies.

574 **$InsP_6$ potentiation on CSN deneddylation activity requires kinase-active ITPK1**

575 The catalytic activity-dependent association of IPK1 with the CSN subunits empirically
576 correlates with the $InsP_6$-dependent enhancement of CSN deneddylase activity, which we
577 observed in our assays (Figure 3B). Similar potentiation by $InsP_6$ is also seen for the
578 mammalian CSN holo-complex (Lin et al., 2020; Scherer et al., 2016). Structural studies show
579 that holo-complex integrated CSN5 interfaces with CSN4-CSN6 subunits that, in turn, inhibit
580 its deneddylase function in the absence of a bound CRL (Enchev et al., 2012; Lingaraju et al.,
581 2014). Upon binding a neddylated CRL, a series of conformational changes prompted by CSN4
582 orients the CSN5 catalytic site towards the neddylated cullins. Conserved neighboring lysines
583 in CSN2 α-helices, proximal to the CSN5 catalytic pocket, coordinate $InsP_6$ to bridge and
584 stabilize these CRL associations likely for subsequent deneddylation of cullins (Lin et al.,
585 2020). Arabidopsis CSN2 harbors most of these conserved lysines (Supplementary Figure
586 10B). Therefore, compromised $InsP_6$ synthesis in *ipk1-1* plants agrees with the reduced
587 deneddylation rates by the CSN holo-complex (Figure 3B). However, lower $InsP_6$ availability
588 would also antagonize the catalytic activity of ITPK1, thereby reducing $InsP_7$ synthesis. Our
589 observation that *itpk1-2* plants, which are deficient in $InsP_7$ synthesis but have wild-type levels
590 of $InsP_6$, exhibit deneddylation defects similar to those in *ipk1-1* plants (Figure 3C) strongly
591 suggests that $InsP_7$ is the primary potentiator of the holo-complex's deneddylation activity. Our
592 data demonstrating that exogenously supplemented $InsP_6$ recovers deneddylation defects of
593 *ipk1-1* but not *itpk1-2* or *GFP-ITPK1*^{D288A}*/itpk1-2* supports this interpretation (Figure 3D). The
594 steric clashes that an $InsP_7$ molecule is predicted to impose at the CRL-CSN juncture may
595 provide the stimulus to potentiate deneddylation on the bound cullin. This, in turn, would
596 destabilize the complex, causing the dissociation of CUL1, CSN5, and the InsP-kinases from
597 the CSN holo-complex, reverting back to its inert state. We acknowledge that conclusive results

598 can only be obtained from direct tests of $InsP_7$ effects in potentiating the deneddylation
599 efficiency of CSN holo-complex and in the recovery of deneddylation defects of *itpk1-2* and
600 perhaps *ipk1-1* plants. However, the limited availability of pure $InsP_7$ prevents us from
601 performing these assays.

602 **Pi-starvation suppresses CSN deneddylation efficiency and targets SPX4 via CRLs**

603 A previous study has demonstrated the proteasome-dependent turnover of SPX4 in Pi-deplete
604 samples (Osorio et al., 2019). However, CSN-CRL activities have not been directly implicated
605 in this turnover or in the downstream response to Pi-starvation. Here, we show that
606 pharmacological inhibition of neddylation with MLN4924 suppresses SPX4 degradation
607 during PSR (Figures 5B, C). The lower SPX4 stability in *ipk1-1* plants is also restored to wild-
608 type levels with MLN4924 or MG132 treatments (Figures 5E, F). Furthermore, MLN4924
609 suppresses the constitutive PSR and elevated Pi-levels in the two InsP-kinase mutants (Figure
610 4A; and Supplementary Fig. 11A). In wild-type plants, this inhibitor also dampened the
611 upregulation of *PSI*-gene expression under Pi-deplete conditions (Figure 4B). These data,
612 combined with the observation of elevated $CUL1^{Nedd8}$ levels in extracts of Pi-deficient plants,
613 which are abolished by MLN4924 or restored to basal levels upon Pi resupply (Figure 4C, D),
614 strongly support the idea that CRL activities play a key role in the elicitation of PSR.

615 Similarly, the very critical modulatory role of CSN deneddylase functions in the transduction
616 of PSR via CRL activities is also emphasized in our data. We show that Pi starvation is
617 associated with reduced deneddylation rates and higher holo-complex associated pools of
618 CSN5, which overall mirror the patterns from the two InsP-kinase mutants (Figures 2B; 4E-G;
619 Supplementary Figure 11C). Reduced cellular levels of $InsP_7$, which occur under Pi-deplete
620 conditions (Riemer et al., 2021), also strongly parallel the two InsP-kinase mutants and can be
621 attributed to the observed consequences. Furthermore, the increased CRL activities resulting
622 from their heightened neddylated status likely orchestrate PSR processes, such as SPX4
623 turnover, as shown in our data.

624 Most importantly, our study reveals that the physiological response to Pi-starvation involves
625 more complex cellular adaptations, which can be only partially ascribed to functional changes
626 of the two InsP-kinases and the deneddylation activity of CSN holo-complex. This is best
627 evident in the observations that the two InsP-kinase mutants and the *csn5a-2* plants remain
628 recalcitrant to primary root growth inhibition under Pi-deplete conditions (Supplementary
629 Figures 13B, C). Additionally, these mutants and the CSN5i-3-treated plants are inefficient in

630 inducing *PSI*-gene expressions under low Pi (Supplementary Figures 13E-G). Additionally,
631 basal expression levels of *PSI*-genes are not altered either in *csn5a-2* or upon CSN5i-3
632 treatment on Col-0 (Supplementary Figures 13E, G). Further, global ubiquitination levels are
633 not enhanced in Pi-deplete extracts, unlike those observed in the InsP-kinase mutants (Figure
634 5A; Supplementary Figure 14A). These results advocate that the constitutive inhibition of
635 CSN5 or of the InsP-kinase activities is detrimental to the successful transduction of PSR.
636 Indeed, under low Pi conditions, ITPK1 was shown to switch its kinase role to an ADP-
637 phosphotransferase that converts $InsP_7$ back to $InsP_6$ (Riemer et al., 2021; Whitfield et al.,
638 2020). Further investigations are needed to explore the detailed activities of the InsP-kinases
639 and CSN holo-complex under stressed conditions. In conclusion, our studies here highlight the
640 remarkable coordination of plant IPK1 and ITPK1 roles in regulating CRL-CSN functions and
641 their further implications in responding to Pi-imbalances.

642 **Materials and Methods**

643 **Plant material and growth conditions.** Details of *Arabidopsis thaliana* (ecotype Col-0) T-
644 DNA insertion lines *ipk1-1, itpk1-2, ipk2β-1*, *itpk4-1*, *csn5a-2*, *vih2-4, ITPK1-GFP/itpk1-2,*
645 and *Myc-IPK1/ipk1-1* have been described earlier (Gulabani et al., 2022; Jia et al., 2015; Kuo
646 et al., 2014; Kuo et al., 2018; Laha et al., 2015; Laha et al., 2022; Riemer et al., 2021). T-DNA
647 and respective gene-specific primers used for genotyping are listed in Table S1. Seeds were
648 stratified for 2 days at 4°C in the dark and then sterilized using a 30% bleach solution. They
649 were germinated either directly on soil or on ½ strength Murashige and Skoog (MS) Pi-replete
650 (625 µM KH_2PO_4) agar plates in growth chambers maintained at 22°C with 70% Relative
651 humidity (RH) and 16 hrs: 8 hrs; light: dark having light intensity 100 µmol $\mu m^{-2}s^{-1}$. For
652 fractionation, Pi-starvation assays, and inhibitor treatments, plants grown on media plates as
653 above were transferred 7 days post-germination to liquid ½ MS medium in 12-well sterile
654 culture plates and proceeded accordingly as indicated in respective experiments. For
655 immunoprecipitation assays, either 4-week-old soil-grown plants or plants subjected to Pi-
656 changes with or without inhibitors for the indicated time period were used.

657 **Generation of constructs.** Arabidopsis *IPK1*, *ITPK1*, *CSN1*, *CSN2* and *CSN5* cDNAs were
658 amplified via RT-PCR (iScript cDNA Synthesis Kit, Bio-Rad, USA) from total RNA isolated
659 from 2-week-old Col-0 plants using RNAiso (Takara-Bio, Japan). Primers for these are listed
660 in Supplementary Table 1. Gateway cloning was first performed into *p*DONR207 and then into
661 *p*BA-Myc (for Myc-IPK1), *p*BA-HA (for HA-CSN2) (Bhattacharjee et al., 2011), *p*SITE-2CA

662 (Chakrabarty et al., 2007) (for GFP-ITPK1), nVenus- or cCFP binary vectors (Bhattacharjee
663 et al., 2011) using BP and LR Clonase, respectively (Invitrogen, USA). BiFC vectors for GUS
664 expression have been described earlier (Bhattacharjee et al., 2011).

665 For generating wild-type and kinase-deficient constructs of the InsP-kinases ($IPK1^{K168A}$ and
666 $ITPK1^{D288A}$), and $InsP_6$ binding-deficient clone of CSN2 ($CSN2^{K3A}$), overlapping PCR with
667 indicated primers using the respective wild-type clones in *p*DONR207 were performed. The
668 confirmed $IPK1^{K168A}$ and $ITPK1^{D288A}$ plasmids were sub-cloned into *p*MDC43 (GFP-
669 containing binary vector (Curtis and Grossniklaus, 2003) using the LR Clonase to generate
670 GFP-$IPK1^{K168A}$ or GFP-$ITPK1^{D288A}$, respectively. The above binary vector clones were
671 electroporated into the agrobacterium strain GV3101 for further *in planta* expression assays.

672 For generating clones for expression and purification of recombinant proteins (His-GFP, His-
673 rCSN2, His-$rCSN2^{K3A}$, His-rIPK1, or His-rITPK1), the constructs were generated via Clonase
674 LR reaction with corresponding *p*DONR207 vectors and *p*DEST17 (Thermo Fisher Scientific,
675 USA). BL21 (DE3) cells were transformed with the confirmed vectors (or clones), induced,
676 and respective proteins purified using Ni^{2+} affinity resin and size exclusion chromatography.
677 Approximately, 5 µg of indicated proteins were used for enrichment assays.

678 **Generation of transgenic lines.** For generating wild-type and kinase-deficient IPK1 or ITPK1
679 expressing transgenic plants, *ipk1-1* or *itpk1-2* plants, as appropriate, were floral-dipped with
680 the respective agrobacterium strains (Clough and Bent, 1998). Multiple independent T1
681 transgenic plants were selected on hygromycin (20 µg/ml) containing ½ MS agar plates,
682 propagated to homozygosity, and then used for indicated assays.

683 *SPX4p:SPX4-LUC/ipk1-1, SPX4p:SPX4-LUC/ipk2β-1,* or *SPX4p:SPX4-LUC/csn5a-2* plants
684 were generated by crosses between the respective parents. F2 and F3 segregating populations
685 were screened by genotyping PCR to identify the appropriate lines. The primers used are
686 according to previous reports (Dohmann et al., 2005; Gulabani et al., 2022; Osorio et al., 2019)
687 and are also listed in Supplementary Table 1.

688 **Yeast two-hybrid assays.** The indicated constructs were first generated via Gateway cloning
689 into destination *p*BK-RC (bait) and *p*GAD-RC (prey) plasmids (Ito et al., 2000), respectively.
690 The investigated bait and prey combinations were then used to co-transform yeast strain
691 MaV203 using the commercial Yeast Transformation Kit (Sigma-Aldrich, USA), and
692 transformants were selected on SD/LT- media plates. Five independent transformants for each

693 combination were resuspended separately in 100 µl of sterile water, adjusted to similar density,
694 and their serial dilutions were spotted on SD/LT- and SD/HLT- containing 15 mM 3-AT (3-
695 Amino-1,2,4-triazole) plates. The growth of the yeast cells was noted and imaged after 3-days
696 post-incubation. Qualitative X-Gal (5-bromo-4-chloro-3-in-dolyl-β-d-galactoside) and
697 quantitative ONPG (O-nitrophenyl β-d-galactopyranoside) cleavage assays were performed as
698 described earlier (Mockli and Auerbach, 2004). Briefly for X-gal assays, transformants grown
699 in liquid SD/LT- media till 0.8-1 OD_{600nm} were pelleted and permeabilized by three repeats of
700 freeze-thaw cycles of 3 mins each with liquid N_2 and incubation in a 37ºC water bath. The
701 pellet was then resuspended in 20 µl of water and added to 96 well plates containing 100 µl of
702 1X PBS 7.4 pH with 500 µg/ml of X-Gal (Sigma-Aldrich, USA), 0.5% Agarose (w/v), 0.05%
703 (v/v) β-mercaptoethanol and incubated at 30ºC. Images were acquired at 12 hours post-
704 incubation. For quantitative ONPG assays, transformants harvested as earlier were resuspended
705 in Breaking Buffer (100 mM Tris-HCl pH 8.0, 4% Glycerol, 1 mM β-Mercaptoethanol, 1X
706 Protease inhibitor cocktail; G-biosciences, USA) and an equal volume of acid-washed beads
707 (Sigma-Aldrich, USA). The suspension was lysed via vortexing (3 cycles of 2 min vortex
708 followed by 1 min rest) and then pelleted by centrifugation at 15000 rpm for 15 mins at 4ºC.
709 To a 96-well plate with each well containing 140 µl Z buffer (60 mM Na_2PO_4, 40 mM KH_2PO_4,
710 10 mM KCl, 1 mM $MgSO_4$), 20 µl of the supernatant was added. The reaction was started by
711 adding 40 µl of ONPG (4 mg/ml stock; Sigma-Aldrich, USA) to each well, and the plate was
712 incubated at 30ºC. After 4 hours post-incubation, the reaction was stopped by adding 100 µl of
713 1 M Na_2CO_3 to each reaction well, and absorbance was measured at 420 nm. The total protein
714 content in each lysate was determined by the Bradford method. Miller Unit was calculated
715 using the standard formula (Miller Units = (Abs_{420nm}/ ml of cell lysate) * (1000) / (mg of total
716 protein/ ml of lysate) * (reaction time in minutes).

717 **Phosphate-starvation/re-supplementation assays.** After germination of seeds as described
718 earlier, seedlings were transferred to liquid ½ MS medium in 12-well sterile culture plates with
719 Pi-replete conditions (625 µM KH_2PO_4) and placed in the growth chamber. At 4 days post-
720 transfer, the plants were either maintained with Pi-replete or transferred to Pi-deplete (10 µM
721 KH_2PO_4) liquid media and continued for another 6 days (total of 17 days post-germination)
722 before being used for Pi-estimation, qRT-PCR, total protein extraction, fractionation, or
723 immuno-precipitation assays. For Pi-resupply, plants in Pi-deplete medium were transferred to
724 Pi-replete medium for 24 hrs before analysis.

725 **Pull down assay/Immunoprecipitation assays.** For co-immunoprecipitation assays between
726 Myc-IPK1 and GFP-ITPK1, agro-infiltrated *N. benthamiana* leaves harvested at 48 hpi were
727 used. For pull-downs, including from Arabidopsis transgenic lines *Myc-IPK1/ipk1-1*, *ITPK1-*
728 *GFP/itpk1-2*, or *35S:GFP* plants, extracts were homogenized in cold RIPA buffer [5 mM Tris-
729 HCl pH 7.5, 150 mM NaCl, 10 mM $MgCl_2$, 1 mM EDTA, 1% NP-40, 1 mM Sodium
730 deoxycholate and 1X protease inhibitor cocktail (Sigma-Aldrich, USA)]. After removing cell
731 debris via centrifugation, the supernatant was pre-cleared with IgG agarose beads (Sigma-
732 Aldrich, USA) at 4°C for 1 hr with rotation. The mix was then centrifuged, IgG agarose bead-
733 pellet washed and saved as non-specific controls. The supernatant was added to indicated
734 antibody-conjugated beads (anti-GFP Agarose, BioBharati Life Sciences, India; anti-Myc
735 Agarose, Sigma-Aldrich, USA). After tumbling overnight at 4°C, the mix was centrifuged, and
736 agarose-bead pellet washed 3-times with RIPA buffer. Beads were then resuspended in 1X
737 Laemmli loading dye and used for immunoblots.

738 **Protein extraction and immunoblots.** Total protein extracts from plants were prepared in 6
739 M urea and used for western blots. For immuno-detection, anti-GFP, anti-Myc (BioBharati
740 Life Sciences, India), anti-CSN1, anti-CSN2, anti-CSN4, anti-CSN5, anti-CUL1 antibodies
741 (ENZO Life Sciences, USA; AS23 4927 Agrisera, Sweden), anti-ACT1 (Abiocode, USA), or
742 anti-LUC (Santa Cruz Biotechnology, USA), as indicated were used. The blots were developed
743 using an ECL kit (Bio-Rad, USA) and imaged in the Alpha Image Quant system (GE-
744 Healthcare, USA).

745 **Bimolecular Fluorescence Complementation (BiFC) assays.** Agrobacterium strains
746 containing the indicated combination of binary vectors were co-infiltrated at equal cell
747 densities into mature *N. benthamiana* leaves. At 48 hpi (hrs post-infiltration), tissue sections
748 from the infiltrated patches were viewed under an SP8 confocal microscope (Leica-
749 microsystems, Germany). Images were acquired with both bright field and YFP filters.

750 **Size-exclusion chromatography of plant extracts.** Gel-filtration protocol was according to
751 (Huang et al., 2013). Briefly, 14-day-old plants ground to a fine powder with liquid nitrogen
752 were homogenized in Gel filtration buffer (50 mM Tris-HCl pH 7.5, 150 mM NaCl, 1 mM
753 EDTA, 10% Glycerol, 10 mM $MgCl_2$, 1 mM DTT, 1 mM PMSF and 1X Protease inhibitor
754 cocktail). Homogenates were centrifuged for 10 mins at 4°C, and supernatant passed through
755 0.2 μM syringe filters. Total protein extracts were fractionated through Superdex 10/300 GL
756 Column (GE- Healthcare, USA) and eluted in the fractionation buffer at 0.2 mL/min flow rate.

757 The eluents were TCA (Trichloroacetic acid) precipitated, washed with acetone, and
758 resuspended in 1X Laemmli loading dye and used for indicated immunoblots.

759 ***In lysate* deneddylation assay.** *In lysate* deneddylayion assay was performed according to Lin
760 et al., (2020). Briefly, 14-day-old seedlings were quickly homogenized in deneddylayion buffer
761 (10 mM Tris-HCl pH7.5, 150 mM NaCl and 0.5% NP-40) in the absence of protease inhibitors.
762 The extracts were incubated at 37°C for indicated times, the reaction stopped by adding
763 Laemmli loading dye to 1X, and then used for immunoblots.

764 ***In vitro* deneddylation assays.** CSN holo-complex was collected by pooling the HMW
765 fractions (#9-12) from the indicated plant extracts via size exclusion chromatography, as earlier
766 (the gel filtration buffer lacked EDTA and protease inhibitors to maintain CSN activity). Total
767 protein was concentrated using Amicon ultracentrifuge filters (Merck Millipore, USA). Nedd8-
768 AML was obtained from Novus Biologicals (USA), and stocks were made in 50 mM HEPES
769 pH 7.5, 100 mM NaCl. For each reaction, ~15-30 μg protein from the CSN holo-complex pools
770 were used with 1 μM Nedd8-AML in a total reaction volume of 20 μL in Buffer A (20 mM
771 Tris-HCl pH 7.6, 8 mM EDTA, 2 mM ATP). The reaction tube was incubated in the dark at
772 37^{0}C for 30 mins. The entire reaction volume was then transferred to a 96-well luminometer
773 plate, and 80 μL of Assay Buffer B (20 mM Tris-HCl pH 7.6, 8 mM $MgSO_4$, and freshly added
774 2 mM ATP, 6 mg/ml BSA, 33 mM DTT) containing 10 ng of QuantiLum recombinant
775 Luciferase (Promega, USA) was added. For testing effects on deneddylation efficiencies,
776 indicated amounts of $InsP_6$ (Sigma-Aldrich, USA), rUCHL3, or CSN5i-3 (10 μM) were added
777 to the reaction prior to the incubation step. Luminescence was measured in a GloMax
778 Luminometer (Promega, USA) and represented as RLU (Relative Luminescence Unit).

779 **qRT-PCR analysis.** cDNAs prepared as earlier, were used for qRT-PCRs with HOT FIREPol
780 EvaGreen qPCR Mix Plus (ROX) (Solis BioDyne, USA) and primer combinations according
781 to the manufacturer's instructions. Primers used are listed in Supplementary Table 1. The
782 reaction was performed on QuantStudio 6 Flex Real-Time PCR system (Applied Biosystems,
783 USA) with three biological and technical replicates. *MON1* (*At2g28390*) expressions were used
784 as internal control (Gulabani et al., 2022; Kim et al., 2010). Relative expression was calculated
785 according to the PCR efficiency^-ΔΔCt formula.

786 **Pi-estimation assay.** Total Pi measurements are according to (Chiou et al., 2006). In brief,
787 fresh tissue was frozen with liquid nitrogen and homogenized in extraction buffer (10 mM Tris-

788 HCl, 1 mM EDTA, 100 mM NaCl, 1 mM PMSF). The homogenized sample was mixed in a
789 ratio of 1:9 with 1% glacial acetic acid and incubated at 42ºC for 30 mins. Then, the reaction
790 was mixed in a ratio of 3:7 with Pi-assay solution (0.35% NH_4MoO_4, 0.86 N H_2SO_4 and 1.4%
791 ascorbic acid) and incubated at 42ºC for 30 mins. Pi content was measured at $A820_{nm}$ using a
792 spectrophotometer. The standard graph was made with known amounts of KH_2PO_4.

793 **Luciferase imaging and quantification.** Bioluminescence assays for Luciferase expression
794 and quantification of Luciferase activity (Luciferase assay system, Promega, USA) in the
795 indicated plants were performed according to Osorio et al., (2019). Imaging of LUC expression
796 was done with the Bio-Rad ChemiDoc system (Bio-Rad, USA). Serial dilution of QuantiLum
797 Recombinant Luciferase (Promega, USA) was used to generate the standard graph and values
798 from plant samples presented as fmol/mg total protein.

799 **Inhibitor treatments.** Stock solutions of MLN4924 (Cayman Chemicals, USA), CSN5i-3
800 (Novartis Inc, Switzerland), and MG132 (Cayman Chemicals, USA) were prepared in DMSO.
801 For treatments,10 µM final concentration of MLN4924 or CSN5i-3 was used. MG132 was
802 used at 50 µM final concentration. For assays on Col-0, *ipk1-1*, or *itpk1-2*, inhibitor treatments
803 were performed 24 hrs prior to analysis. For effects on PSR, inhibitors were added 24 hrs prior
804 to harvesting the samples for analysis.

805 ***In vitro* ITPK1 kinase, inhibition and recovery assays.**

806 The $InsP_6$ kinase assay was performed according to the previously published protocol (Riemer
807 et al., 2021) Briefly, 5 µM of purified recombinant ITPK1 (rITPK1) or its kinase-deficient
808 version ($rITPK1^{D288A}$) was used in a reaction buffer containing 5 mM of $MgCl_2$, 20 mM of
809 HEPES (pH 7.5), 1 mM of DTT, 12.5 mM ATP, 1 mM of IP_6 (Calbiochem, USA), 5 mM of
810 phosphocreatine, and 1 unit creatine kinase. After incubation at room temperature for 6 hrs the
811 reaction separated by 33% PAGE and visualized by staining with toluidine blue. To test CSN2
812 or $CSN2^{K3A}$ ($InsP_6$ binding-deficient version) effects on $InsP_7$ synthesis, 2 µM of the respective
813 purified recombinant protein (His-rCSN2 or His-$rCSN2^{K3A}$) was added to the $InsP_6$ kinase
814 reaction, incubated as above, and analyzed accordingly. Similarly, to test IPK1 effects on
815 CSN2-mediation inhibition on $InsP_6$ kinase activity, 2 µM of recombinant IPK1 (His-rIPK1)
816 was added to the reaction and analyzed as earlier.

817 **Inositol phosphate extraction and CE-ESI-MS analyses**

818 Inositol phosphate extraction from plant tissues was performed as described previously
819 (Pullagurla et al., 2024; Wilson et al., 2015). In short, 12 mg of TiO_2 beads (GL Sciences Inc.,
820 USA) were weighed for each sample and prepared by washing once with ultrapure water and
821 twice with ice-cold 1 M perchloric acid (PA). Using a pestle, the plant tissues were
822 homogenized in ice-cold PA and incubated on ice for 10 minutes, then centrifuged at 18,000 ×
823 g for 10 minutes at 4 °C. The collected supernatants were transferred into new 1.5 mL tubes,
824 and the centrifugation step was repeated for another 10 minutes at 20,000 × g at 4 °C. The
825 supernatants were then mixed with the pre-washed TiO_2 beads and incubated for 30 to 60
826 minutes at 4 °C on a rotor. After incubation, the TiO_2 beads in the supernatant were pelleted
827 by centrifugation at 6,000 × g for 1 minute at 4 °C. The pelleted TiO_2 beads were washed twice
828 with 500 µL of ice-cold PA (1 M). Next, to elute the inositol phosphates, the beads were
829 resuspended in 200 µL of freshly prepared 10% ammonium hydroxide and incubated on
830 rotation for 5 minutes at room temperature. After centrifugation, the supernatants were
831 transferred into 1.5 mL tubes, and the elution was repeated. The eluted samples were
832 lyophilized using a speed-vac. CE–ESI–MS analyses of the plant extracts were performed as
833 previously detailed (Chalak et al., 2024; Qiu et al., 2023).

834 **Global and SPX4-LUC ubiquitination assays.** For determining global polyubiquitination
835 levels, extracts from indicated plants prepared in Gel filtration buffer in the presence of 50 µM
836 proteasome inhibitor MG132 were incubated on ice for 2 hrs. Immunoblotting was then
837 performed with anti-ubiquitin antibodies (P4D1; SantaCruz Biotechnology, USA). For
838 investigating SPX4-LUC ubiquitination, total protein extracts from Pi-replete, Pi-deplete, or
839 Pi-resupply samples were homogenized in Immunoprecipitation (IP) buffer (25 mM Tris-HCl,
840 7.5 pH; 150 mM NaCl; 0.5% Sodium deoxycholate; 1% Triton X-100; 0.1% NP-40; 40 µM
841 MG-132; 20 mM Iodoacetamide; 10 mM N-ethylmaleimide; 5 µM PR-619 (Cayman
842 Chemicals, USA); 1 mM PMSF; 2X plant protease arrest). The homogenates were centrifuged
843 at 11000 g at 4°C for 5 mins to remove cell debris. To the supernatant, anti-luciferase antibodies
844 conjugated to protein A^{PLUS} beads (BioBharati Life Sciences, India) were added and kept for
845 binding at 4°C with constant rotation for 5 hrs. The samples were then centrifuged at 2000 rpm
846 for 5 minutes at 4°C to pellet the beads. The supernatant was discarded, and the beads were
847 washed three times with IP buffer (without inhibitors). After the third wash, the beads were
848 resuspended in 2X Laemmli loading dye and used for immunoblots.

849 **Densitometric analysis.** The densitometric analysis of the protein bands was performed using
850 the ImageJ Software (NIH, USA). The values presented are normalized to the indicated
851 controls.

852 **Statistical analysis.** All data presented here are representative of at least three biological and
853 technical replicates for each. Statistical analysis details are mentioned in the respective figure
854 legends.

855 **Funding**

856 This work was supported by financial support from Regional Centre for Biotechnology (RCB)
857 core funds and Grants (No. BT/PR45561/AGIII/103/103/2023 and EMR/2016/001899) to SB
858 and SB, Young Investigator award and DBT-RA fellowship (DBT-RA/2021/January/N/218)
859 to YW, and SERB N-PDF award (No. PDF/2023/001938) to BCS. DL acknowledges the
860 Indian Institute of Science for start-up funds and Infosys Young Investigator award (IISc). G.S.
861 acknowledges funding from the Deutsche Forschungsgemeinschaft under Germany's
862 Excellence Strategy – EXC 2070 – 390732324 (PhenoRob) and grant SCHA 1274/5-1.

863 **Author Contributions**

864 SB, YW, MN and SB conceived and designed the research. SB generated all transgenic lines
865 used here. SB and YW generated all constructs and performed most experiments unless
866 otherwise indicated. IB performed the Y2H assays. MN performed all PAGE assays. SB, YW,
867 and MN performed SPX4-LUC experiments. YW, MN, and SD purified recombinant proteins
868 used here. BCS contributed to several size exclusion assays reported here. SB, YW, and MK
869 performed qRT-PCR assays on InsP-mutants upon Pi-changes. InsP extraction and
870 measurements were done by NJP, DL and HJ. SB, DL and GS analyzed the data. SB wrote the
871 manuscript with inputs from all authors.

872 **Acknowledgements**

873 We thank Dr. Ricarda Jost, La Trobe Institute for Agriculture and Food, Australia, for
874 *SPX4p:SPX4-LUC* seeds, Dr. Tushar Maiti, RCB, for rUCHL3, Dr. Eva Altmann, Novartis
875 Institutes for BioMedical Research, Switzerland for sharing CSN5i-3, Swaroop Peddiraju and
876 Dr. Divya Chandran, RCB for help with transcriptomic data analysis of *csn* mutants, Abhisha
877 Roy for specific SPX4-LUC assays, and Dr. Nripendra Singh and his team at Advanced
878 Technology Platform Centre (ATPC), Faridabad, India for constant support with sample

fractionations, and Marília Kamleitner, Department of Plant Nutrition, Institute of Crop Science and Resource Conservation, University of Bonn, for critically reading this manuscript. The authors declare no conflict of interest in this study.

References

Adepoju, O., Williams, S.P., Craige, B., Cridland, C.A., Sharpe, A.K., Brown, A.M., Land, E., Perera, I.Y., Mena, D., Sobrado, P., et al. (2019). Inositol Trisphosphate Kinase and Diphosphoinositol Pentakisphosphate Kinase Enzymes Constitute the Inositol Pyrophosphate Synthesis Pathway in Plants. bioRxiv:724914. 10.1101/724914.

Alcazar-Roman, A.R., Bolger, T.A., and Wente, S.R. (2010). Control of mRNA export and translation termination by inositol hexakisphosphate requires specific interaction with Gle1. J Biol Chem **285**:16683-16692. 10.1074/jbc.M109.082370.

Bhattacharjee, S., Halane, M.K., Kim, S.H., and Gassmann, W. (2011). Pathogen effectors target Arabidopsis EDS1 and alter its interactions with immune regulators. Science **334**:1405-1408. 10.1126/science.1211592.

Bustos, R., Castrillo, G., Linhares, F., Puga, M.I., Rubio, V., Pérez-Pérez, J., Solano, R., Leyva, A., and Paz-Ares, J. (2010). A Central Regulatory System Largely Controls Transcriptional Activation and Repression Responses to Phosphate Starvation in Arabidopsis. PLOS Genetics **6**:e1001102. 10.1371/journal.pgen.1001102.

Chakrabarty, R., Banerjee, R., Chung, S.M., Farman, M., Citovsky, V., Hogenhout, S.A., Tzfira, T., and Goodin, M. (2007). PSITE vectors for stable integration or transient expression of autofluorescent protein fusions in plants: probing *Nicotiana benthamiana*-virus interactions. Mol Plant Microbe Interact **20**:740-750. 10.1094/MPMI-20-7-0740.

Chalak, K., Yadav, R., Liu, G., Rana, P., Jessen, H.J., and Laha, D. (2024). Functional Conservation of the DDP1-type Inositol Pyrophosphate Phosphohydrolases in Land Plant. Biochemistry 10.1021/acs.biochem.4c00458.

Chamovitz, D.A., and Segal, D. (2001). JAB1/CSN5 and the COP9 signalosome. EMBO reports **2**:96-101. https://doi.org/10.1093/embo-reports/kve028.

Chiou, T.-J., Aung, K., Lin, S.-I., Wu, C.-C., Chiang, S.-F., and Su, C.-l. (2006). Regulation of Phosphate Homeostasis by MicroRNA in Arabidopsis. The Plant Cell **18**:412-421. 10.1105/tpc.105.038943.

Christmann, M., Schmaler, T., Gordon, C., Huang, X., Bayram, Ö., Schinke, J., Stumpf, S., Dubiel, W., and Braus, G.H. (2013). Control of Multicellular Development by the Physically Interacting Deneddylases DEN1/DenA and COP9 Signalosome. PLOS Genetics **9**:e1003275. 10.1371/journal.pgen.1003275.

Clough, S.J., and Bent, A.F. (1998). Floral dip: a simplified method for Agrobacterium-mediated transformation of *Arabidopsis thaliana*. Plant J **16**:735-743. 10.1046/j.1365-313x.1998.00343.x.

Collins, E., Shou, H., Mao, C., Whelan, J., and Jost, R. (2024). Dynamic interactions between SPX proteins, the ubiquitination machinery, and signalling molecules for stress adaptation at a whole-plant level. Biochem J **481**:363-385. 10.1042/BCJ20230163.

Cope, G.A., Suh, G.S., Aravind, L., Schwarz, S.E., Zipursky, S.L., Koonin, E.V., and Deshaies, R.J. (2002). Role of predicted metalloprotease motif of Jab1/Csn5 in cleavage of Nedd8 from Cul1. Science **298**:608-611. 10.1126/science.1075901.

Cridland, C., and Gillaspy, G. (2020). Inositol Pyrophosphate Pathways and Mechanisms: What Can We Learn from Plants? Molecules **25**10.3390/molecules25122789.

Curtis, M.D., and Grossniklaus, U. (2003). A gateway cloning vector set for high-throughput functional analysis of genes in planta. Plant Physiol **133**:462-469. 10.1104/pp.103.027979.

Desai, M., Rangarajan, P., Donahue, J.L., Williams, S.P., Land, E.S., Mandal, M.K., Phillippy, B.Q., Perera, I.Y., Raboy, V., and Gillaspy, G.E. (2014). Two inositol hexakisphosphate kinases drive inositol pyrophosphate synthesis in plants. Plant J **80**:642-653. 10.1111/tpj.12669.

927 **Dohmann, E.M., Kuhnle, C., and Schwechheimer, C.** (2005). Loss of the CONSTITUTIVE
928 PHOTOMORPHOGENIC9 signalosome subunit 5 is sufficient to cause the *cop/det/fus* mutant
929 phenotype in Arabidopsis. Plant Cell **17**:1967-1978. 10.1105/tpc.105.032870.
930 **Dohmann, E.M., Levesque, M.P., Isono, E., Schmid, M., and Schwechheimer, C.** (2008). Auxin
931 responses in mutants of the Arabidopsis CONSTITUTIVE PHOTOMORPHOGENIC9 signalosome. Plant
932 Physiol **147**:1369-1379. 10.1104/pp.108.121061.
933 **Dong, J., Ma, G., Sui, L., Wei, M., Satheesh, V., Zhang, R., Ge, S., Li, J., Zhang, T.E., Wittwer, C., et al.**
934 (2019). Inositol Pyrophosphate InsP(8) Acts as an Intracellular Phosphate Signal in Arabidopsis. Mol
935 Plant **12**:1463-1473. 10.1016/j.molp.2019.08.002.
936 **Dubiel, D., Rockel, B., Naumann, M., and Dubiel, W.** (2015). Diversity of COP9 signalosome structures
937 and functional consequences. FEBS Letters **589**:2507-2513.
938 https://doi.org/10.1016/j.febslet.2015.06.007.
939 **Duda, D.M., Borg, L.A., Scott, D.C., Hunt, H.W., Hammel, M., and Schulman, B.A.** (2008). Structural
940 insights into NEDD8 activation of cullin-RING ligases: conformational control of conjugation. Cell
941 **134**:995-1006. 10.1016/j.cell.2008.07.022.
942 **Enchev, R.I., Scott, D.C., da Fonseca, P.C., Schreiber, A., Monda, J.K., Schulman, B.A., Peter, M., and**
943 **Morris, E.P.** (2012). Structural basis for a reciprocal regulation between SCF and CSN. Cell Rep **2**:616-
944 627. 10.1016/j.celrep.2012.08.019.
945 **Feng, S., Ma, L., Wang, X., Xie, D., Dinesh-Kumar, S.P., Wei, N., and Deng, X.W.** (2003). The COP9
946 signalosome interacts physically with SCF COI1 and modulates jasmonate responses. Plant Cell
947 **15**:1083-1094. 10.1105/tpc.010207.
948 **Franco-Zorrilla, J.M., González, E., Bustos, R., Linhares, F., Leyva, A., and Paz-Ares, J.** (2004). The
949 transcriptional control of plant responses to phosphate limitation. Journal of Experimental Botany
950 **55**:285-293. 10.1093/jxb/erh009.
951 **Fukumoto, A., Tomoda, K., Kubota, M., Kato, J.-y., and Yoneda-Kato, N.** (2005). Small Jab1-containing
952 subcomplex is regulated in an anchorage- and cell cycle-dependent manner, which is abrogated by ras
953 transformation. FEBS Letters **579**:1047-1054. https://doi.org/10.1016/j.febslet.2004.12.076.
954 **Füzesi-Levi, M.G., Fainer, I., Ivanov Enchev, R., Ben-Nissan, G., Levin, Y., Kupervaser, M., Friedlander,**
955 **G., Salame, T.M., Nevo, R., Peter, M., et al.** (2020). CSNAP, the smallest CSN subunit, modulates
956 proteostasis through cullin-RING ubiquitin ligases. Cell Death Differ **27**:984-998. 10.1038/s41418-019-
957 0392-8.
958 **Gillaspy, G.E.** (2013). The role of phosphoinositides and inositol phosphates in plant cell signaling.
959 Advances in experimental medicine and biology **991**:141-157. 10.1007/978-94-007-6331-9_8.
960 **Gray, W., Del pozo, J., Walker, L., Hobbie, L., Risseeuw, E., Banks, T., Crosby, W., Yang, M., Ma, H.,**
961 **and Estelle, M.** (1999). Identification of an SCF ubiquitin-ligase complex required for auxin response
962 in *Arabidopsis thaliana*. Genes Dev **13**:1678-1691. 10.1101/gad.13.13.1678.
963 **Gray, W.M., Kepinski, S., Rouse, D., Leyser, O., and Estelle, M.** (2001). Auxin regulates SCF^{TIR1}-
964 dependent degradation of AUX/IAA proteins. Nature **414**:271-276. 10.1038/35104500.
965 **Guan, Z., Zhang, Q., Zhang, Z., Zuo, J., Chen, J., Liu, R., Savarin, J., Broger, L., Cheng, P., Wang, Q., et**
966 **al.** (2022). Mechanistic insights into the regulation of plant phosphate homeostasis by the rice SPX2 -
967 PHR2 complex. Nat Commun **13**:1581. 10.1038/s41467-022-29275-8.
968 **Gulabani, H., Goswami, K., Walia, Y., Roy, A., Noor, J.J., Ingole, K.D., Kasera, M., Laha, D., Giehl,**
969 **R.F.H., Schaaf, G., et al.** (2022). Arabidopsis inositol polyphosphate kinases IPK1 and ITPK1 modulate
970 crosstalk between SA-dependent immunity and phosphate-starvation responses. Plant Cell Reports
971 **41**:347-363. 10.1007/s00299-021-02812-3.
972 **Gusmaroli, G., Feng, S., and Deng, X.W.** (2004). The Arabidopsis CSN5A and CSN5B subunits are
973 present in distinct COP9 signalosome complexes, and mutations in their JAMM domains exhibit
974 differential dominant negative effects on development. Plant Cell **16**:2984-3001.
975 10.1105/tpc.104.025999.

Gusmaroli, G., Figueroa, P., Serino, G., and Deng, X.W. (2007). Role of the MPN subunits in COP9 signalosome assembly and activity, and their regulatory interaction with Arabidopsis Cullin3-based E3 ligases. The Plant cell **19**:564-581. 10.1105/tpc.106.047571.

Hakenjos, J.P., Richter, R., Dohmann, E.M.N., Katsiarimpa, A., Isono, E., and Schwechheimer, C. (2011). MLN4924 Is an Efficient Inhibitor of NEDD8 Conjugation in Plants Plant Physiology **156**:527-536. 10.1104/pp.111.176677.

Ham, B.K., Chen, J., Yan, Y., and Lucas, W.J. (2018). Insights into plant phosphate sensing and signaling. Curr Opin Biotechnol **49**:1-9. 10.1016/j.copbio.2017.07.005.

Hemelaar, J., Borodovsky, A., Kessler, B., Reverter, D., Cook, J., Kolli, N., Gan-Erdene, T., Wilkinson, K., Gill, G., Lima, C., et al. (2004). Specific and Covalent Targeting of Conjugating and Deconjugating Enzymes of Ubiquitin-Like Proteins. Molecular and cellular biology **24**:84-95. 10.1128/MCB.24.1.84-95.2004.

Hotton, S.K., and Callis, J. (2008). Regulation of Cullin RING Ligases. Annual Review of Plant Biology **59**:467-489. 10.1146/annurev.arplant.58.032806.104011.

Hua, Z., and Vierstra, R.D. (2011). The cullin-RING ubiquitin-protein ligases. Annu Rev Plant Biol **62**:299-334. 10.1146/annurev-arplant-042809-112256.

Huang, H., Quint, M., and Gray, W.M. (2013). The *eta7/csn3-3* auxin response mutant of Arabidopsis defines a novel function for the CSN3 subunit of the COP9 signalosome. PLoS One **8**:e66578. 10.1371/journal.pone.0066578.

Ito, T., Tashiro, K., Muta, S., Ozawa, R., Chiba, T., Nishizawa, M., Yamamoto, K., Kuhara, S., and Sakaki, Y. (2000). Toward a protein-protein interaction map of the budding yeast: A comprehensive system to examine two-hybrid interactions in all possible combinations between the yeast proteins. Proc Natl Acad Sci U S A **97**:1143-1147. 10.1073/pnas.97.3.1143.

Jia, Q., Kong, D., Li, Q., Sun, S., Song, J., Zhu, Y., Liang, K., Ke, Q., Lin, W., and Huang, J. (2019). The Function of Inositol Phosphatases in Plant Tolerance to Abiotic Stress. Int J Mol Sci **20**10.3390/ijms20163999.

Jia, X., Chanda, B., Zhao, M., Brunner, A.M., and Beers, E.P. (2015). Instability of the Arabidopsis mutant csn5a-2 caused by epigenetic modification of intronic T-DNA. Plant Sci **238**:53-63. 10.1016/j.plantsci.2015.05.015.

Kim, S., Bhandari, R., Brearley, C.A., and Saiardi, A. (2024). The inositol phosphate signalling network in physiology and disease. Trends Biochem Sci **49**:969-985. 10.1016/j.tibs.2024.08.005.

Kim, S.H., Gao, F., Bhattacharjee, S., Adiasor, J.A., Nam, J.C., and Gassmann, W. (2010). The Arabidopsis resistance-like gene SNC1 is activated by mutations in SRFR1 and contributes to resistance to the bacterial effector AvrRps4. PLoS Pathog **6**:e1001172. 10.1371/journal.ppat.1001172.

Kuo, H.F., Chang, T.Y., Chiang, S.F., Wang, W.D., Charng, Y.Y., and Chiou, T.J. (2014). Arabidopsis inositol pentakisphosphate 2-kinase, AtIPK1, is required for growth and modulates phosphate homeostasis at the transcriptional level. Plant J **80**:503-515. 10.1111/tpj.12650.

Kuo, H.F., Hsu, Y.Y., Lin, W.C., Chen, K.Y., Munnik, T., Brearley, C.A., and Chiou, T.J. (2018). Arabidopsis inositol phosphate kinases IPK1 and ITPK1 constitute a metabolic pathway in maintaining phosphate homeostasis. Plant J 10.1111/tpj.13974.

Laha, D., Portela-Torres, P., Desfougères, Y., and Saiardi, A. (2021). Inositol phosphate kinases in the eukaryote landscape. Advances in Biological Regulation **79**:100782. https://doi.org/10.1016/j.jbior.2020.100782.

Laha, D., Parvin, N., Dynowski, M., Johnen, P., Mao, H., Bitters, S.T., Zheng, N., and Schaaf, G. (2016). Inositol Polyphosphate Binding Specificity of the Jasmonate Receptor Complex. Plant Physiol **171**:2364-2370. 10.1104/pp.16.00694.

Laha, D., Parvin, N., Hofer, A., Giehl, R.F.H., Fernandez-Rebollo, N., von Wirén, N., Saiardi, A., Jessen, H.J., and Schaaf, G. (2019). Arabidopsis ITPK1 and ITPK2 Have an Evolutionarily Conserved Phytic Acid Kinase Activity. ACS Chemical Biology **14**:2127-2133. 10.1021/acschembio.9b00423.

Laha, D., Johnen, P., Azevedo, C., Dynowski, M., Weiss, M., Capolicchio, S., Mao, H., Iven, T., Steenbergen, M., Freyer, M., et al. (2015). VIH2 Regulates the Synthesis of Inositol Pyrophosphate

1027 InsP8 and Jasmonate-Dependent Defenses in Arabidopsis. Plant Cell **27**:1082-1097.
1028 10.1105/tpc.114.135160.
1029 **Laha, N.P., Giehl, R.F.H., Riemer, E., Qiu, D., Pullagurla, N.J., Schneider, R., Dhir, Y.W., Yadav, R.,**
1030 **Mihiret, Y.E., Gaugler, P., et al.** (2022). INOSITOL (1,3,4) TRIPHOSPHATE 5/6 KINASE1-Dependent
1031 Inositol Polyphosphates Regulate Auxin Responses in Arabidopsis. Plant Physiology
1032 10.1093/plphys/kiac425.
1033 **Land, E.S., Cridland, C.A., Craige, B., Dye, A., Hildreth, S.B., Helm, R.F., Gillaspy, G.E., and Perera, I.Y.**
1034 (2021). A Role for Inositol Pyrophosphates in the Metabolic Adaptations to Low Phosphate in
1035 Arabidopsis. Metabolites **11**10.3390/metabo11090601.
1036 **Lin, H., Zhang, X., Liu, L., Fu, Q., Zang, C., Ding, Y., Su, Y., Xu, Z., He, S., Yang, X., et al.** (2020). Basis
1037 for metabolite-dependent Cullin-RING ligase deneddylation by the COP9 signalosome. Proceedings of
1038 the National Academy of Sciences **117**:4117-4124. doi:10.1073/pnas.1911998117.
1039 **Lingaraju, G.M., Bunker, R.D., Cavadini, S., Hess, D., Hassiepen, U., Renatus, M., Fischer, E.S., and**
1040 **Thoma, N.H.** (2014). Crystal structure of the human COP9 signalosome. Nature **512**:161-165.
1041 10.1038/nature13566.
1042 **Lv, Q., Zhong, Y., Wang, Y., Wang, Z., Zhang, L., Shi, J., Wu, Z., Liu, Y., Mao, C., Yi, K., et al.** (2014).
1043 SPX4 Negatively Regulates Phosphate Signaling and Homeostasis through Its Interaction with PHR2 in
1044 Rice The Plant Cell **26**:1586-1597. 10.1105/tpc.114.123208.
1045 **Lyapina, S., Cope, G., Shevchenko, A., Serino, G., Tsuge, T., Zhou, C., Wolf, D.A., Wei, N., Shevchenko,**
1046 **A., and Deshaies, R.J.** (2001). Promotion of NEDD-CUL1 conjugate cleavage by COP9 signalosome.
1047 Science **292**:1382-1385. 10.1126/science.1059780.
1048 **Mergner, J., Heinzlmeir, S., Kuster, B., and Schwechheimer, C.** (2015). DENEDDYLASE1 Deconjugates
1049 NEDD8 from Non-Cullin Protein Substrates in *Arabidopsis thaliana*. The Plant Cell **27**:741-753.
1050 10.1105/tpc.114.135996.
1051 **Mockli, N., and Auerbach, D.** (2004). Quantitative beta-galactosidase assay suitable for high-
1052 throughput applications in the yeast two-hybrid system. Biotechniques **36**:872-876.
1053 10.2144/04365PT03.
1054 **Monserrate, J.P., and York, J.D.** (2010). Inositol phosphate synthesis and the nuclear processes they
1055 affect. Current opinion in cell biology **22**:365-373. 10.1016/j.ceb.2010.03.006.
1056 **Mosadeghi, R., Reichermeier, K.M., Winkler, M., Schreiber, A., Reitsma, J.M., Zhang, Y., Stengel, F.,**
1057 **Cao, J., Kim, M., Sweredoski, M.J., et al.** (2016). Structural and kinetic analysis of the COP9-
1058 Signalosome activation and the cullin-RING ubiquitin ligase deneddylation cycle. Elife
1059 **5**10.7554/eLife.12102.
1060 **Murphy, A.M., Otto, B., Brearley, C.A., Carr, J.P., and Hanke, D.E.** (2008). A role for inositol
1061 hexakisphosphate in the maintenance of basal resistance to plant pathogens. Plant J **56**:638-652.
1062 10.1111/j.1365-313X.2008.03629.x.
1063 **Oh, W., Lee, E.-W., Sung, Y.H., Yang, M.-R., Ghim, J., Lee, H.-W., and Song, J.** (2006). Jab1 Induces the
1064 Cytoplasmic Localization and Degradation of p53 in Coordination with Hdm2*. Journal of Biological
1065 Chemistry **281**:17457-17465. https://doi.org/10.1074/jbc.M601857200.
1066 **Oron, E., Mannervik, M., Rencus, S., Harari-Steinberg, O., Neuman-Silberberg, S., Segal, D., and**
1067 **Chamovitz, D.A.** (2002). COP9 signalosome subunits 4 and 5 regulate multiple pleiotropic pathways in
1068 *Drosophila melanogaster*. Development **129**:4399-4409. 10.1242/dev.129.19.4399.
1069 **Osorio, M.B., Ng, S., Berkowitz, O., De Clercq, I., Mao, C., Shou, H., Whelan, J., and Jost, R.** (2019).
1070 SPX4 Acts on PHR1-Dependent and -Independent Regulation of Shoot Phosphorus Status in
1071 Arabidopsis. Plant Physiology **181**:332-352. 10.1104/pp.18.00594.
1072 **Poon, J.S.Y., Le Fevre, R.E., Carr, J.P., Hanke, D.E., and Murphy, A.M.** (2020). Inositol
1073 hexakisphosphate biosynthesis underpins PAMP-triggered immunity to *Pseudomonas syringae* pv.
1074 *tomato* in *Arabidopsis thaliana* but is dispensable for establishment of systemic acquired resistance.
1075 Mol Plant Pathol **21**:376-387. 10.1111/mpp.12902.
1076 **Puga, M.I., Mateos, I., Charukesi, R., Wang, Z., Franco-Zorrilla, J.M., de Lorenzo, L., Irigoyen, M.L.,**
1077 **Masiero, S., Bustos, R., Rodriguez, J., et al.** (2014). SPX1 is a phosphate-dependent inhibitor of

Phosphate Starvation Response 1 in Arabidopsis. Proc Natl Acad Sci U S A **111**:14947-14952. 10.1073/pnas.1404654111.

Pullagurla, N.J., Shome, S., Yadav, R., and Laha, D. (2023). ITPK1 Regulates Jasmonate-Controlled Root Development in *Arabidopsis thaliana*. Biomolecules **13**10.3390/biom13091368.

Pullagurla, N.J., Shome, S., Liu, G., Jessen, H.J., and Laha, D. (2024). Orchestration of phosphate homeostasis by the ITPK1-type inositol phosphate kinase in the liverwort *Marchantia polymorpha*. Plant Physiol 10.1093/plphys/kiae454.

Qin, Z.-X., Chen, Q.-J., Tong, Z., and Wang, X.-C. (2005). The Arabidopsis inositol 1,3,4-trisphosphate 5/6 kinase, AtITPK-1, is involved in plant photomorphogenesis under red light conditions, possibly via interaction with COP9 signalosome. Plant physiology and biochemistry : PPB / Société française de physiologie végétale **43**:947-954. 10.1016/j.plaphy.2005.08.006.

Qiu, D., Gu, C., Liu, G., Ritter, K., Eisenbeis, V.B., Bittner, T., Gruzdev, A., Seidel, L., Bengsch, B., Shears, S.B., et al. (2023). Capillary electrophoresis mass spectrometry identifies new isomers of inositol pyrophosphates in mammalian tissues. Chem Sci **14**:658-667. 10.1039/d2sc05147h.

Rao, F., Xu, J., Khan, A.B., Gadalla, M.M., Cha, J.Y., Xu, R., Tyagi, R., Dang, Y., Chakraborty, A., and Snyder, S.H. (2014). Inositol hexakisphosphate kinase-1 mediates assembly/disassembly of the CRL4-signalosome complex to regulate DNA repair and cell death. Proc Natl Acad Sci U S A **111**:16005-16010. 10.1073/pnas.1417900111.

Ren, Y., Jiang, M., Zhu, J.K., Zhou, W., and Zhao, C. (2024). Simultaneous mutations in ITPK4 and MRP5 genes result in a low phytic acid level without compromising salt tolerance in Arabidopsis. J Integr Plant Biol **66**:2109-2125. 10.1111/jipb.13745.

Ried, M.K., Wild, R., Zhu, J., Pipercevic, J., Sturm, K., Broger, L., Harmel, R.K., Abriata, L.A., Hothorn, L.A., Fiedler, D., et al. (2021). Inositol pyrophosphates promote the interaction of SPX domains with the coiled-coil motif of PHR transcription factors to regulate plant phosphate homeostasis. Nat Commun **12**:384. 10.1038/s41467-020-20681-4.

Riemer, E., Qiu, D., Laha, D., Harmel, R.K., Gaugler, P., Gaugler, V., Frei, M., Hajirezaei, M.-R., Laha, N.P., Krusenbaum, L., et al. (2021a). ITPK1 is an InsP(6)/ADP phosphotransferase that controls phosphate signaling in Arabidopsis. Molecular plant **14**:1864-1880. 10.1016/j.molp.2021.07.011.

Ruan, W., Guo, M., Wang, X., Guo, Z., Xu, Z., Xu, L., Zhao, H., Sun, H., Yan, C., and Yi, K. (2019). Two RING-Finger Ubiquitin E3 Ligases Regulate the Degradation of SPX4, An Internal Phosphate Sensor, for Phosphate Homeostasis and Signaling in Rice. Mol Plant **12**:1060-1074. 10.1016/j.molp.2019.04.003.

Rubio, V., Linhares, F., Solano, R., Martín, A.C., Iglesias, J., Leyva, A., and Paz-Ares, J. (2001). A conserved MYB transcription factor involved in phosphate starvation signaling both in vascular plants and in unicellular algae. Genes Dev **15**:2122-2133. 10.1101/gad.204401.

Scherer, P.C., Ding, Y., Liu, Z., Xu, J., Mao, H., Barrow, J.C., Wei, N., Zheng, N., Snyder, S.H., and Rao, F. (2016). Inositol hexakisphosphate (IP6) generated by IP5K mediates cullin-COP9 signalosome interactions and CRL function. Proc Natl Acad Sci U S A **113**:3503-3508. 10.1073/pnas.1525580113.

Schlierf, A., Altmann, E., Quancard, J., Jefferson, A.B., Assenberg, R., Renatus, M., Jones, M., Hassiepen, U., Schaefer, M., Kiffe, M., et al. (2016). Targeted inhibition of the COP9 signalosome for treatment of cancer. Nature Communications **7**:13166. 10.1038/ncomms13166.

Schwechheimer, C. (2001). Interactions of the COP9 signalosome with the E3 ubiquitin ligase SCF. Science.

Schwechheimer, C. (2018). NEDD8—its role in the regulation of Cullin-RING ligases. Current Opinion in Plant Biology **45**:112-119. https://doi.org/10.1016/j.pbi.2018.05.017.

Sheard, L.B., Tan, X., Mao, H., Withers, J., Ben-Nissan, G., Hinds, T.R., Kobayashi, Y., Hsu, F.F., Sharon, M., Browse, J., et al. (2010). Jasmonate perception by inositol-phosphate-potentiated COI1-JAZ co-receptor. Nature **468**:400-405. 10.1038/nature09430.

Shears, S.B., and Wang, H. (2019). Inositol phosphate kinases: Expanding the biological significance of the universal core of the protein kinase fold. Adv Biol Regul **71**:118-127. 10.1016/j.jbior.2018.10.006.

Soucy, T.A., Smith, P.G., Milhollen, M.A., Berger, A.J., Gavin, J.M., Adhikari, S., Brownell, J.E., Burke, K.E., Cardin, D.P., Critchley, S., et al. (2009). An inhibitor of NEDD8-activating enzyme as a new approach to treat cancer. Nature **458**:732-736. 10.1038/nature07884.

Stevenson-Paulik, J., Bastidas, R.J., Chiou, S.T., Frye, R.A., and York, J.D. (2005). Generation of phytate-free seeds in Arabidopsis through disruption of inositol polyphosphate kinases. Proc Natl Acad Sci U S A **102**:12612-12617. 10.1073/pnas.0504172102.

Stuttmann, J., Lechner, E., Guérois, R., Parker, J.E., Nussaume, L., Genschik, P., and Noël, L.D. (2009). COP9 signalosome- and 26S proteasome-dependent regulation of SCF^{TIR1} accumulation in Arabidopsis. J Biol Chem **284**:7920-7930. 10.1074/jbc.M809069200.

Sun, L., Song, L., Zhang, Y., Zheng, Z., and Liu, D. (2016). Arabidopsis PHL2 and PHR1 Act Redundantly as the Key Components of the Central Regulatory System Controlling Transcriptional Responses to Phosphate Starvation. Plant Physiol **170**:499-514. 10.1104/pp.15.01336.

Sun, Y., Wilson, M.P., and Majerus, P.W. (2002). Inositol 1,3,4-trisphosphate 5/6-kinase associates with the COP9 signalosome by binding to CSN1. The Journal of biological chemistry **277**:45759-45764. 10.1074/jbc.m208709200.

Tan, X., Calderon-Villalobos, L.I., Sharon, M., Zheng, C., Robinson, C.V., Estelle, M., and Zheng, N. (2007). Mechanism of auxin perception by the TIR1 ubiquitin ligase. Nature **446**:640-645. 10.1038/nature05731.

Tomoda, K., Kubota, Y., Arata, Y., Mori, S., Maeda, M., Tanaka, T., Yoshida, M., Yoneda-Kato, N., and Kato, J.-y. (2002). The Cytoplasmic Shuttling and Subsequent Degradation of p27Kip1 Mediated by Jab1/CSN5 and the COP9 Signalosome Complex. Journal of Biological Chemistry **277**:2302-2310. https://doi.org/10.1074/jbc.M104431200.

Veiga, N.s., Torres, J., DomÌnguez, S., Mederos, A., Irvine, R.F., DÌaz, l., and Kremer, C. (2006). The behaviour of myo-inositol hexakisphosphate in the presence of magnesium(II) and calcium(II): Protein-free soluble InsP6 is limited to 49 microM under cytosolic/nuclear conditions. Journal of Inorganic Biochemistry **100**:1800 - 1810.

Wada, H., Kito, K., Caskey, L.S., Yeh, E.T.H., and Kamitani, T. (1998). Cleavage of the C-Terminus of NEDD8 by UCH-L3. Biochemical and Biophysical Research Communications **251**:688-692. https://doi.org/10.1006/bbrc.1998.9532.

Whitfield, H., White, G., Sprigg, C., Riley, A.M., Potter, B.V.L., Hemmings, A.M., and Brearley, C.A. (2020). An ATP-responsive metabolic cassette comprised of inositol tris/tetrakisphosphate kinase 1 (ITPK1) and inositol pentakisphosphate 2-kinase (IPK1) buffers diphosphosphoinositol phosphate levels. Biochem J **477**:2621-2638. 10.1042/BCJ20200423.

Wild, R., Gerasimaite, R., Jung, J.-Y., Truffault, V., Pavlovic, I., Schmidt, A., Saiardi, A., Jessen, H.J., Poirier, Y., Hothorn, M., et al. (2016). Control of eukaryotic phosphate homeostasis by inositol polyphosphate sensor domains. Science **352**:986-990. doi:10.1126/science.aad9858.

Williams, C., Fernández-Calvo, P., Colinas, M., Pauwels, L., and Goossens, A. (2019). Jasmonate and auxin perception: how plants keep F-boxes in check. Journal of experimental botany **70**10.1093/jxb/erz272.

Williams, S.P., Gillaspy, G.E., and Perera, I.Y. (2015). Biosynthesis and possible functions of inositol pyrophosphates in plants. Front Plant Sci **6**:67. 10.3389/fpls.2015.00067.

Wilson, M.S., Livermore, T.M., and Saiardi, A. (2013). Inositol pyrophosphates: between signalling and metabolism. Biochem J **452**:369-379. 10.1042/BJ20130118.

Wilson, M.S., Bulley, S.J., Pisani, F., Irvine, R.F., and Saiardi, A. (2015). A novel method for the purification of inositol phosphates from biological samples reveals that no phytate is present in human plasma or urine. Open Biol **5**:150014. 10.1098/rsob.150014.

Wu, J.-T., Chan, Y.-R., and Chien, C.-T. (2006). Protection of cullin-RING E3 ligases by CSN-UBP12. Trends in cell biology **16**:362-369. 10.1016/j.tcb.2006.05.001.

Xu, L., Liu, F., Lechner, E., Genschik, P., Crosby, W.L., Ma, H., Peng, W., Huang, D., and Xie, D. (2002). The SCFCOI1 Ubiquitin-Ligase Complexes Are Required for Jasmonate Response in Arabidopsis. The Plant Cell **14**:1919-1935. 10.1105/tpc.003368.

1178 **Zheng, N., Schulman, B., Song, L., Miller, J., Jeffrey, P., Wang, P., Chu, C., Koepp, D., Elledge, S.,**
1179 **Pagano, M., et al.** (2002). Structure of the Cul1-Rbx1-Skp1-F boxSkp2 SCF ubiquitin ligase complex.
1180 Nature **416**:703-709. 10.1038/416703a.
1181 **Zhong, Y., Wang, Y., Guo, J., Zhu, X., Shi, J., He, Q., Liu, Y., Wu, Y., Zhang, L., Lv, Q., et al.** (2018). Rice
1182 SPX6 negatively regulates the phosphate starvation response through suppression of the transcription
1183 factor PHR2. New Phytol **219**:135-148. 10.1111/nph.15155.
1184 **Zhou, J., Jiao, F., Wu, Z., Li, Y., Wang, X., He, X., Zhong, W., and Wu, P.** (2008). OsPHR2 is involved in
1185 phosphate-starvation signaling and excessive phosphate accumulation in shoots of plants. Plant
1186 Physiol **146**:1673-1686. 10.1104/pp.107.111443.
1187 **Zhu, J., Lau, K., Puschmann, R., Harmel, R.K., Zhang, Y., Pries, V., Gaugler, P., Broger, L., Dutta, A.K.,**
1188 **Jessen, H.J., et al.** (2019). Two bifunctional inositol pyrophosphate kinases/phosphatases control plant
1189 phosphate homeostasis. eLife **8**:e43582. 10.7554/eLife.43582.
1190 **Zhu, S., Goeres, J., Sixt, K.M., Bekes, M., Zhang, X.D., Salvesen, G.S., and Matunis, M.J.** (2009).
1191 Protection from isopeptidase-mediated deconjugation regulates paralog-selective sumoylation of
1192 RanGAP1. Mol Cell **33**:570-580. 10.1016/j.molcel.2009.02.008.

1193 **Figure legends**

1194 **Figure 1. Arabidopsis IPK1 and ITPK1 interact with the CSN holo-complex and**
1195 **modulate its deneddylation activity.**

1196 **(A)** Anti-CUL1 immunoblot showing basal levels of neddylated: unneddylated CUL1
1197 ($CUL1^{Nedd8}$: CUL1) in *ipk1-1* or *itpk1-2* relative to Col-0. Anti-ACT1 immunoblot or Ponceau
1198 S staining for rubisco large subunit denote comparable protein loading across samples. The
1199 numerical values below the images indicate the percentage of $CUL1^{Nedd8}$ relative to
1200 unneddylated CUL1.

1201 **(B)** Immuno-enrichments (IP) of IPK1 or ITPK1 from the corresponding complemented lines
1202 (*Myc-IPK1/ipk1-1* or *ITPK1-GFP/itpk1-2*, respectively) probed (IB) with anti-CSN1/2/4/5,
1203 anti-CUL1, anti-Myc, or anti-GFP antibodies. IgG-agarose enrichments were used as negative
1204 controls. Respective protein amounts in the input extracts are also indicated.

1205 **(C and D)** Growth phenotypes of indicated plants at 21 days post-germination.

1206 **(E and F)** Immuno-enrichment (IP) of GFP-tagged wild-type or kinase-dead versions of IPK1
1207 or ITPK1 from transgenic plants probed (IB) with the indicated CSN antibodies. The numerical
1208 values below the images represent the levels of the probed CSN subunit normalized to the
1209 corresponding immuno-enriched InsP-kinase. Respective protein amounts in the input extracts
1210 are also indicated.

1211 **Figure 2. Perturbed InsP-kinase or deneddylation activities disrupt the dissociation**
1212 **equilibrium of CSN4/5 subunits from the holo-complex.**

1213 **(A)** Affinity enrichment (IP) of His-rCSN2 from Col-0, *ipk1-1*, or *itpk1-2* plants probed (IB)
1214 with the indicated antibodies. The numerical values below the immunoblots represent the
1215 probed CSN subunit, or CUL1 levels normalized to the corresponding amounts of affinity-
1216 enriched His-rCSN2. Respective protein amounts in the input extracts are also shown.

1217 **(B)** Size exclusion partitioning profiles of CSN5 and CSN4 from indicated plants probed (IB)
1218 with anti-CSN5 or anti-CSN4 antibodies.

1219 **(C)** Anti-CUL1 blots from control, CSN5i-3, or MLN4924 treated Col-0 samples at 24 hours
1220 post-treatment (hpt). Relative migration positions of $CUL1^{Nedd8}$: CUL1 are indicated. Ponceau
1221 S staining shows comparable protein loading across samples. The numerical values below the
1222 immunoblot images represent the percentage of $CUL1^{Nedd8}$ relative to unneddylated CUL1.

1223 **(D)** Size exclusion partitioning profile of CSN5 and CUL1 from mock (DMSO) or CSN5i-3
1224 treated Col-0 probed (IB) with anti-CSN5, or anti-CUL1 antibodies.

1225 **(E)** Affinity enrichment (IP) of His-rCSN2 from control and CSN5i-3-treated plants probed
1226 (IB) with the indicated antibodies. The numerical values below the immunoblots represent the
1227 CSN subunit or CUL1 amounts relative to the levels of affinity-enriched His-rCSN2.

1228 **(F)** Affinity enrichment (IP) of His-rIPK1 or His-rITPK1 from control and CSN5i-3-treated
1229 plants probed (IB) with the indicated antibodies. The numerical values below the immunoblots
1230 indicate the CSN subunit or CUL1 amounts normalized to the corresponding affinity-enriched
1231 recombinant InsP-kinase.

1232 In all fractionation data, the fraction numbers and elution positions of molecular weight
1233 standards (in kDa) are marked. HMW (high molecular weight) or LMW (low molecular
1234 weight) refers to the expected partitioning positions of CSN holo-complex and subunit
1235 monomers, respectively. Protein amounts in the input extracts are also indicated for the
1236 respective blots.

1237 **Figure 3. $InsP_6$ potentiation on CSN deneddylase activity requires a kinase-active ITPK1.**

1238 **(A)** *In vitro* deneddylation activity of isolated Col-0 CSN holo-complex on Nedd8-AML
1239 substrate. Indicated amounts (in μg) of total CSN holo-complex co-fractionated proteins, or

1240 recombinant rUCHL3 were incubated with Nedd8-AML and the Luciferase activity measured.
1241 The inhibition assay was performed with CSN5i-3 (10 μM) supplemented to the CSN holo-
1242 complex protein pool (30 μg).

1243 **(B)** Dose-dependent enhancement in deneddylation activity of isolated Col-0 CSN holo-
1244 complex in the presence of indicated amounts of $InsP_6$.

1245 **(C)** Kinetics of deneddylation rates by the CSN holo-complex isolated from *ipk1-1* or *itpk1-2*
1246 plants relative to Col-0. Time points of incubation (mpi, minutes post-incubation) with the
1247 substrate are indicated.

1248 **(D)** Deneddylation activity of isolated CSN holo-complex from the indicated plants
1249 supplemented with or without $InsP_6$ (50 nM).

1250 **(E)** $InsP_7$ synthesis *in vitro* by ITPK1 is inhibited by CSN2 and restored by IPK1. Numerical
1251 values below the gel image represent $InsP_7$ levels relative to the only ITPK1 reaction.

1252 Data shown is mean ± SD (n=3) and represented as relative luminescence units (RLU) **(A and**
1253 **D)**, or relative to minus $InsP_6$ sample **(B)**, or as fold-change relative to Col-0 **(C)**. Statistical
1254 analysis is according to **(A and D)** Student's *t*-test with pairwise comparison to minus CSN
1255 holo-complex protein samples, (***P<0.0001, ns= not significant), or **(B)** with ANOVA
1256 (Tukey, $p < 0.05$).

1257 **Figure 4. InsP-kinase and CUL^{Nedd8} activities are essential for *PSI*-gene induction during**
1258 **PSR.**

1259 **(A and B)** *PSI*-gene expression in *ipk1-1, itpk1-2,* or in Pi-replete (+Pi) or Pi-deplete (-Pi) Col-
1260 0 in the presence or absence of MLN4924. Gene expressions are relative to *MON1* internal
1261 control. Data is mean ± SD (n=3). Heatmaps were generated using GraphPad Prism 8.4.3
1262 software using the single gradient function.

1263 **(C and D)** Anti-CUL1 immunoblot showing relative levels of neddylated: unneddylated CUL1
1264 ($CUL1^{Nedd8}$: CUL1) in the indicated samples (+Pi: Pi-replete; -Pi: Pi-deplete; -Pi + MLN: Pi-
1265 deplete samples treated with MLN4924; Pi-Resupply: Pi-deplete samples replenished with Pi).

1266 **(E)** Size exclusion fractionation profile of CSN5 from extracts of Pi-replete (+Pi), Pi-deplete
1267 (-Pi), or Pi-Resupply plants. Fraction numbers, elution positions of molecular weight standards
1268 (in kDa), and expected fractions indicative of CSN holo-complex-incorporated (HMW) or free

1269 CSN5 subunit monomers (LMW) are marked. Input panels show protein amounts in the total
1270 extracts.

1271 **(F)** *In lysate* deneddylation assays at indicated time points (mpi, minutes post-incubation) on
1272 Pi-replete or Pi-deplete Col-0 extracts probed (IB) with anti-CUL1 antibodies.

1273 **(G)** Scatter plot showing the half-life of $CUL1^{Nedd8}$ in the Pi-replete or Pi-deplete Col-0
1274 extracts.

1275 In the above immunoblots, the relative migration positions of $CUL1^{Nedd8}$: CUL1 are marked.
1276 Ponceau S staining denotes comparable protein loading across samples. The numerical values
1277 below images **(C and D)** represent the percentage of $CUL1^{Nedd8}$ relative to unneddylated
1278 CUL1.

1279 **Figure 5. Activated CRLs target SPX4 degradation during PSR.**

1280 **(A)** Total poly-ubiquitin conjugates in protein extracts of Col-0, *ipk1-1, itpk1-2,* and the
1281 respective complemented lines, detected with anti-Ub antibodies.

1282 **(B and C)** LUC luminescence and SPX4-protein levels in the *SPX4p:SPX4-LUC* transgenic
1283 plants subjected to Pi-replete (+Pi), or Pi-deplete (-Pi) conditions in the absence or presence of
1284 MLN4924, MG132, or CSN5i-3.

1285 **(D)** Polyubiquitinated SPX4-LUC in +Pi, -Pi and Pi-resupply (-Pi + Pi) detected via immuno-
1286 enrichment (IP) with anti-LUC antibodies and probed (IB) with anti-Ub antibodies. Relative
1287 levels of unmodified SPX4-LUC are shown with anti-LUC immunoblot. Migration position of
1288 molecular weight standards (in kDa) are indicated.

1289 **(E and F)** LUC luminescence and SPX4-protein levels in *SPX4p:SPX4-LUC* plants in wild-
1290 type (Col-0), *ipk2b-1*, untreated *ipk1-1*, and *ipk1-1* treated with MLN4924 or MG132
1291 inhibitors.

1292 Anti-ACT1 immunoblot or Ponceau S staining for rubisco large subunit represents comparable
1293 protein loading across samples. Numerical values below the immunoblots **(C and F)** represent
1294 SPX4-LUC levels normalized to the corresponding ACT1 levels.

1295 **Figure 6. Schematic model of dynamics of COP9 signalosome (CSN) deneddylation cycles**
1296 **regulated by IPK1 and ITPK1.**

1297 The kinase activity of ITPK1 at the CSN platform is inhibited by CSN2, either through
1298 allosteric interactions or via direct competition for $InsP_6$ binding. The rate-limiting $InsP_7$
1299 synthesis affects the deneddylation rates of the holo-complex. Kinase activity-dependent
1300 interaction of IPK1 with CSN2 increases the local synthesis of $InsP_6$, relieving the suppression
1301 of ITPK1 activity and enhancing subsequent $InsP_7$ production. Increased concentration of this
1302 metabolite stimulates the deneddylation activity of the holo-complex on cullins (ON). The
1303 deneddylation activity leads to the dissociation of deneddylated cullins, CSN4, CSN5 and the
1304 InsP-kinases from the holo-complex, thereby causing its inactivation (OFF). The dynamics of
1305 these processes maintain the equilibrium of active CRLs that, in turn, regulate the steady-state
1306 fate and function of SPX4 in phosphate homeostasis and phosphate starvation response. N8,
1307 Nedd8; CUL1, Cullin1.

1308 **Figure 1**

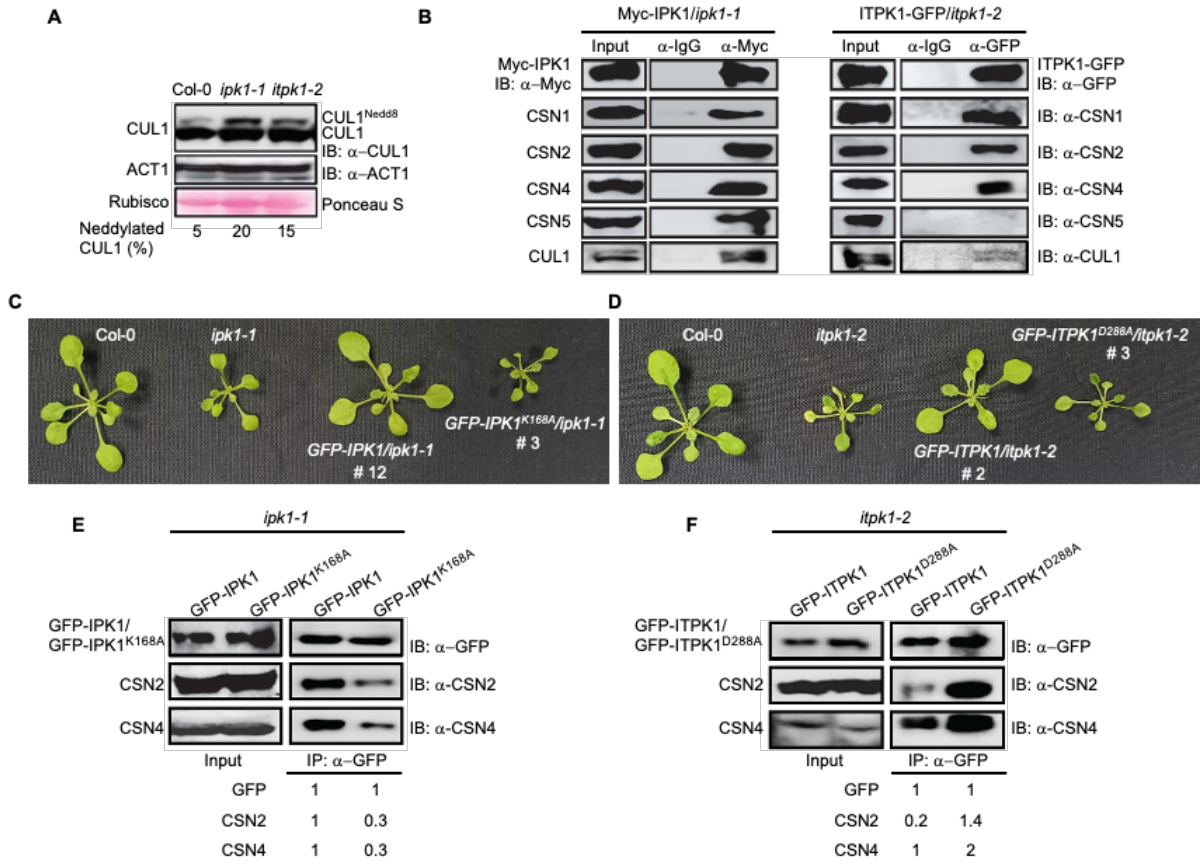

1309

1310 **Figure 1. Arabidopsis IPK1 and ITPK1 interact with the CSN holo-complex subunits and**
1311 **modulate its deneddylation activity.**

1312 **(A)** Anti-CUL1 immunoblot showing basal levels of neddylated: unneddylated CUL1
1313 ($CUL1^{Nedd8}$: CUL1) in *ipk1-1* or *itpk1-2* relative to Col-0. Anti-ACT1 immunoblot or Ponceau
1314 S staining for rubisco large subunit denote comparable protein loading across samples. The
1315 numerical values below the images indicate the percentage of $CUL1^{Nedd8}$ relative to
1316 unneddylated CUL1.
1317 **(B)** Immuno-enrichments (IP) of IPK1 or ITPK1 from the corresponding complemented lines
1318 (*Myc-IPK1/ipk1-1* or *ITPK1-GFP/itpk1-2*, respectively) probed (IB) with anti-CSN1/2/4/5,
1319 anti-CUL1, anti-Myc, or anti-GFP antibodies. IgG-agarose enrichments were used as negative
1320 controls. Respective protein amounts in the input extracts are also indicated.
1321 **(C and D)** Growth phenotypes of indicated plants at 21 days post-germination.
1322 **(E and F)** Immuno-enrichment (IP) of GFP-tagged wild-type or kinase-dead versions of IPK1
1323 or ITPK1 from transgenic plants probed (IB) with the indicated CSN antibodies. The numerical
1324 values below the images represent the levels of the probed CSN subunit normalized to the
1325 corresponding immuno-enriched InsP-kinase. Respective protein amounts in the input extracts
1326 are also indicated.

Figure 2

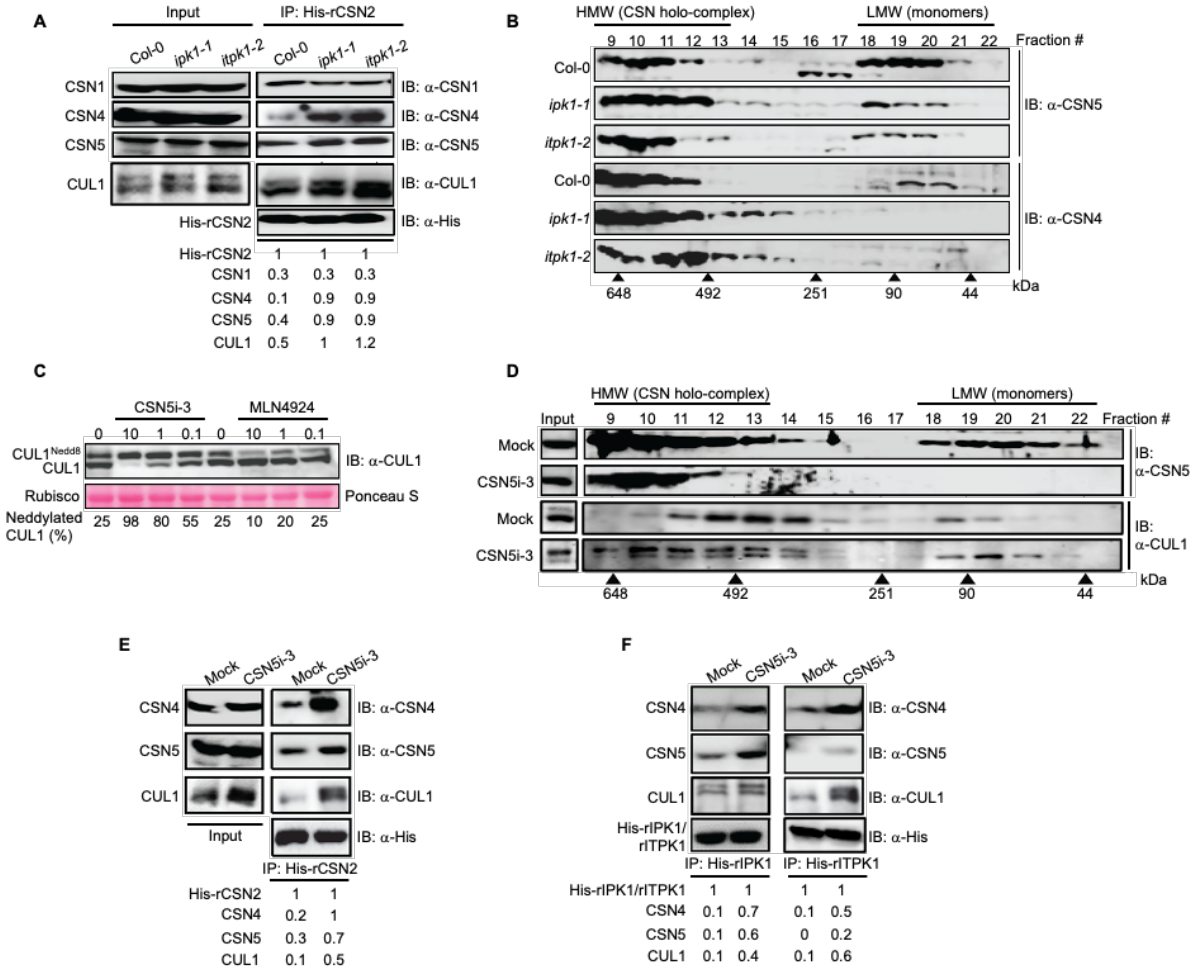

Figure 2. Perturbed InsP-kinase or deneddylation activities disrupt the dissociation equilibrium of CSN4/5 subunits from the holo-complex.

(A) Affinity enrichment (IP) of His-rCSN2 from Col-0, *ipk1-1*, or *itpk1-2* plants probed (IB) with the indicated antibodies. The numerical values below the immunoblots represent the probed CSN subunit, or CUL1 levels normalized to the corresponding amounts of affinity-enriched His-rCSN2. Respective protein amounts in the input extracts are also shown.
(B) Size exclusion CSN5 and CSN4 partitioning profiles from indicated plants probed (IB) with anti-CSN5 or anti-CSN4 antibodies.
(C) Anti-CUL1 blots from control, CSN5i-3, or MLN4924 treated Col-0 samples at 24 hours post-treatment (hpt). Relative migration positions of $CUL1^{Nedd8}$: CUL1 are indicated. Ponceau S staining shows comparable protein loading across samples. The numerical values below the immunoblot images represent the percentage of $CUL1^{Nedd8}$ relative to unneddylated CUL1.
(D) Size exclusion partitioning profile of CSN5 and CUL1 from mock (DMSO) or CSN5i-3 treated Col-0 probed (IB) with anti-CSN5 or anti-CUL1 antibodies.
(E) Affinity enrichment (IP) of His-rCSN2 from control and CSN5i-3-treated plants probed (IB) with the indicated antibodies. The numerical values below the immunoblots represent the CSN subunit or CUL1 amounts relative to the levels of affinity-enriched His-rCSN2.

1346 **(F)** Affinity enrichment (IP) of His-rIPK1 or His-rITPK1 from control and CSN5i-3-treated
1347 plants probed (IB) with the indicated antibodies. The numerical values below the immunoblots
1348 indicate the CSN subunit or CUL1 amounts normalized to the corresponding affinity-enriched
1349 recombinant InsP-kinase.
1350 In all fractionation data, the fraction numbers and elution positions of molecular weight
1351 standards (in kDa) are marked. HMW (high molecular weight) or LMW (low molecular
1352 weight) refers to the expected partitioning positions of CSN holo-complex and subunit
1353 monomers, respectively. Protein amounts in the input extracts are also indicated for the
1354 respective blots.

1355 **Figure 3**

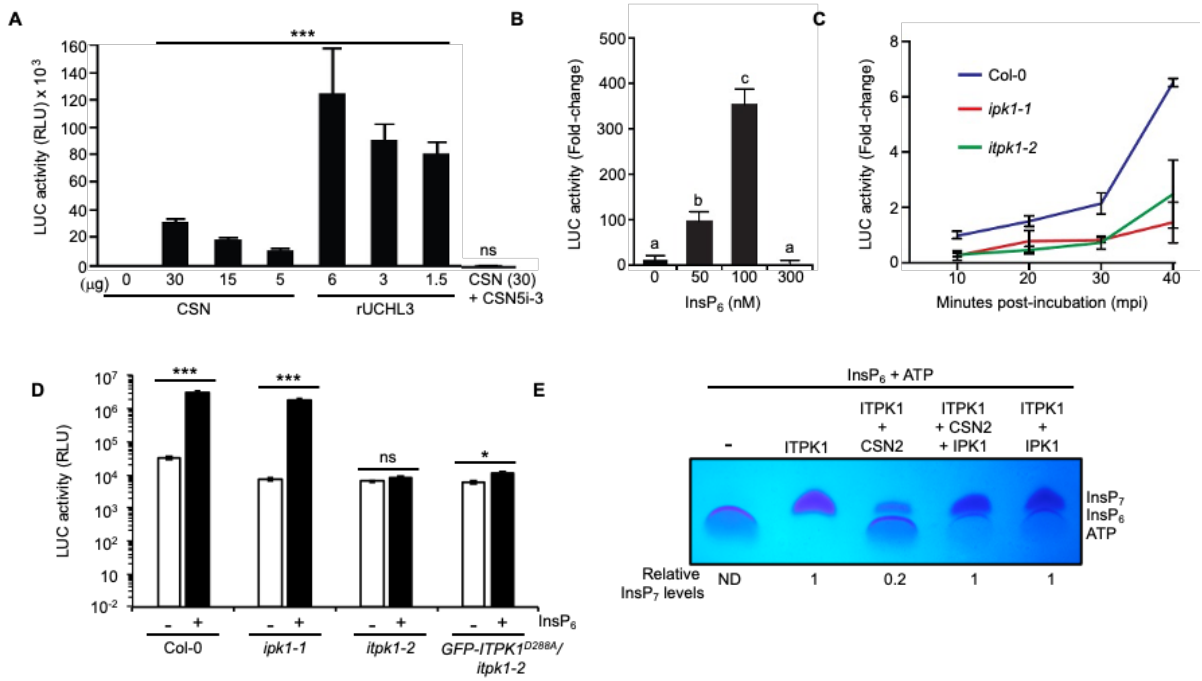

1356

1357 **Figure 3. $InsP_6$ potentiation on CSN deneddylase activity requires a kinase-active ITPK1.**

1358 **(A)** *In vitro* deneddylation activity of isolated Col-0 CSN holo-complex on Nedd8-AML
1359 substrate. Indicated amounts (in µg) of total CSN holo-complex co-fractionated proteins, or
1360 recombinant rUCHL3 were incubated with Nedd8-AML and the Luciferase activity measured.
1361 The inhibition assay was performed with CSN5i-3 (10 µM) supplemented to the CSN holo-
1362 complex protein pool (30 µg).
1363 **(B)** Dose-dependent enhancement in deneddylation activity of isolated Col-0 CSN holo-
1364 complex in the presence of indicated amounts of $InsP_6$.
1365 **(C)** Kinetics of deneddylation rates by the CSN holo-complex isolated from *ipk1-1* or *itpk1-2*
1366 plants relative to Col-0. Time points of incubation (mpi, minutes post-incubation) with the
1367 substrate are indicated.
1368 **(D)** Deneddylation activity of isolated CSN holo-complex from the indicated plants
1369 supplemented with or without $InsP_6$ (50 nM).
1370 **(E)** $InsP_7$ synthesis *in vitro* by ITPK1 is inhibited by CSN2 and restored by IPK1. Numerical
1371 values below the gel image represent $InsP_7$ levels relative to the only ITPK1 reaction.
1372 Data shown is mean ± SD (n=3) and represented as relative luminescence units (RLU) **(A and**
1373 **D)**, or relative to minus $InsP_6$ sample **(B)**, or as fold-change relative to Col-0 **(C)**. Statistical
1374 analysis is according to **(A and D)** Student's *t*-test with pairwise comparison to minus CSN
1375 holo-complex protein samples, (***P<0.0001, ns= not significant), or **(B)** with ANOVA
1376 (Tukey, $p < 0.05$).

1377 **Figure 4**

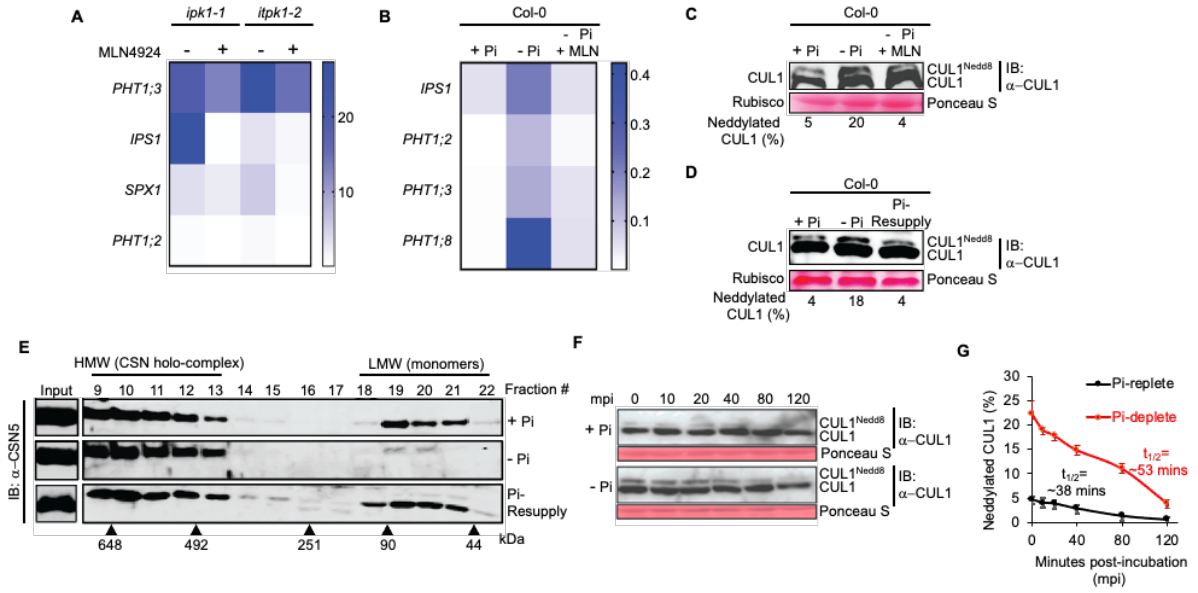

1378

1379 **Figure 4. InsP-kinase and CUL^{Nedd8} activities are essential for *PSI*-gene induction during**
1380 **PSR.**

1381 **(A and B)** *PSI*-gene expression in *ipk1-1, itpk1-2,* or in Pi-replete (+Pi) or Pi-deplete (-Pi) Col-
1382 0 in the presence or absence of MLN4924. Gene expressions are relative to *MON1* internal
1383 control. Data is mean ± SD (n=3). Heatmaps were generated using GraphPad Prism 8.4.3
1384 software using the single gradient function.
1385 **(C and D)** Anti-CUL1 immunoblot showing relative levels of neddylated: unneddylated CUL1
1386 (CUL1^{Nedd8}: CUL1) in the indicated samples (+Pi: Pi-replete; -Pi: Pi-deplete; -Pi + MLN: Pi-
1387 deplete samples treated with MLN4924; Pi-Resupply: Pi-deplete samples replenished with Pi).
1388 **(E)** Size exclusion fractionation profile of CSN5 from extracts of Pi-replete (+Pi), Pi-deplete
1389 (-Pi), or Pi-Resupply plants. Fraction numbers, elution positions of molecular weight standards
1390 (in kDa), and expected fractions indicative of CSN holo-complex-incorporated (HMW) or free
1391 CSN5 subunit monomers (LMW) are marked. Input panels show protein amounts in the total
1392 extracts.
1393 **(F)** *In lysate* deneddylation assays at indicated time points (mpi, minutes post-incubation) on
1394 Pi-replete or Pi-deplete Col-0 extracts probed (IB) with anti-CUL1 antibodies.
1395 **(G)** Scatter plot showing half-life CUL1^{Nedd8} in the Pi-replete or Pi-deplete Col-0 extracts.
1396 In the above immunoblots, the relative migration positions of CUL1^{Nedd8}: CUL1 are marked.
1397 Ponceau S staining denotes comparable protein loading across samples. The numerical values
1398 below images (C and D) represent the percentage of CUL1^{Nedd8} relative to unneddylated CUL1.

1399 **Figure 5**

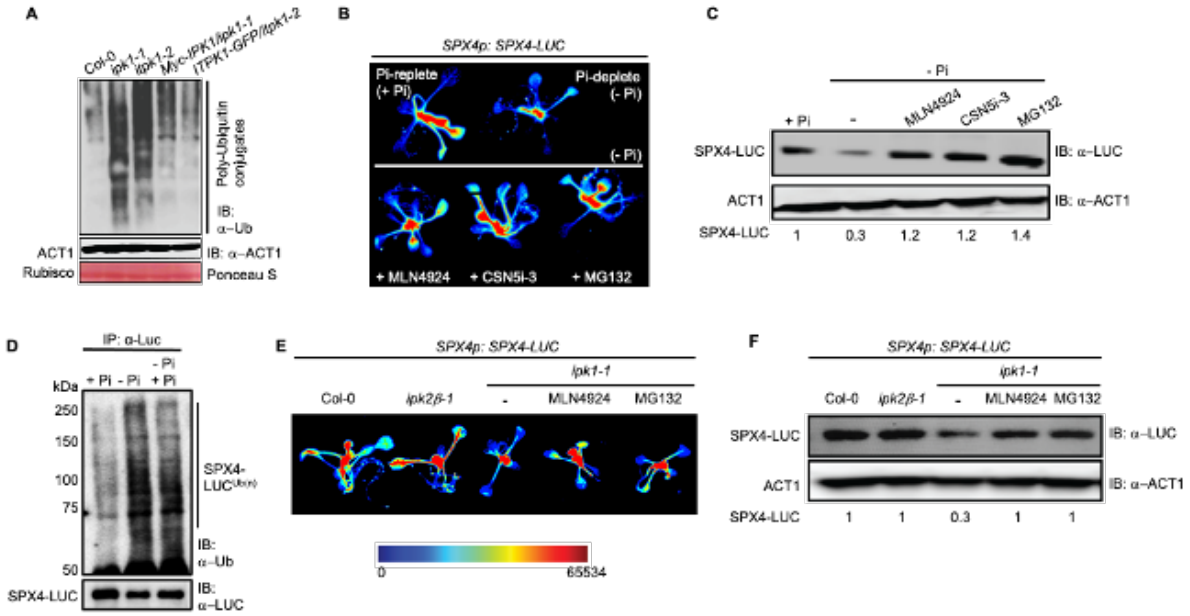

1400

1401 **Figure 5. CRLs target SPX4 degradation during PSR.**

1402 **(A)** Total poly-ubiquitin conjugates in protein extracts of Col-0, *ipk1-1, itpk1-2,* and the
1403 respective complemented lines detected with anti-Ub antibodies.
1404 **(B and C)** LUC luminescence and SPX4-protein levels in the *SPX4p:SPX4-LUC* transgenic
1405 plants when subjected to Pi-replete (+Pi), or Pi-deplete (-Pi) conditions in the absence or
1406 presence of MLN4924, MG132, or CSN5i-3.
1407 **(D)** Polyubiquitinated SPX4-LUC in +Pi, -Pi and Pi-resupply (-Pi + Pi) detected via immuno-
1408 enrichment (IP) with anti-LUC antibodies and probed (IB) with anti-Ub antibodies. Relative
1409 levels of unmodified SPX4-LUC are shown with anti-LUC immunoblot. Migration position of
1410 molecular weight standards (in kDa) are indicated.
1411 **(E and F)** LUC luminescence and SPX4-protein levels in *SPX4p:SPX4-LUC* plants in wild-
1412 type (Col-0), *ipk2β-1*, untreated *ipk1-1*, and *ipk1-1* treated with MLN4924 or MG132
1413 inhibitors.
1414 Anti-ACT1 immunoblot or Ponceau S staining for rubisco large subunit represents comparable
1415 protein loading across samples. Numerical values below the immunoblots **(C and F)** represent
1416 SPX4-LUC levels normalized to the corresponding ACT1 levels.

1417 **Figure 6**

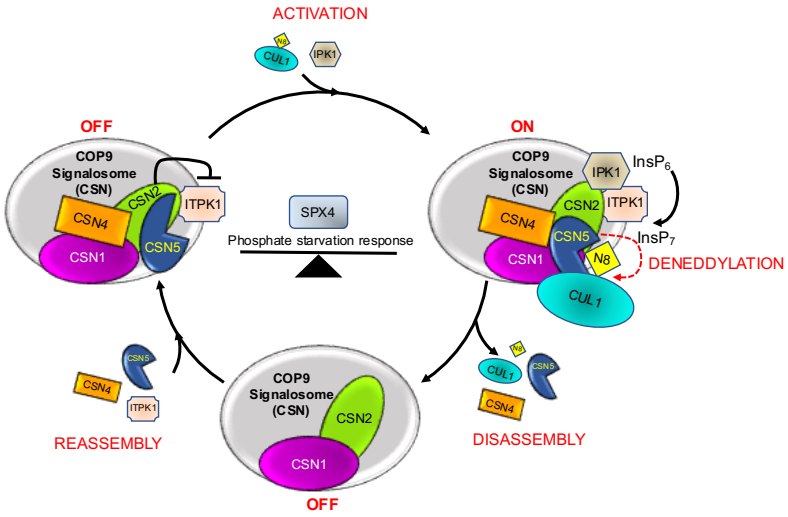

1418

1419 **Figure 6. Schematic model of dynamics of COP9 signalosome (CSN) deneddylation cycles**
1420 **regulated by IPK1 and ITPK1.**

The kinase activity of ITPK1 at the CSN platform is inhibited by CSN2, either through allosteric interactions or via direct competition for $InsP_6$ binding. The rate-limiting $InsP_7$ synthesis affects the deneddylation rates of the holo-complex. Kinase activity-dependent interaction of IPK1 with CSN2 increases the local synthesis of $InsP_6$, relieving the suppression of ITPK1 activity and enhancing subsequent $InsP_7$ production. Increased concentration of this metabolite stimulates the deneddylation activity of the holo-complex on cullins (ON). The deneddylation activity leads to the dissociation of deneddylated cullins, CSN4, CSN5 and the InsP-kinases from the holo-complex, thereby causing its inactivation (OFF). The dynamics of these processes maintain the equilibrium of active CRLs that, in turn, regulate the steady-state fate and function of SPX4 in phosphate homeostasis and phosphate starvation response. N8, Nedd8; CUL1, Cullin1.

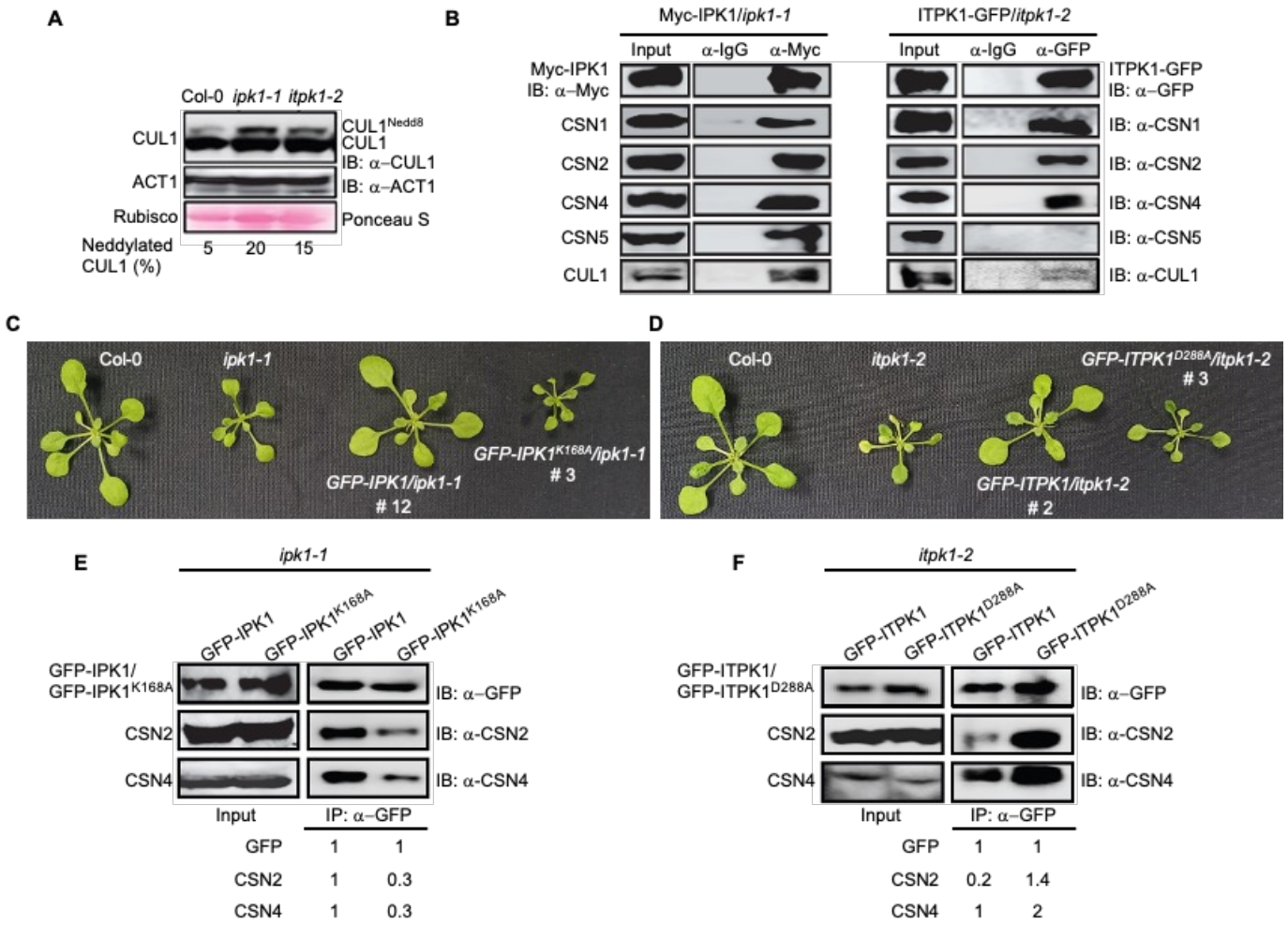

Figure 1. Arabidopsis IPK1 and ITPK1 interact with the CSN holo-complex and modulate its deneddylation activity.

(A) Anti-CUL1 immunoblot showing basal levels of neddylated: unneddylated CUL1 ($CUL1^{Nedd8}$: CUL1) in *ipk1-1* or *itpk1-2* relative to Col-0. Anti-ACT1 immunoblot or Ponceau S staining for rubisco large subunit denote comparable protein loading across samples. The numerical values below the images indicate the percentage of $CUL1^{Nedd8}$ relative to unneddylated CUL1.

(B) Immuno-enrichments (IP) of IPK1 or ITPK1 from the corresponding complemented lines (*Myc-IPK1/ipk1-1* or *ITPK1-GFP/itpk1-2*, respectively) probed (IB) with anti-CSN1/2/4/5, anti-CUL1, anti-Myc, or anti-GFP antibodies. IgG-agarose enrichments were used as negative controls. Respective protein amounts in the input extracts are also indicated.

(C and D) Growth phenotypes of indicated plants at 21 days post-germination.

(E and F) Immuno-enrichment (IP) of GFP-tagged wild-type or kinase-dead versions of IPK1 or ITPK1 from transgenic plants probed (IB) with the indicated CSN antibodies. The numerical values below the images represent the levels of the probed CSN subunit normalized to the corresponding immuno-enriched InsP-kinase. Respective protein amounts in the input extracts are also indicated.

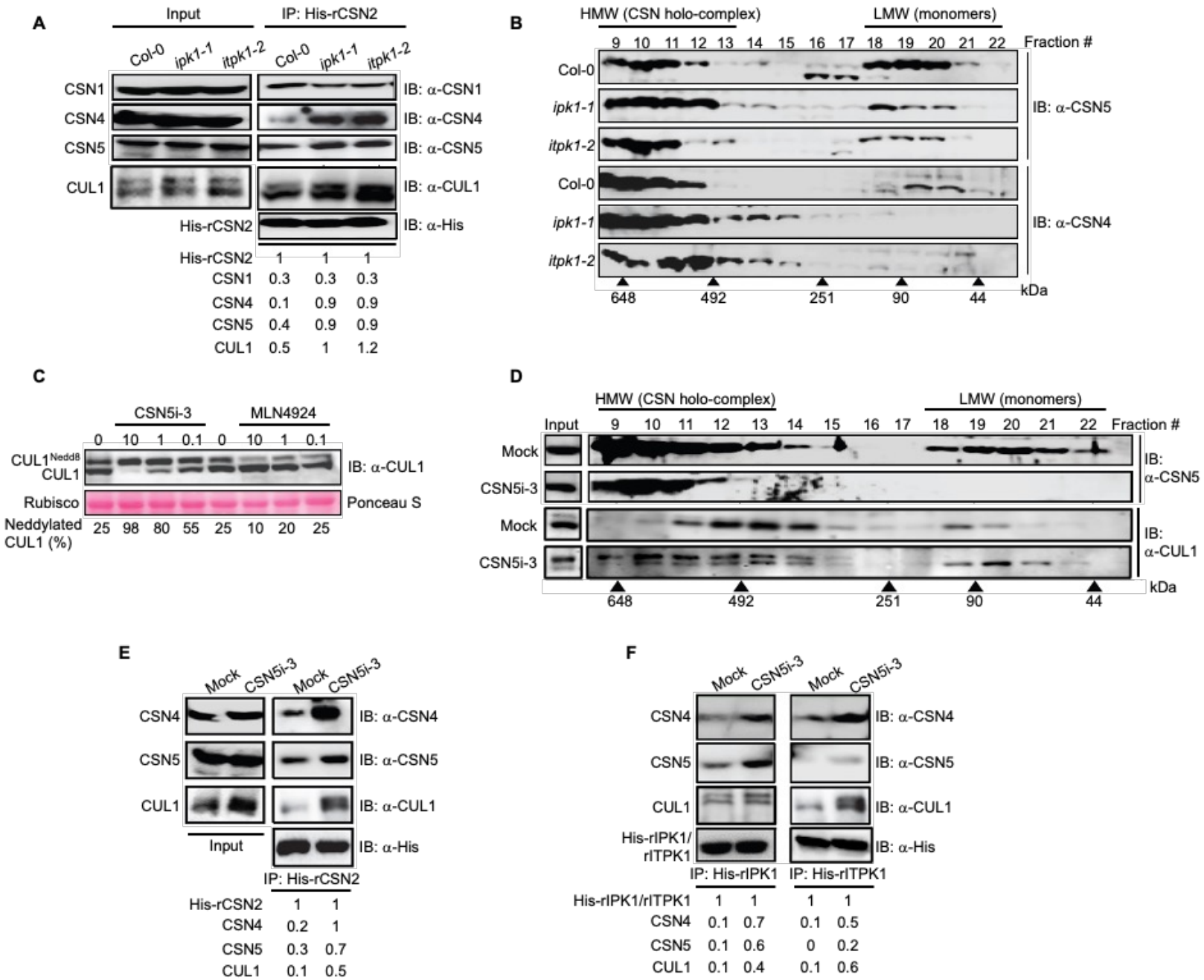

Figure 2. Perturbed InsP-kinase or deneddylation activities disrupt the dissociation equilibrium of CSN4/5 subunits from the holo-complex.

(A) Affinity enrichment (IP) of His-rCSN2 from Col-0, *ipk1-1*, or *itpk1-2* plants probed (IB) with the indicated antibodies. The numerical values below the immunoblots represent the probed CSN subunit, or CUL1 levels normalized to the corresponding amounts of affinity-enriched His-rCSN2. Respective protein amounts in the input extracts are also shown.

(B) Size exclusion CSN5 and CSN4 partitioning profiles from indicated plants probed (IB) with anti-CSN5 or anti-CSN4 antibodies.

(C) Anti-CUL1 blots from control, CSN5i-3, or MLN4924 treated Col-0 samples at 24 hours post-treatment (hpt). Relative migration positions of $CUL1^{Nedd8}$: CUL1 are indicated. Ponceau S staining shows comparable protein loading across samples. The numerical values below the immunoblot images represent the percentage of $CUL1^{Nedd8}$ relative to unneddylated CUL1.

(D) Size exclusion partitioning profile of CSN5 and CUL1 from mock (DMSO) or CSN5i-3 treated Col-0 probed (IB) with anti-CSN5 or anti-CUL1 antibodies.

(E) Affinity enrichment (IP) of His-rCSN2 from control and CSN5i-3-treated plants probed (IB) with the indicated antibodies. The numerical values below the immunoblots represent the CSN subunit or CUL1 amounts relative to the levels of affinity-enriched His-rCSN2.

(F) Affinity enrichment (IP) of His-rIPK1 or His-rITPK1 from control and CSN5i-3-treated plants probed (IB) with the indicated antibodies. The numerical values below the immunoblots indicate the CSN subunit or CUL1 amounts normalized to the corresponding affinity-enriched recombinant InsP-kinase.

In all fractionation data, the fraction numbers and elution positions of molecular weight standards (in kDa) are marked. HMW (high molecular weight) or LMW (low molecular weight) refers to the expected partitioning positions of CSN holo-complex and subunit monomers, respectively. Protein amounts in the input extracts are also indicated for the respective blots.

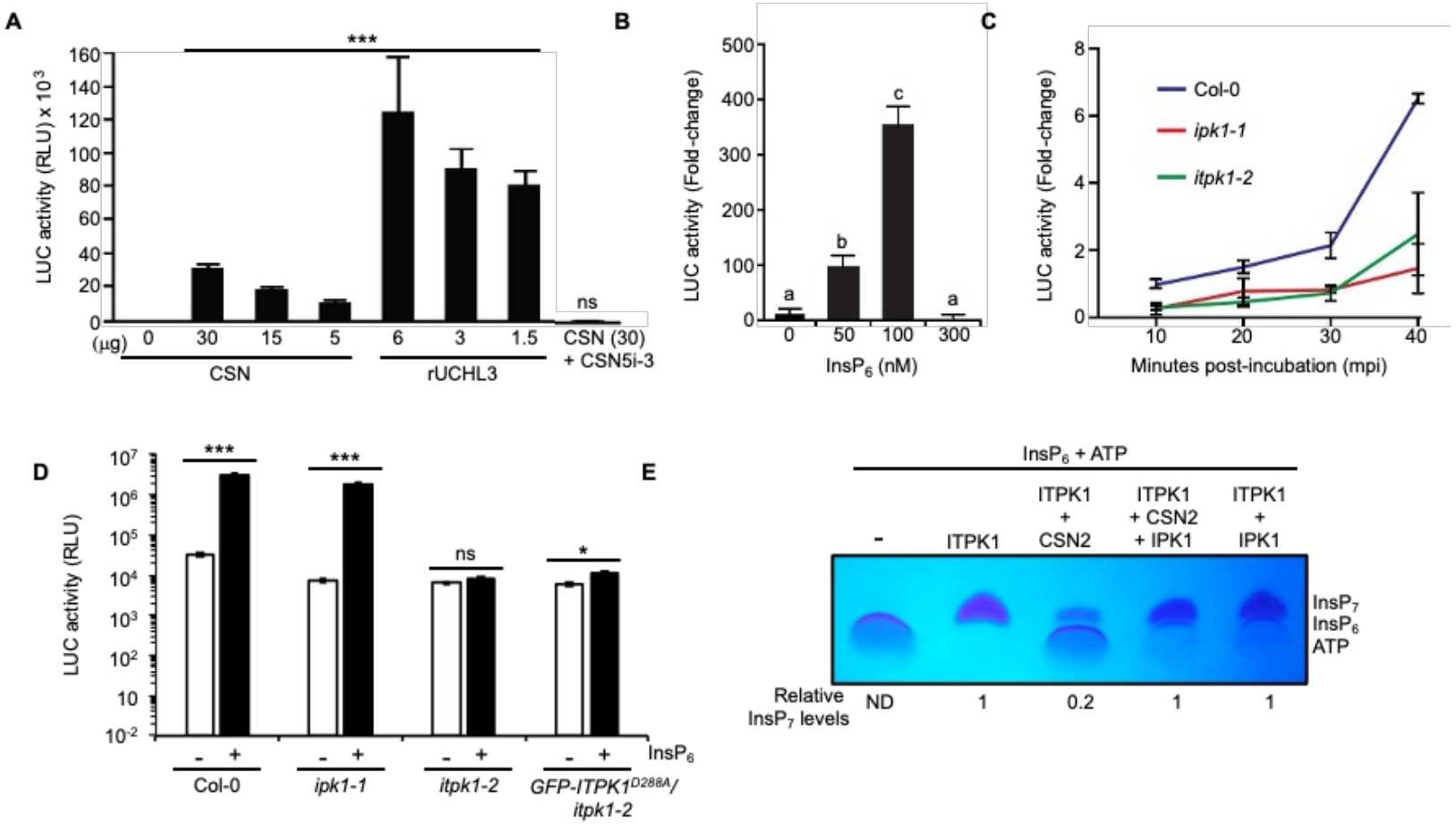

Figure 3. $InsP_6$ potentiation on CSN deneddylase activity requires a kinase-active ITPK1.

(A) *In vitro* deneddylation activity of isolated Col-0 CSN holo-complex on Nedd8-AML substrate. Indicated amounts (in µg) of total CSN holo-complex co-fractionated proteins, or recombinant rUCHL3 were incubated with Nedd8-AML and the Luciferase activity measured. The inhibition assay was performed with CSN5i-3 (10 µM) supplemented to the CSN holo-complex protein pool (30 µg).

(B) Dose-dependent enhancement in deneddylation activity of isolated Col-0 CSN holo-complex in the presence of indicated amounts of $InsP_6$.

(C) Kinetics of deneddylation rates by the CSN holo-complex isolated from *ipk1-1* or *itpk1-2* plants relative to Col-0. Time points of incubation (mpi, minutes post-incubation) with the substrate are indicated.

(D) Deneddylation activity of isolated CSN holo-complex from the indicated plants supplemented with or without $InsP_6$ (50 nM).

(E) $InsP_7$ synthesis *in vitro* by ITPK1 is inhibited by CSN2 and restored by IPK1. Numerical values below the gel image represent $InsP_7$ levels relative to the only ITPK1 reaction.

Data shown is mean ± SD (n=3) and represented as relative luminescence units (RLU) **(A and D)**, or relative to minus $InsP_6$ sample **(B)**, or as fold-change relative to Col-0 **(C)**. Statistical analysis is according to **(A and D)** Student's *t*-test with pairwise comparison to minus CSN holo-complex protein samples, (***$P<0.0001$, ns= not significant), or **(B)** with ANOVA (Tukey, $p < 0.05$).

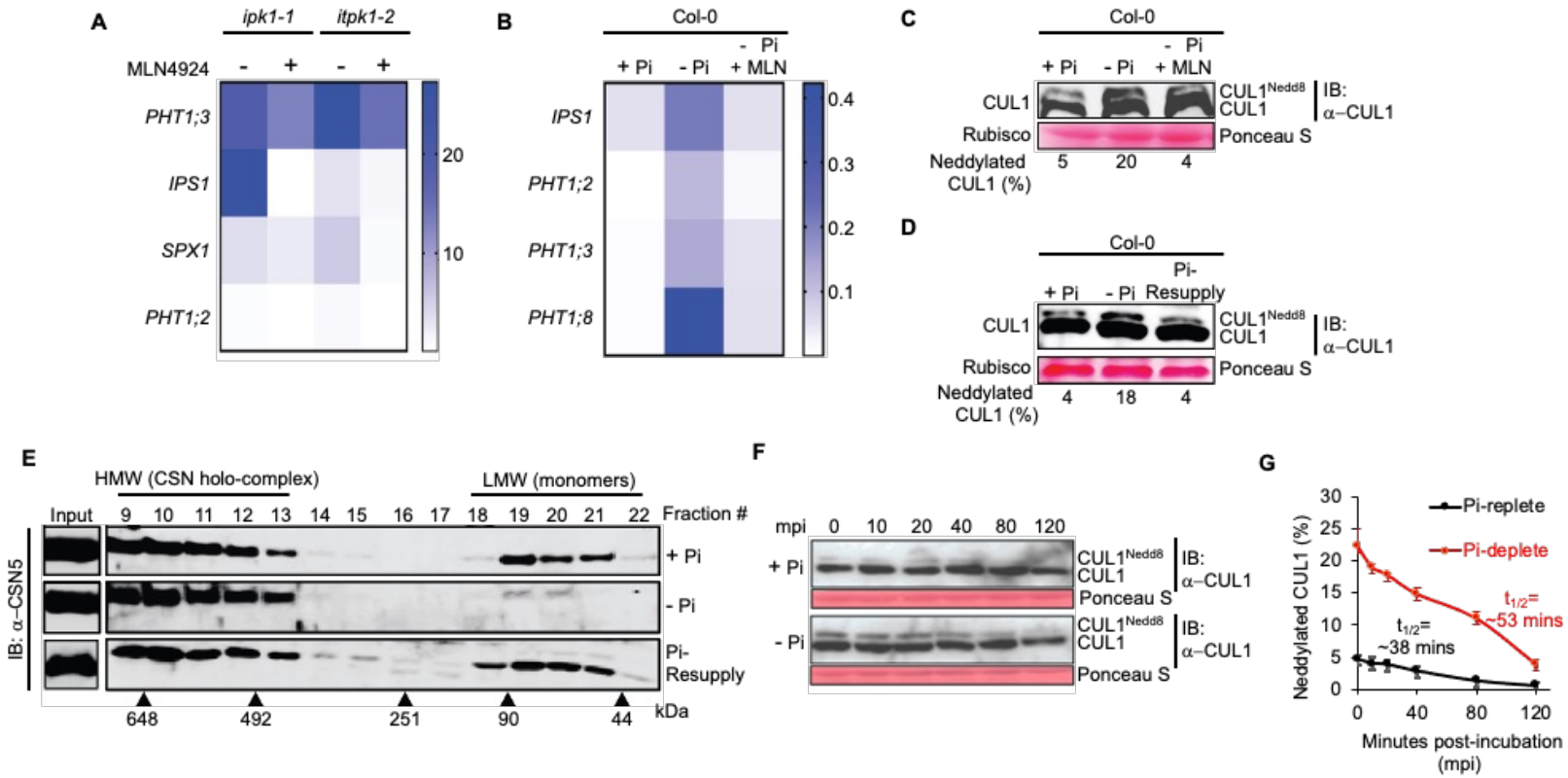

Figure 4. InsP-kinase and CUL^{Nedd8} activities are essential for *PSI*-gene induction during PSR.

(A and B) *PSI*-gene expression in *ipk1-1, itpk1-2,* or in Pi-replete (+Pi) or Pi-deplete (-Pi) Col-0 in the presence or absence of MLN4924. Gene expressions are relative to *MON1* internal control. Data is mean ± SD (n=3). Heatmaps were generated using GraphPad Prism 8.4.3 software using the single gradient function.

(C and D) Anti-CUL1 immunoblot showing relative levels of neddylated: unneddylated CUL1 (CUL1^{Nedd8}: CUL1) in the indicated samples (+Pi: Pi-replete; -Pi: Pi-deplete; -Pi + MLN: Pi-deplete samples treated with MLN4924; Pi-Resupply: Pi-deplete samples replenished with Pi).

(E) Size exclusion fractionation profile of CSN5 from extracts of Pi-replete (+Pi), Pi-deplete (-Pi), or Pi-Resupply plants. Fraction numbers, elution positions of molecular weight standards (in kDa), and expected fractions indicative of CSN holo-complex-incorporated (HMW) or free CSN5 subunit monomers (LMW) are marked. Input panels show protein amounts in the total extracts.

(F) *In lysate* deneddylation assays at indicated time points (mpi, minutes post-incubation) on Pi-replete or Pi-deplete Col-0 extracts probed (IB) with anti-CUL1 antibodies.

(G) Scatter plot showing the half-life of CUL1^{Nedd8} in the Pi-replete or Pi-deplete Col-0 extracts.

In the above immunoblots, the relative migration positions of CUL1^{Nedd8}: CUL1 are marked. Ponceau S staining denotes comparable protein loading across samples. The numerical values below images **(C and D)** represent the percentage of CUL1^{Nedd8} relative to unneddylated CUL1.

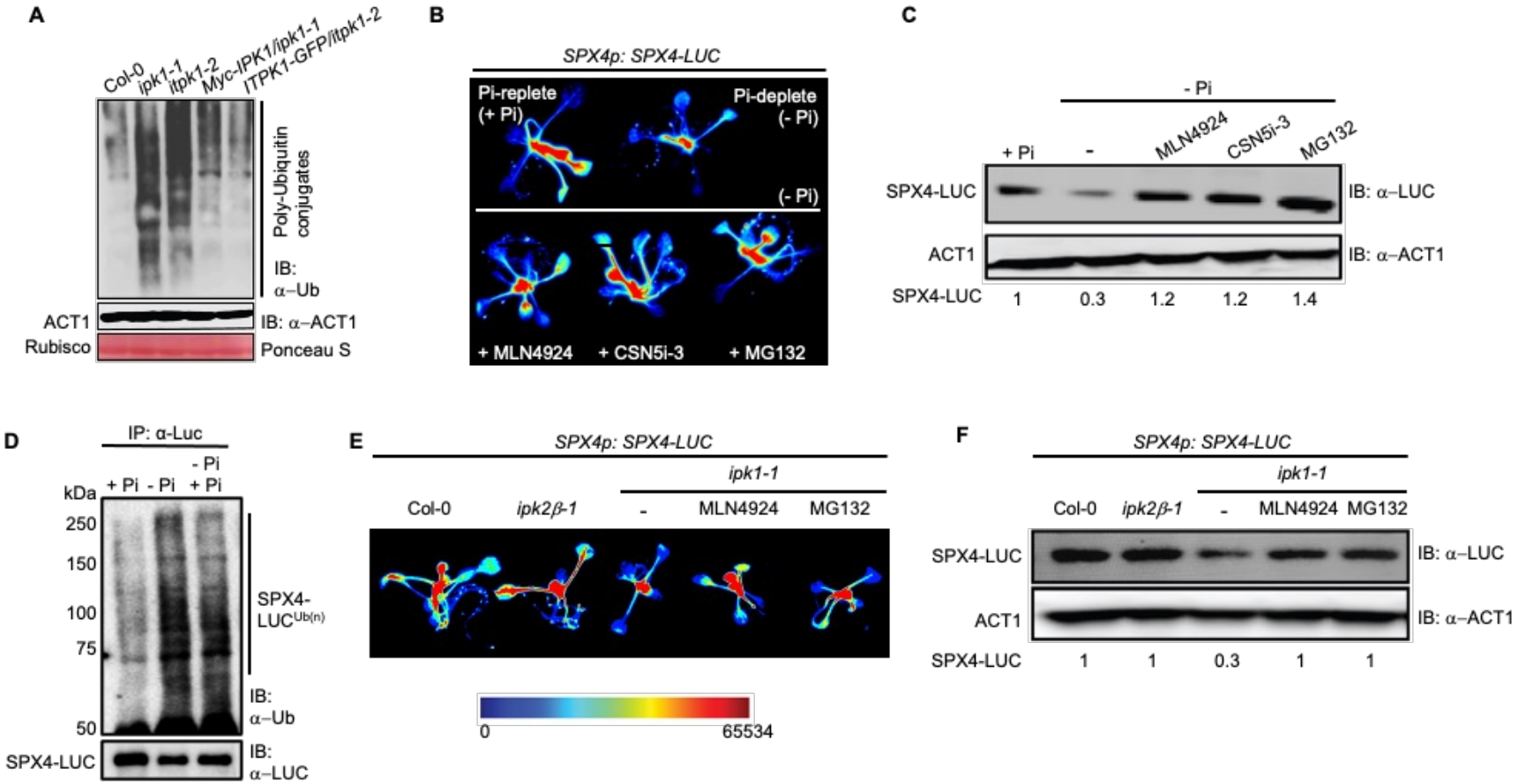

Figure 5. Activated CRLs target SPX4 degradation during PSR.

(A) Total poly-ubiquitin conjugates in protein extracts of Col-0, *ipk1-1, itpk1-2,* and the respective complemented lines, detected with anti-Ub antibodies.

(B and C) LUC luminescence and SPX4-protein levels in the *SPX4p:SPX4-LUC* transgenic plants subjected to Pi-replete (+Pi), or Pi-deplete (-Pi) conditions in the absence or presence of MLN4924, MG132, or CSN5i-3.

(D) Polyubiquitinated SPX4-LUC in +Pi, -Pi and Pi-resupply (-Pi + Pi) detected via immuno-enrichment (IP) with anti-LUC antibodies and probed (IB) with anti-Ub antibodies. Relative levels of unmodified SPX4-LUC are shown with anti-LUC immunoblot. Migration position of molecular weight standards (in kDa) are indicated.

(E and F) LUC luminescence and SPX4-protein levels in *SPX4p:SPX4-LUC* plants in wild-type (Col-0), *ipk2β-1*, untreated *ipk1-1*, and *ipk1-1* treated with MLN4924 or MG132 inhibitors.

Anti-ACT1 immunoblot or Ponceau S staining for rubisco large subunit represents comparable protein loading across samples. Numerical values below the immunoblots **(C and F)** represent SPX4-LUC levels normalized to the corresponding ACT1 levels.

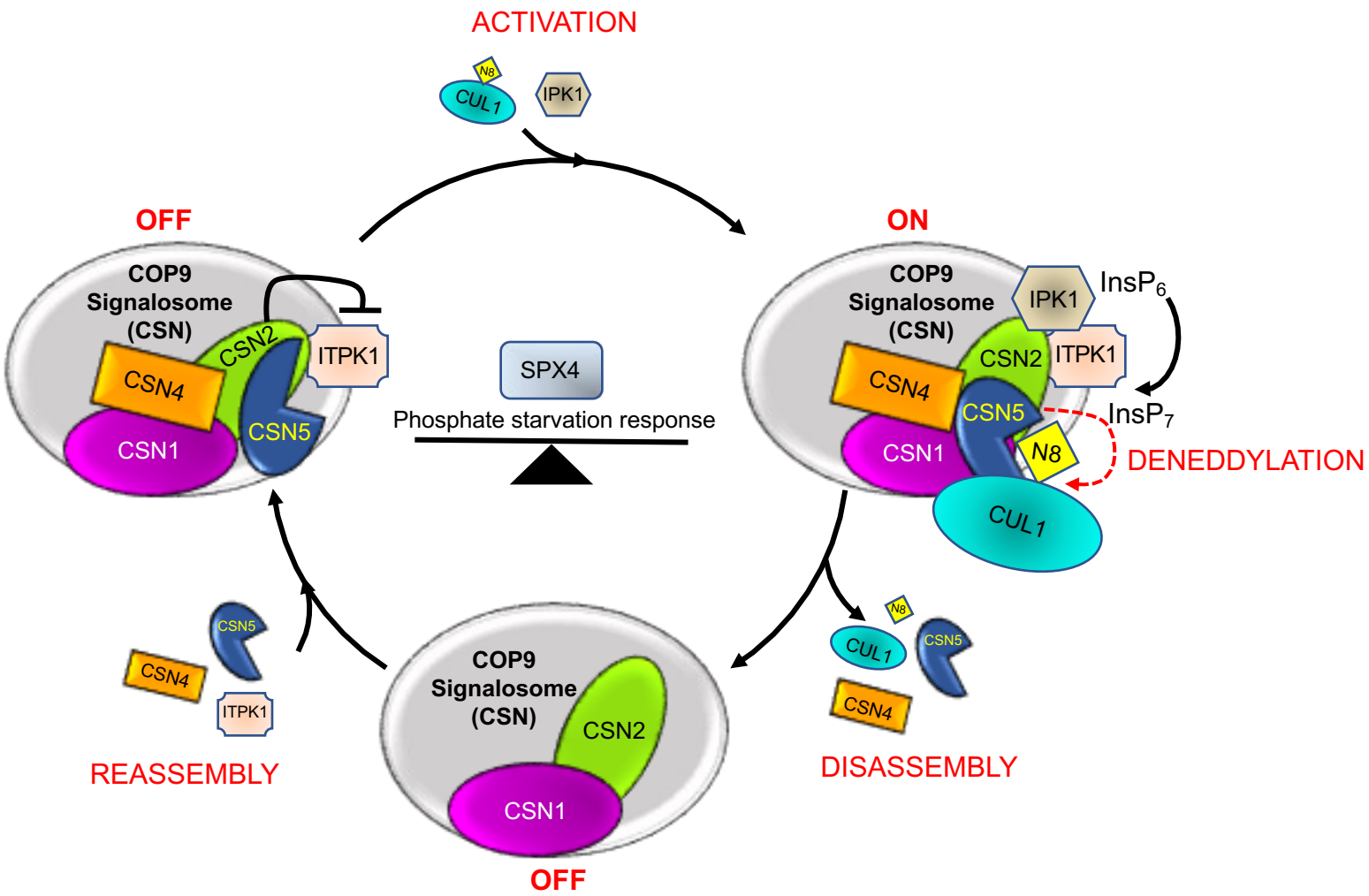

Figure 6. Schematic model of dynamics of COP9 signalosome (CSN) deneddylation cycles regulated by IPK1 and ITPK1.
The kinase activity of ITPK1 at the CSN platform is inhibited by CSN2, either through allosteric interactions or via direct competition for $InsP_6$ binding. The rate-limiting $InsP_7$ synthesis affects the deneddylation rates of the holo-complex. Kinase activity-dependent interaction of IPK1 with CSN2 increases the local synthesis of $InsP_6$, relieving the suppression of ITPK1 activity and enhancing subsequent $InsP_7$ production. Increased concentration of this metabolite stimulates the deneddylation activity of the holo-complex on cullins (ON). The deneddylation activity leads to the dissociation of deneddylated cullins, CSN4, CSN5 and the InsP-kinases from the holo-complex, thereby causing its inactivation (OFF). The dynamics of these processes maintain the equilibrium of active CRLs that, in turn, regulate the steady-state fate and function of SPX4 in phosphate homeostasis and phosphate starvation response. N8, Nedd8; CUL1, Cullin1.

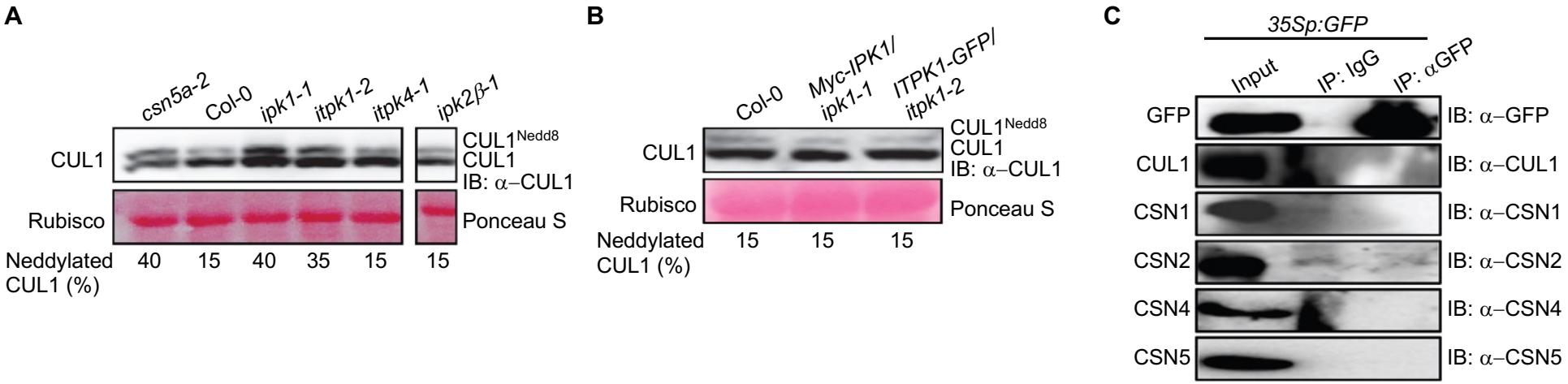

Supplementary Figure 1. Increased CUL1^{Nedd8}: CUL1 ratios are specific to *ipk1-1* or *itpk1-2* but not other InsP-kinase mutants.

(A and B) Anti-CUL1 immunoblot showing relative levels of neddylated: unneddylated CUL1 (CUL1^{Nedd8}: CUL1) in the indicated plant lines. Comparable protein loading between samples is shown by Ponceau S staining for rubisco large subunit. The numerical values below each lane represents the percentage of CUL1^{Nedd8} relative to unneddylated CUL1 for the corresponding sample.

(C) Anti-GFP or anti-IgG-enrichments (IP) from control *35Sp:GFP*-expressing transgenic plants probed (IB) with the indicated antibodies. Relative protein amounts in the input extracts are also shown.

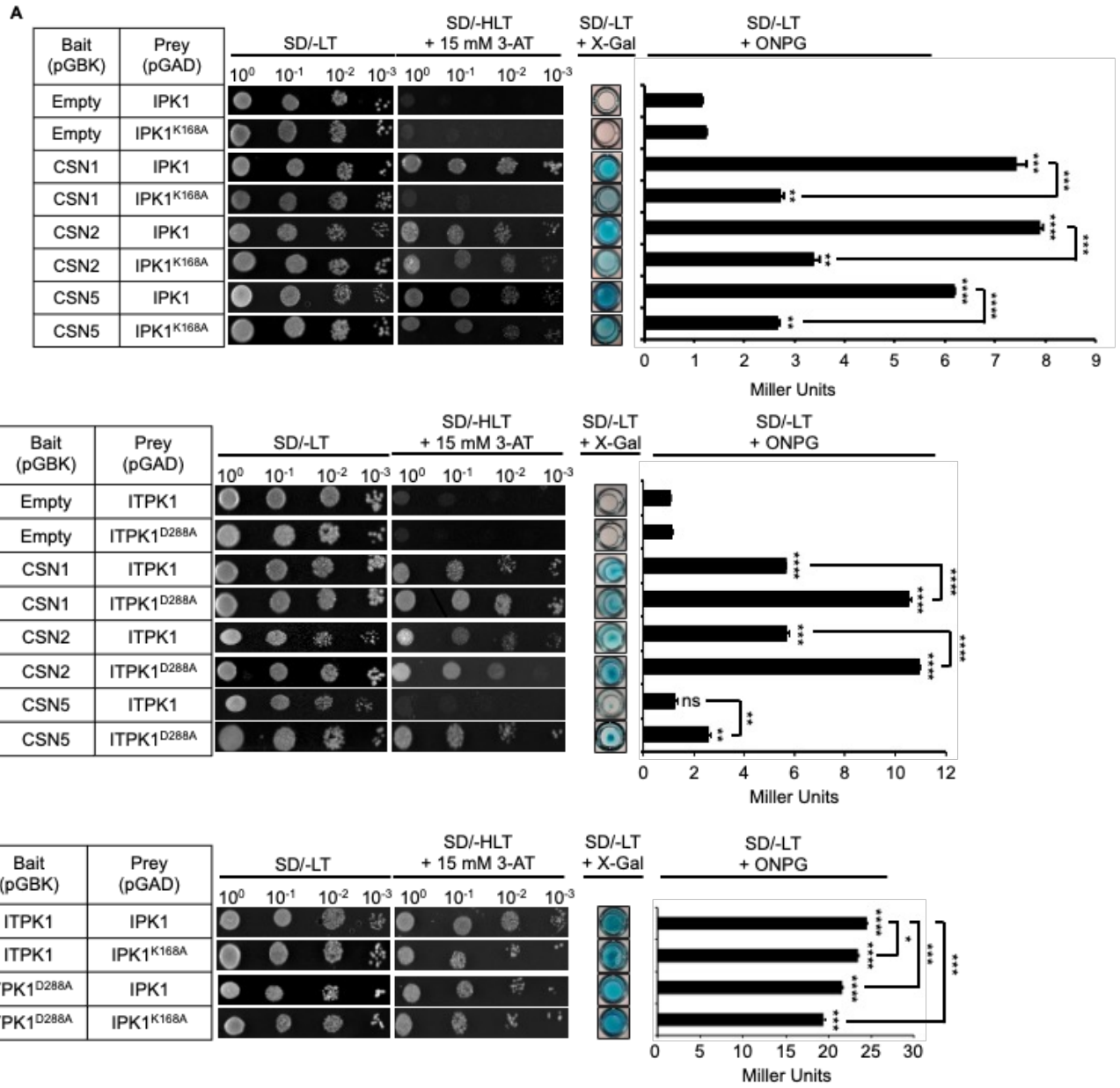

Supplementary Figure 2. Kinase domains of IPK1 and ITPK1 affect their interaction with CSN subunits, but not with each other.

(A) Yeast two-hybrid assays showing stronger interaction of kinase-proficient (IPK1) than kinase-deficient IPK1 ($IPK1^{K168A}$) with CSN1, CSN2, and CSN5 subunits.

(B) Yeast two-hybrid assays showing stronger interaction of kinase-deficient ($ITPK1^{D288A}$) than kinase-proficient ITPK1 (ITPK1) with CSN1, CSN2, and CSN5 subunits.

(C) Yeast two-hybrid assays showing mutual interaction of kinase-deficient and kinase-proficient IPK1 and ITPK1 (ITPK1) with each other.

Yeast transformants containing the indicated bait and prey combinations were plated with the indicated serial dilution on SD/-LT or SD/-HLT + 15 mM 3-AT plates, and the growth of cells was recorded after 3 days. Qualitative X-Gal assays were performed with permeabilized yeast transformants, and the images were acquired 12 hours post-incubation. Quantitative ONPG assays were performed with lysates from the indicated transformants, and color development was measured using a spectrophotometer (420 nm). For each assay , n=3-5.

Statistical analysis is according to Student's *t*-test : firstly, between indicated combinations of the tested InsP-kinase (wild-type or kinase-dead mutant) prey and empty or the indicated CSN subunit bait; secondly, between the indicated combinations of the wild-type InsP-kinase or its kinase-dead prey version with a tested CSN subunit bait; thirdly, between the indicated combinations of wild-type IPK1 and ITPK1 or their indicated kinase dead version (*$P<0.05$, **$P<0.01$, ***$P<0.001$, ****$P<0.0001$, ns=not significant).

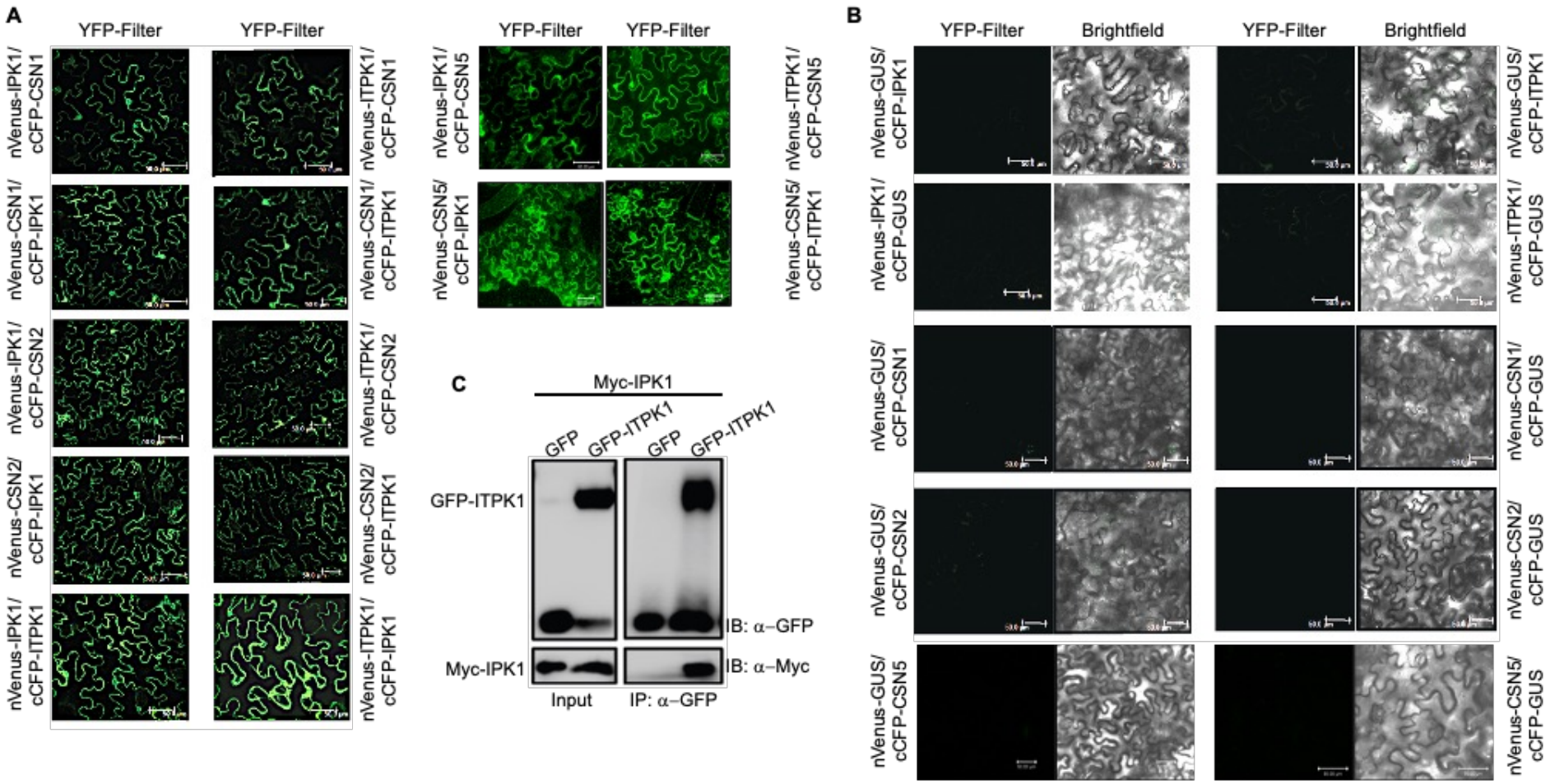

Supplementary Figure 3. ***In vivo*** **interactions between IPK1, ITPK1 and CSN subunits.**

(A) Confocal images of BiFC assays showing interactions between IPK1 and ITPK1 and with CSN1, CSN2, and CSN5 subunits.

(B) Lack of interactions between the negative control GUS with IPK1, ITPK1, CSN1, CSN2 or CSN5.

Images were acquired at 48 hpi (hours post-infiltration) with YFP and brightfield filters. Figures are representative of multiple images obtained for each BiFC combination. Scale bar = 50 μM.

(C) Co-immunoprecipitation of transiently expressed GFP-ITPK1 with Myc-IPK1. Anti-GFP pulldown (IP) from GFP alone or GFP-ITPK1 co-expressed with Myc-IPK1 were probed (IB) with anti-GFP or anti-Myc antibodies. Protein amounts in the input samples are indicated.

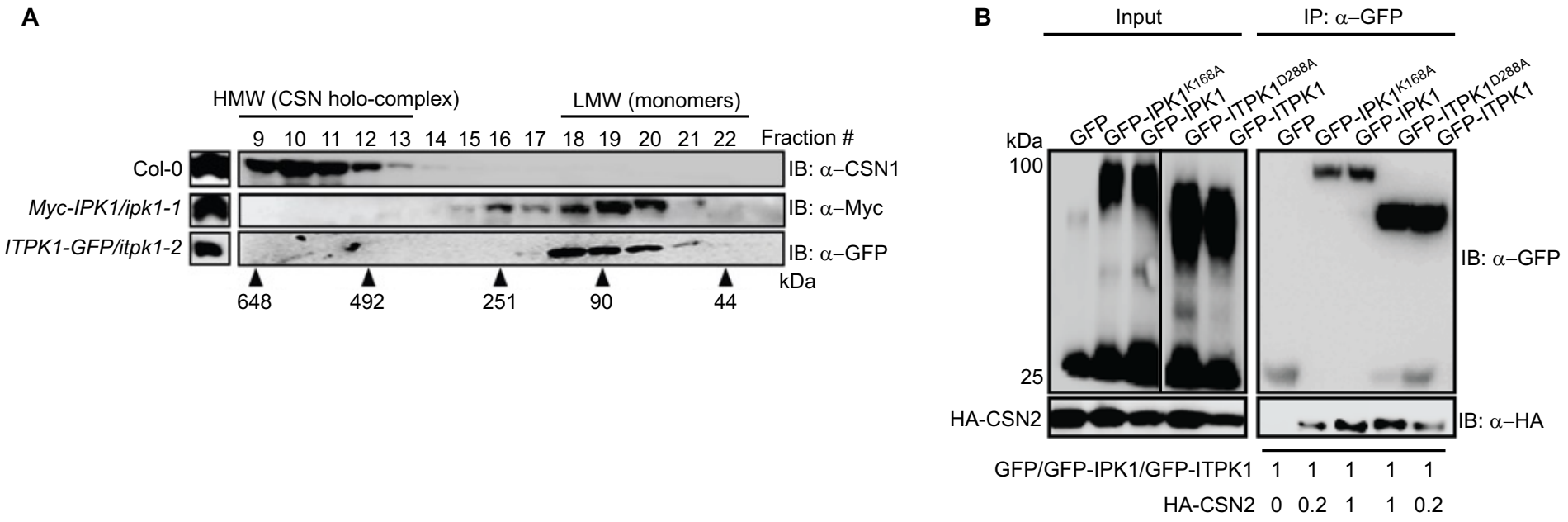

Supplementary Figure 4. CSN2 associations of IPK1 and ITPK1 are conversely affected by their catalytic activities.

(A) Gel-filtration fractionation pattern of Myc-IPK1 or ITPK1-GFP probed (IB) with the indicated antibodies. Fraction numbers and elution positions of molecular weight standards (in kDa) are indicated. CSN1 partitioning profile was used as a reference for the elution pattern of the CSN holo-complex.

(B) Immuno-enrichment of GFP-tagged wild-type or kinase-dead IPK1^{K168A} or ITPK1^{D288A} co-expressed with HA-CSN2 in *N. benthamiana* leaves. Pull-down (IP) was performed with anti-GFP antibodies and the bound proteins were probed (IB) with anti-GFP or anti-HA antibodies. The migration position of molecular weight standards (in kDa) and the total protein amounts in the extracts (input) are shown. The numerical values below the IP image represents the relative CSN2 amounts normalized to the corresponding enriched GFP-tagged InsP-kinase.

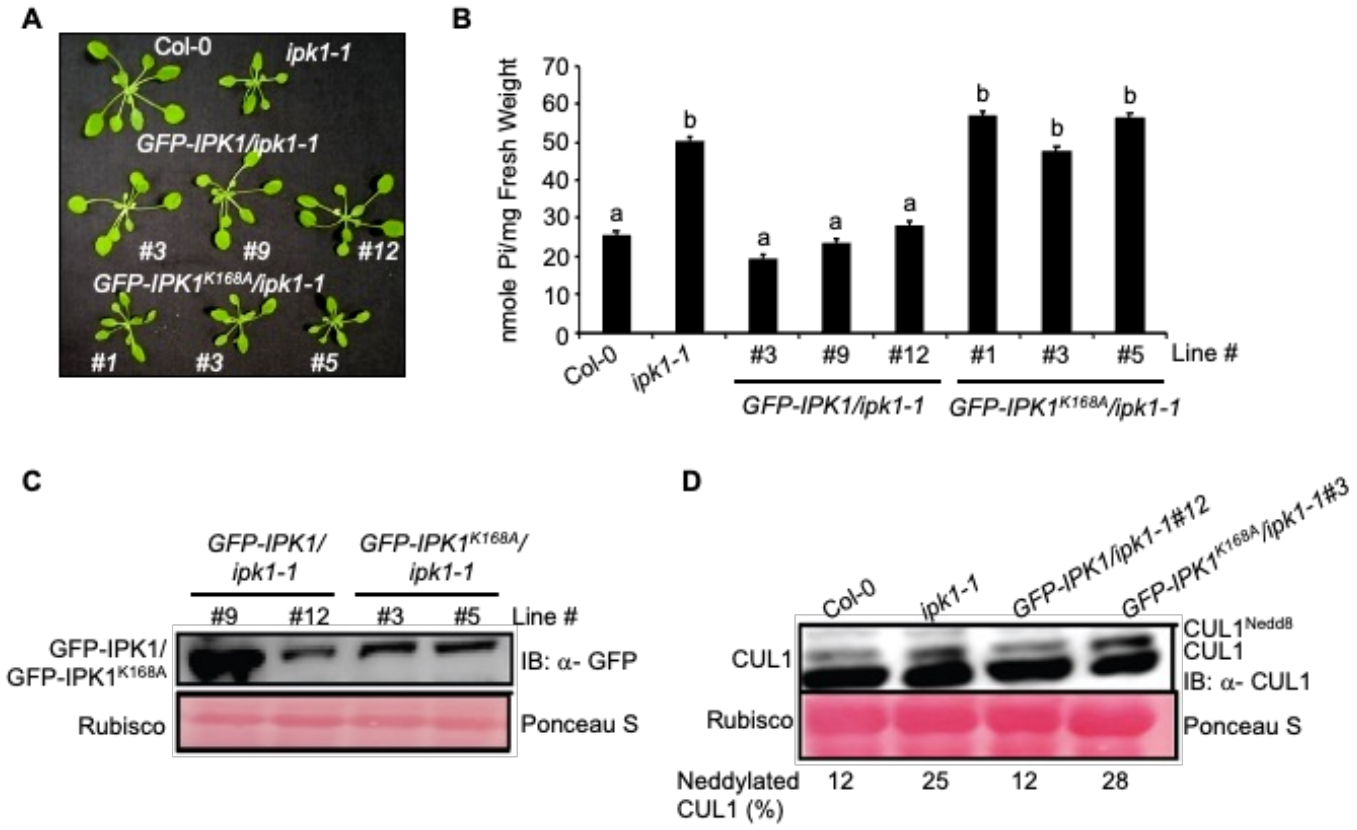

Supplementary Figure 5. Kinase-proficient, but not kinase-deficient IPK1, restore *ipk1-1* defects.

(A) Growth phenotypes of independent transgenic lines of *ipk1-1* plants expressing *GFP-IPK1* or *GFP-IPK1^{K168A}*.

(B) Endogenous Pi levels in the indicated genotypes. The data shown is mean ± SD (n=6-7). Different alphabets indicate significant differences ($P < 0.05$, ANOVA, Tukey) between samples.

(C) Expression levels of GFP-IPK1 or GFP-IPK1^{K168A} in the indicated transgenic lines probed with anti-GFP antibodies.

(D) Relative CUL1^{Nedd8}:CUL1 levels in the indicted plant lines probed (IB) with anti-CUL1 antibodies. Relative migration positions of CUL1^{Nedd8} and CUL1 are marked. The numerical values below the image represent the percentage of CUL1^{Nedd8} relative to unneddylated CUL1 for the corresponding sample.

Ponceau S staining shows loading controls.

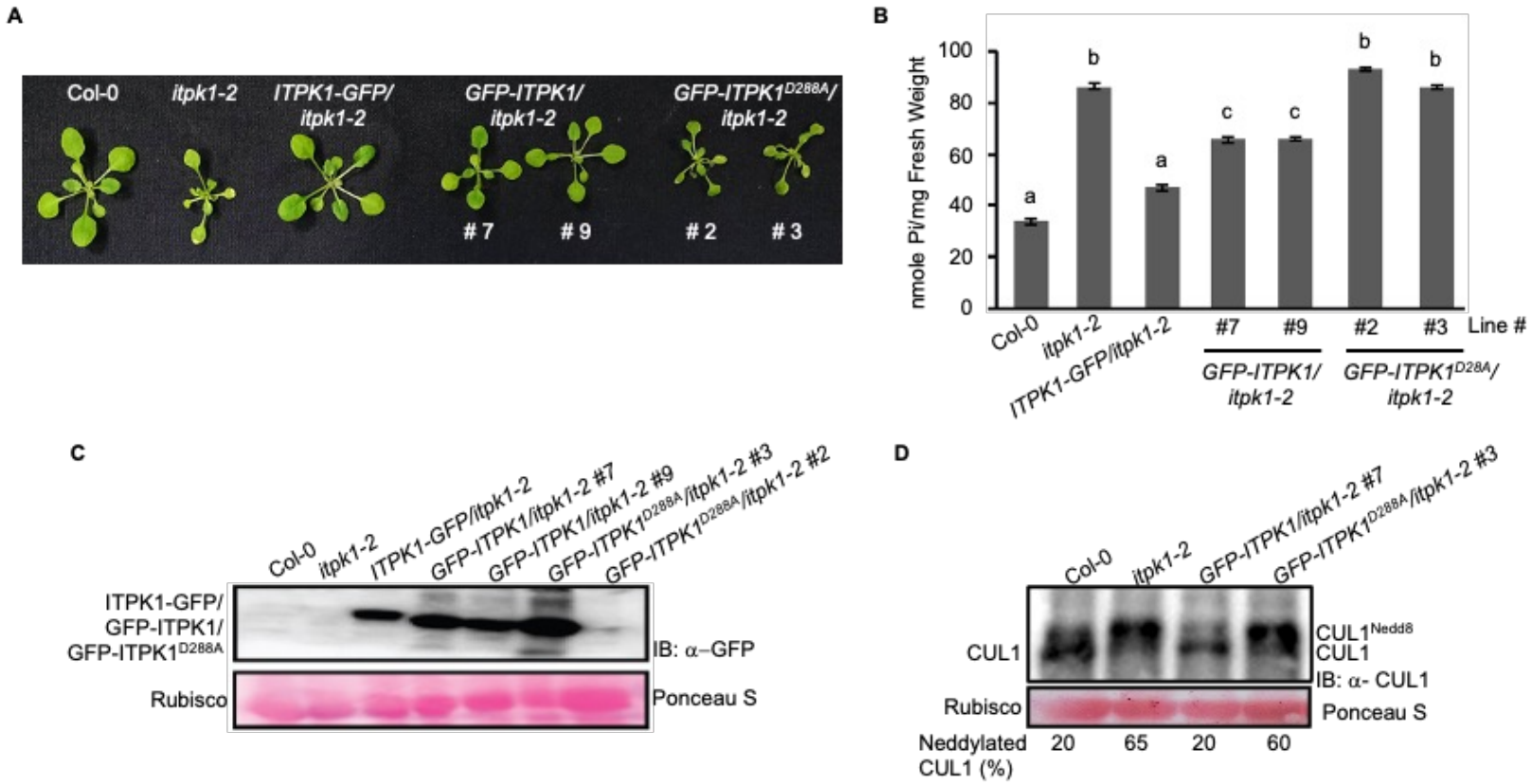

Supplementary Figure 6. Kinase-proficient, but not kinase-deficient ITPK1, restore *itpk1-2* defects.

(A) Growth phenotypes of independent transgenic lines of *itpk1-2* plants expressing *GFP-ITPK1* or *GFP-ITPK1^{D288A}*.

(B) Endogenous Pi levels in the indicated genotypes. The data shown is mean ± SD (n=6-7). Different alphabets indicate significant differences ($P < 0.05$, ANOVA, Tukey) between samples.

(C) Expression levels of GFP-ITPK1 or GFP-ITPK1^{D288A} in the indicated transgenic lines probed with anti-GFP antibodies.

(D) Relative CUL1^{Nedd8}:CUL1 levels in the indicted plant lines probed (IB) with anti-CUL1 antibodies. The migration positions of CUL1^{Nedd8} and CUL1 are marked. The numerical values below the image represent the percentage of CUL1^{Nedd8} relative to unneddylated CUL1 for the corresponding sample.

Ponceau S staining shows loading controls.

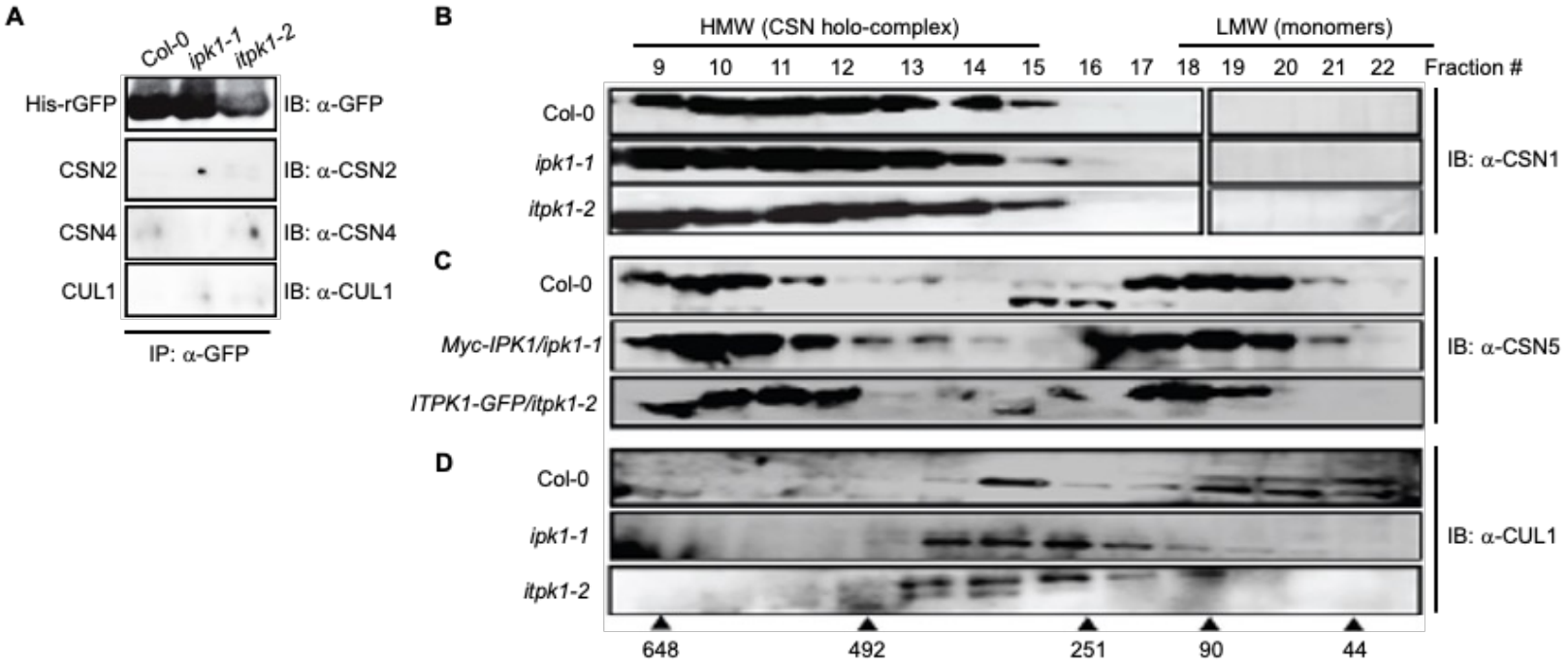

Supplementary Figure 7. Fractionation profiles of CSN subunits and CUL1 in the indicated plants.

(A) Control His-rGFP enrichments (IP) from supplemented extracts of indicated plants probed (IB) with the various antibodies.

(B) Size exclusion partitioning profile of CSN1 from Col-0, *ipk1-1*, and *itpk1-2* extracts. The blots were probed (IB) with anti-CSN1 antibodies.

(C) Size exclusion partitioning profile of CSN5 Col-0, and the complemented lines of *ipk1-1* and *itpk1-2* (*Myc-IPK1/ipk1-1* and *ITPK1-GFP/itpk1-2*, respectively) extraxts. The blots were probed (IB) with anti-CSN5 antibodies.

(D) Size exclusion partitioning profile of CUL1 from Col-0, *ipk1-1*, and *itpk1-2* extracts. The blots were probed (IB) with anti-CUL1 antibodies.

The migration positions of molecular weight standards (in kDa) are shown.

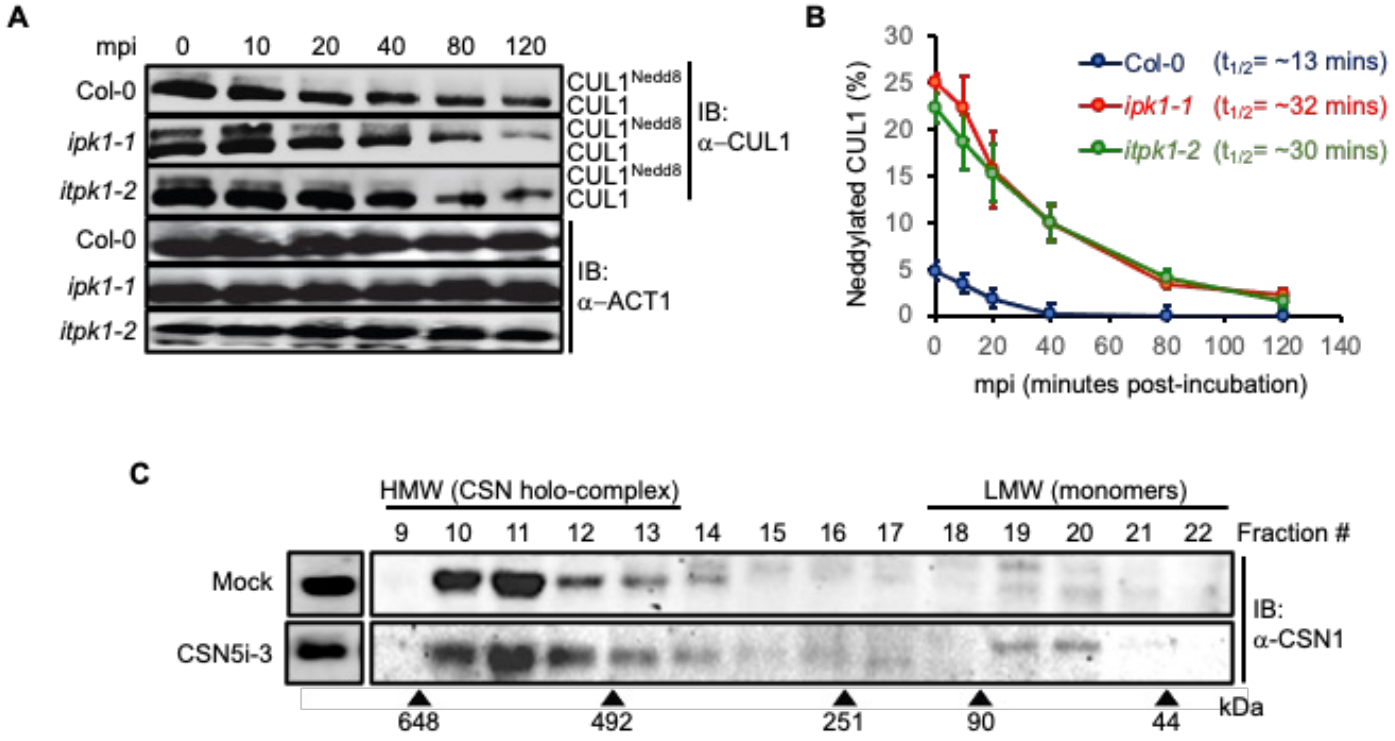

Supplementary Figure 8. CUL1 Deneddylation rates are reduced in the InsP-kinase mutants.

(A) *In lysate* deneddylation assay in Col-0, *ipk1-1*, and *itpk1-2* plants. Total extracts were incubated for indicated time points (mpi, minutes post-incubation) and probed (IB) with anti-CUL1 or anti-ACT1 antibodies.

(B) Scatter plot showing half-life $CUL1^{Nedd8}$ in the indicated plant extracts.

(C) Size exclusion partitioning profile of CSN1 from control (mock) and CSN5i-3 treated Col-0 samples at 24 hours post-treatment (hpt). The migration positions of molecular weight standards (in kDa) are shown.

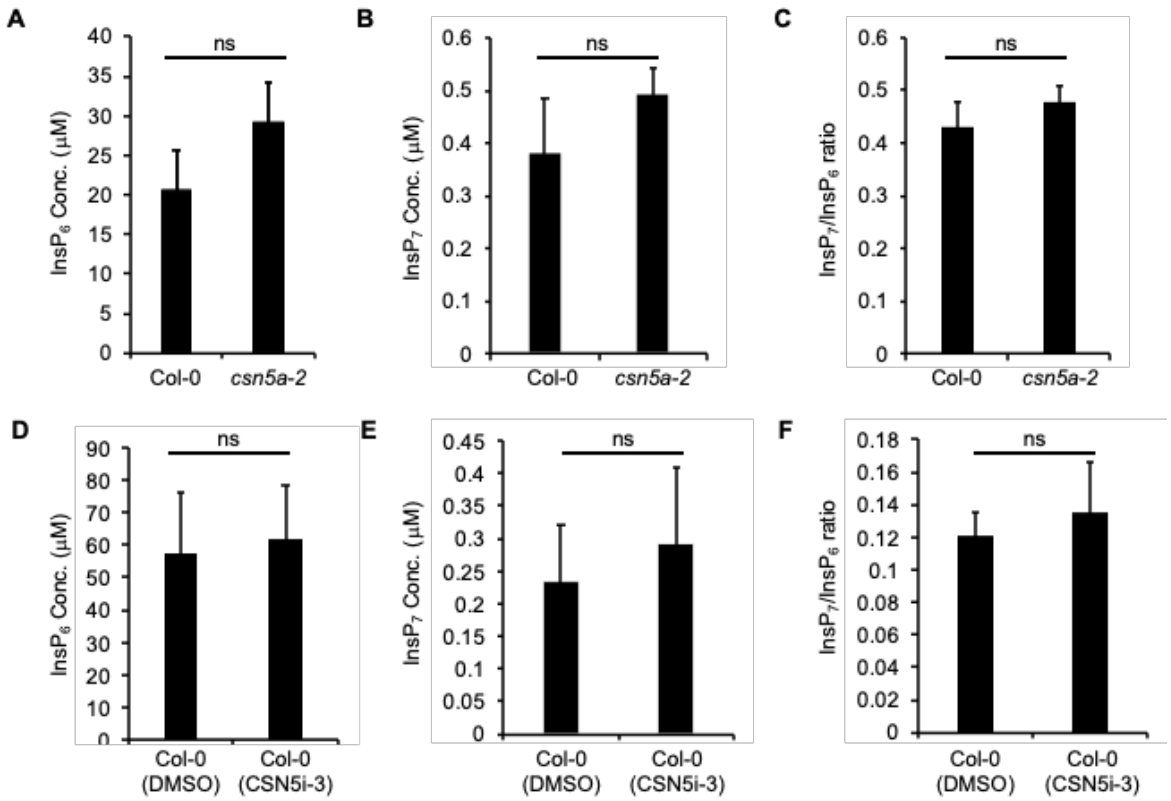

Supplementary Figure 9. $InsP_{6/7}$ levels are unaffected in *csn5a-2* plants or upon CSN5i-3 treatment on Col-0.

(A to C) CE-ESI-MS analysis of $InsP_6$, $InsP_7$ levels and $InsP_6/InsP_7$ ratio in Col-0 and *csn5a-2* plants.

(D to F) CE-ESI-MS analysis of $InsP_6$, $InsP_7$ levels and $InsP_6/InsP_7$ ratio in CSN5i-3-treated and untreated (DMSO) Col-0.

Data shown here is means ± SE (n = 3). Statistical analysis is according to Student's *t*-test (ns= non-significant).

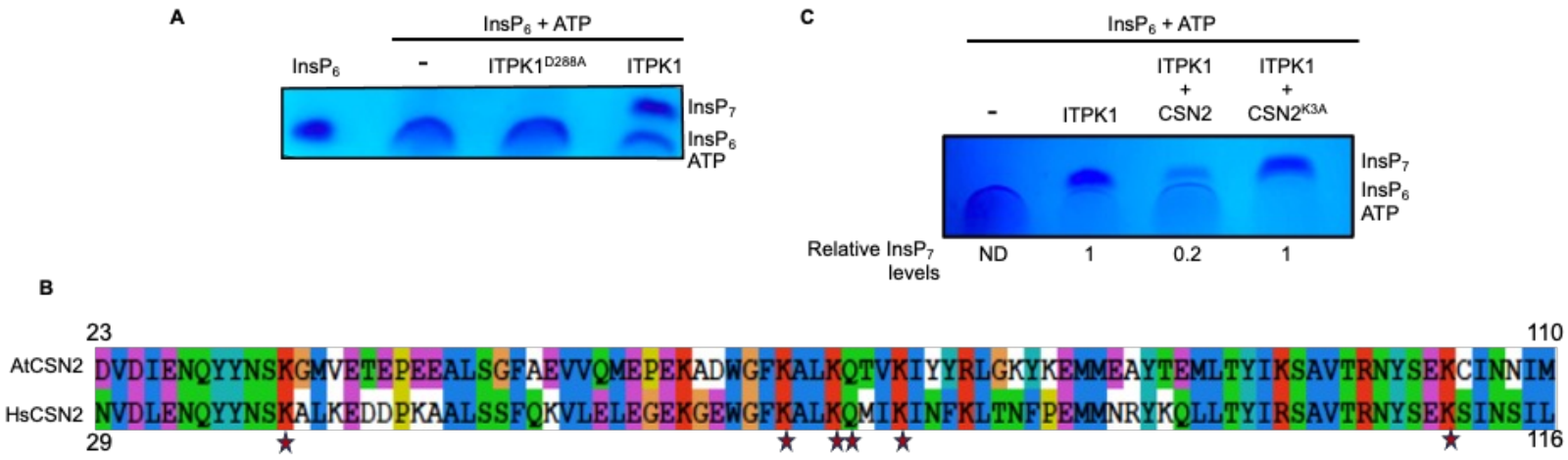

Supplementary Figure 10. Competitive inhibition on ITPK1 kinase activity by CSN2, but not by CSN2^{K3A}.

(A) PAGE analysis of *in vitro* ITPK1 kinase reaction.

(B) Alignment of AtCSN2 and HsCSN2 sequences. The $InsP_6$-binding residues in HsCSN2 and conserved in AtCSN2 are marked with a star sign.

(C) PAGE analysis of *in vitro* ITPK1 kinase reaction in the presence of wild-type and CSN2^{K3A} mutant. The numerical values below the gel image represent $InsP_7$ levels relative to the ITPK1 alone reaction.

The relative migration positions of $InsP_7$, $InsP_6$, and ATP are shown.

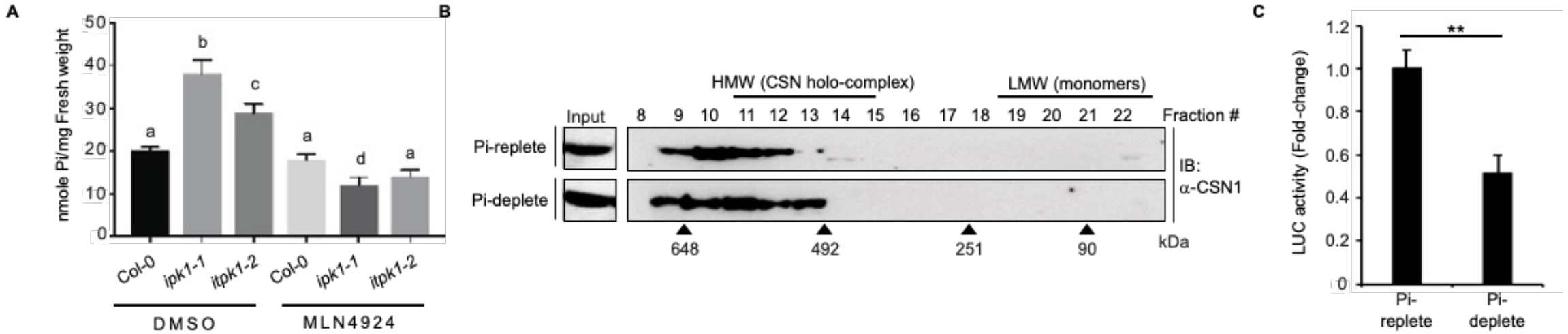

Supplementary Figure 11. MLN4924 suppresses high endogenous Pi accumulation in the InsP kinase mutants.

(A) Endogenous Pi levels in mock-(DMSO) or MLN4924-treated Col-0, *ipk1-1*, or *itpk1-2* plants. The data shown is mean ± SD (n=6-7). Different alphabets indicate significant differences ($P < 0.05$, ANOVA, Tukey) between samples.

(B) CSN1 fractionation profile in Pi-replete or Pi-deplete Col-0 extracts detected via immunoblot (IB) with anti-CSN1 antibodies. Fraction numbers and elution positions of molecular weight standards (in kDa) are marked. CSN1 levels in the input extracts are shown.

(C) Deneddylation activity of isolated CSN holo-complex from the indicated plants tested on Nedd8-AML substrate. LUC activity is presented as fold-change relative to Pi-replete data. Statistical analysis is according to Student's *t*-test (**$P<0.01$).

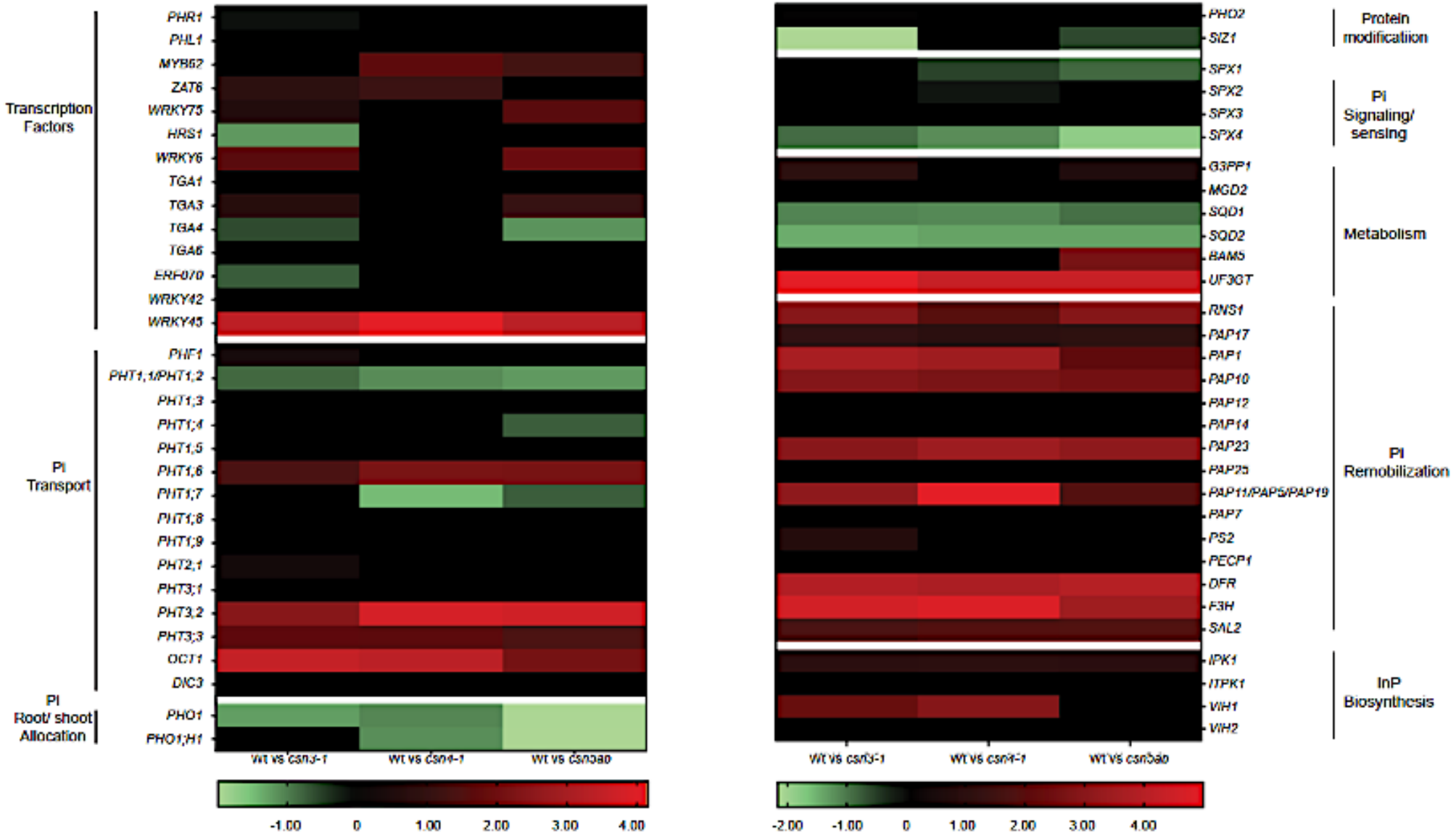

Supplementary Figure 12. Differential expression of *PSI*-genes in *csn* mutants relative to wild-type plants (Wt).

The data was curated from Dohmann *et al* (2008). The heatmap is generated using Graphpad Prism 8.4.3 using double gradient Heatmap function. The expression change is shown as $\log_2$FC (Fold-Change) values of different genes with Green for downregulated genes, Red for upregulated genes and black for either genes which show no change or the genes with expression values which are not significant (Adjusted $P > 0.10$). Functional categorizations are according to Kuo *et al* (2014).

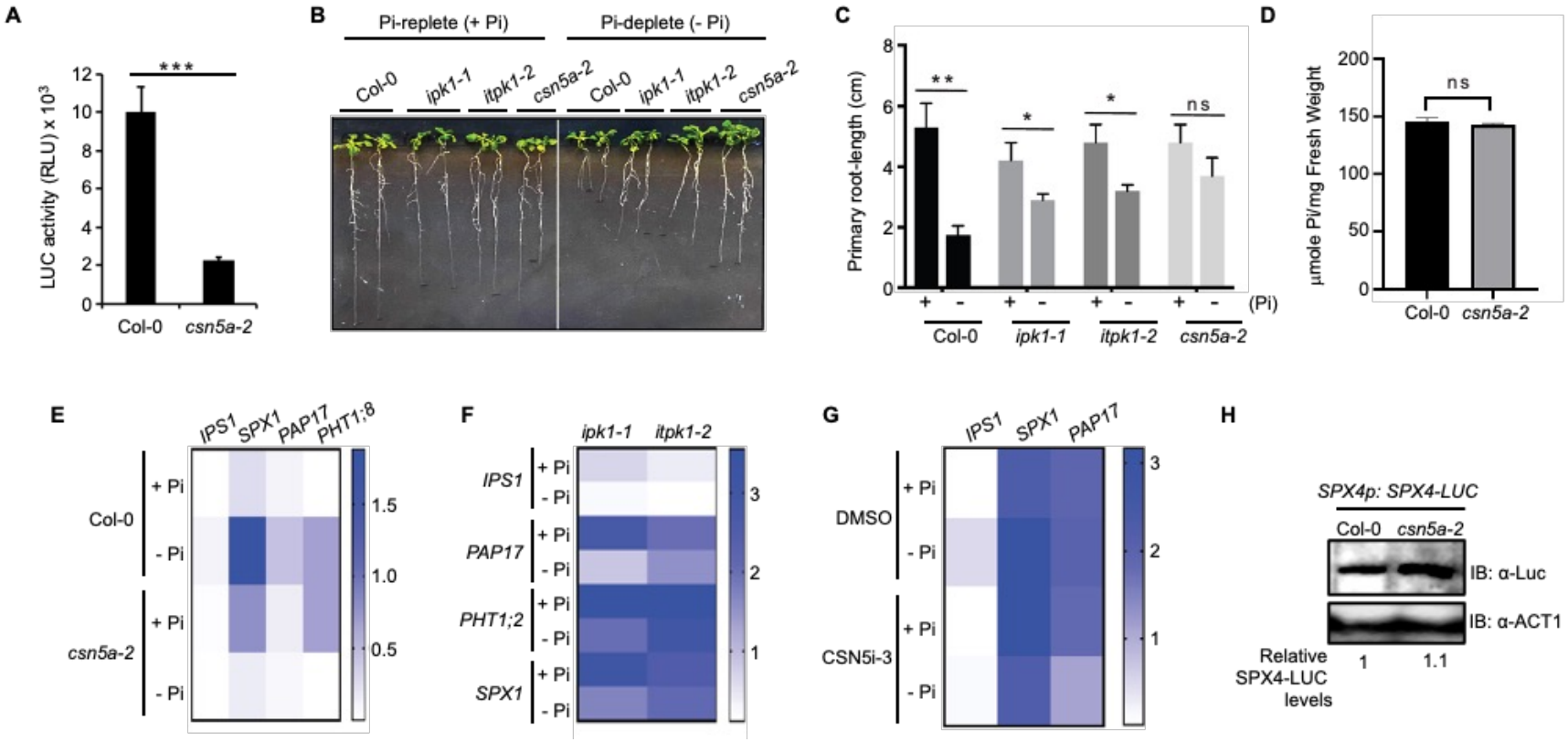

Supplementary Figure 13. Functional inefficiency of CSN5 or InsP-kinases impair PSR.

(A) Deneddylation activity of isolated CSN holo-complex from Col-0 versus *csn5a-2* plants tested on the Nedd8-AML substrate.

(B and C) Primary root-growth inhibition under Pi-deplete (-Pi) versus Pi-replete (+Pi) conditions in Col-0, *csn5a-2*, i*pk1-1*, or *itpk1-2* plants. Data represents the mean (n=~20) ± SD.

(C) Endogenous Pi levels in Col-0 and *csn5a-2* plants. The data shown is mean ± SD (n=6-7).

(E to G) Heatmaps of *PSI*-gene expressions in Col-0 versus *csn5a-2* **(E)**, *itpk1-1* and *itpk1-2* **(F)**, or mock (DMSO)- or CSN5i-3-treated Col-0 **(G)** under Pi-replete (+Pi) or Pi-deplete (-Pi) conditions (n=3). Gene expression were normalized to endogenous *MON1* transcripts. Heatmaps were generated using Graphpad Prism 8.4.3 software using the single gradient function.

Data is indicative of mean values (± SD). Statistical analysis is by pairwise comparison with Student's *t*-test (*P<0.05, **P< 0.01, ns= not significant).

(H) SPX4-LUC levels in Col-0 versus *csn5a-2* plants. Total extracts were immunoblotted (IB) with anti-LUC antibodies. Anti-ACT1 immunoblot shows loading controls. The numbers below the image indicate relative SPX4-LUC amounts normalized to ACT1 levels.

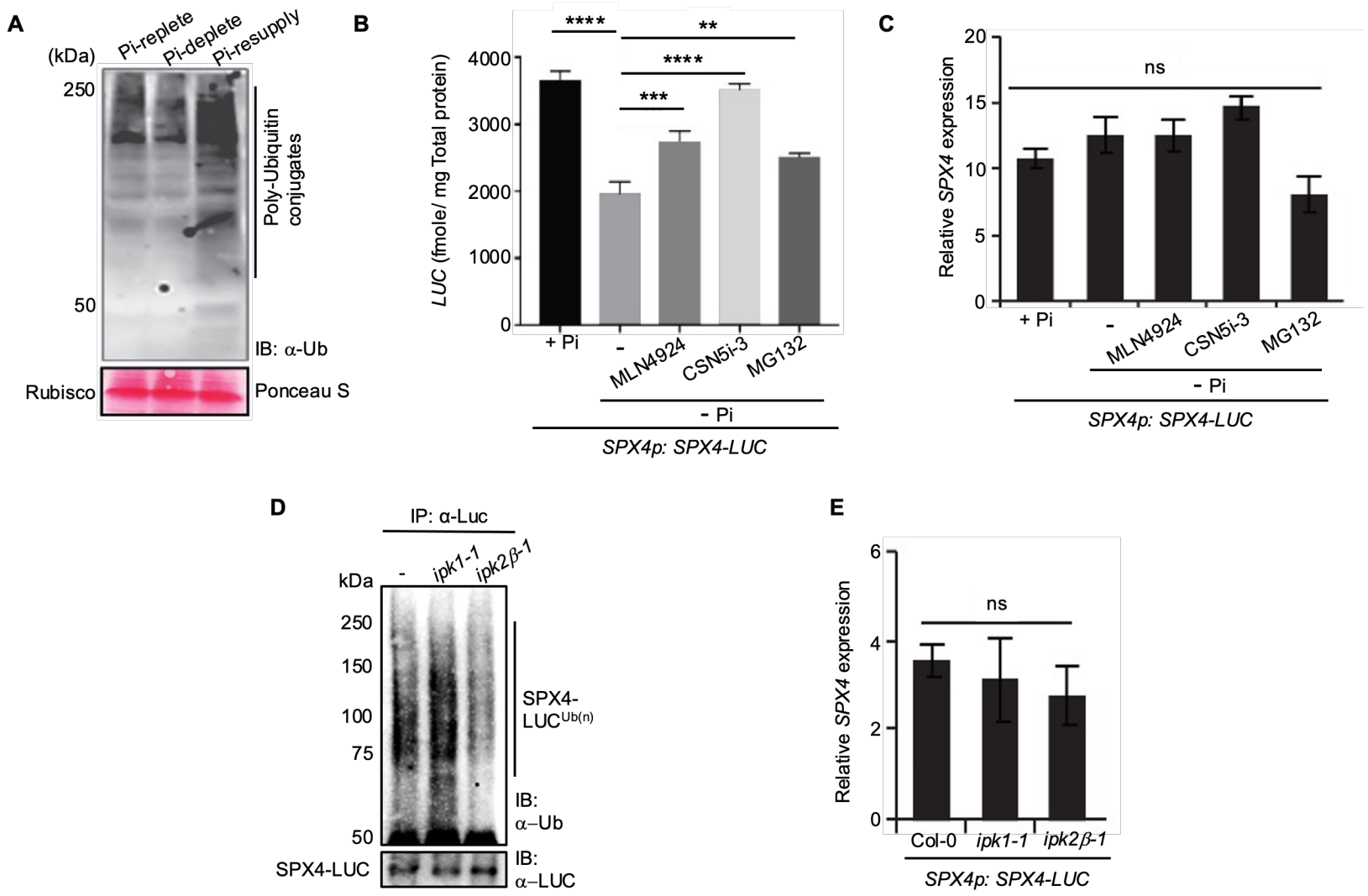

Supplemental Figure 14. Pi-starvation causes CSN-mediated and CRL-dependent degradation of SPX4.

(A) Global poly-ubiquitin conjugates in total extracts from Pi-replete, Pi-deplete, or Pi-deplete + resupply (Pi-resupply) Col-0 plants probed (IB) with anti-ubiquitin (Ub) antibodies. Approximate migration positions of poly-ubiquitin conjugated proteins are marked. Relative migration position of molecular weight standards (in kDa) are shown. Comparable total protein loading between the samples is denoted by Ponceau S staining.

(B) MLN4924 or CSN5i-3 reduce SPX4 degradation upon PSR. Luciferase (LUC) activity is indicative of SPX4-LUC levels under Pi-replete (+ Pi) and Pi-deplete (-Pi) conditions without or with indicated inhibitors.

(C-E) Relative *SPX4* transcript levels in the indicated treatments **(C)**, or in the mentioned genotypes **(E)**.

(D) Polyubiquitinated SPX4-LUC in control (-), *ipk1-1,* and *ipk2β-1* plants detected via immuno-enrichment (IP) with anti-LUC antibodies and probed (IB) with anti-Ub antibodies. Relative levels of unmodified SPX4-LUC are shown with anti-LUC immunoblot. Migration position of molecular weight standards (in kDa) are indicated.

Gene expressions were normalized to endogenous *MON1* transcripts. Data represents mean ± SE (n=3). Statistical analysis is by pairwise comparison to + Pi **(B and C)**, or to Col-0 **(D)** with Student's *t*-test (***P*<0.01; ****P*< 0.001, *****P*<0.0001, ns= not significant).